POLYMER ELECTROLYTES AND PAPER-BASED CURRENT COLLECTORS FOR FLEXIBLE LITHIUM ION BATTERY APPLICATIONS

by

Nojan Aliahmad

A Thesis

Submitted to the Faculty of Purdue University

In Partial Fulfillment of the Requirements for the degree of

Doctor of Philosophy

School of Electrical & Computer Engineering

West Lafayette, Indiana

August 2019

THE PURDUE UNIVERSITY GRADUATE SCHOOL
STATEMENT OF COMMITTEE APPROVAL

Dr. Kody Varahramyan, Co-Chair
School of Electrical and Computer Engineering
Dr. Edward Delp, Co-Chair
School of Electrical and Computer Engineering
Dr. Mangilal Agarwal
School of Mechanical Engineering
Dr. Saeed Mohammadi
School of Electrical and Computer Engineering
Dr. Maher Rizkalla
School of Electrical and Computer Engineering

Approved by:

Dr. Dimitrios Peroulis
Head of the Graduate Program

To my amazing parents, Mitra and Mehrdad,
for their unconditional love and support throughout my journey of life.

ACKNOWLEDGMENTS

I would like to express my gratitude to all my mentors, colleagues, lab mates, and individuals who helped me toward my research. First, I have to gratefully thank, Dr. Kody Varahramyan, Dr. Edward Delp, and Dr. Mangilal Agarwal for providing this opportunity and their supports throughout all the challenges, and their helpful and constructive discussions. I would like to especially thank Dr. Mangilal Agarwal, a great mentor, tireless supervisor, and true scientist. Without his endless support, motivation, trainings, and supervision, none of the success that I have achieved today was possible. I also appreciate Dr. Kody Varahramyan for all the guidance and support towards my research.

I would also like to thank my other thesis committee members for their helpful feedbacks, and time. A great deal of thanks to Dr. Maher Rizkalla, who was my mentor since the early days of undergraduate study, and helped me to live up my potentials. I also would like to thank Dr. Saeed Mohammadi for individual discussions and feedbacks for this dissertation. I would like to acknowledge my colleagues in the Integrated Nanosystems Development Institute, Dr. Dan Minner, Dr. Ali Daneshkhah, and Dr. Amanda Siegel for all their endless support in different aspects of my research from designing of the experiments, to characterization and analyzing data, and their kind assistance in authoring scientific papers. I would like to also aknowledge Dr. Yadong Liu, and Dr. Jian Xie for laboratory assistance and help with the experimental works of this research. I would like to thank, Dr. Brian King, and Ms. Sherrie Tucker for all their support and guidance.

Last but not least, I would also sincerely thank my lovely mom and dad, Mitra Khodayarkhani and Mehrdad Aliahmad, who I owe my existence to them, and I would not be here without their unconditional love and support throughout my entire life. My amazing mom, who took the best care of me all the times and motivated me to achieve the best, and my great dad, who was my first teacher in my life and showed me how to be successful and face the challenges of life.

TABLE OF CONTENTS

LIST OF TABLES

LIST OF FIGURES

LIST OF ABBREVIATIONS

CNT	Carbon nanotubes
CV	Cyclic Voltammogram
DEC	Diethyl carbonate
EC	Ethylene carbonate
GO	Graphene oxide
LbL	Layer-by-Layer self nanoassembly
$LiPF_6$	Lithium phosphorous fluoride
LTO	Lithium titanite
LCO	Lithium cobalt oxide
LMO	Lithium manganese oxide
MWNT	Multi wall carbon nanotube
NMP	N-Methyl-2-pyrrolidone
PAA	Polyacrylic acid PANI: Polyaniline
PANI	Polyaniline
PDMS	Polydimethylsiloxane
PEDOT	Poly (3,4-ethylenedioxythiophene)
PEG	Polyethylene glycol
PEI	Polyethyleneimine
PEO	Polyethylene oxide
PVA	Poly(vinyl alcohol)
PVDF	Polyvinylidene fluoride
PVDF-HFP	Poly(vinylidene fluoride-hexafluoropropylene)
QCM	Quartz crystal microbalance
RFID	Radio-frequency identification
rGO	Reduced graphene oxide
SEI	Solid electrolyte interface
TEGDME	Tetraethylene glycol dimethyl ether
TPU	Thermoplastic polyurethane
TAAPI	Technical Association of Pulp and Paper
V_2O_5	Vanadium pentoxide

V_2O_5/G	Vanadium pentoxide/reduced graphene
SEM	Scanning electron microscope
SWNT	Single wall carbon nanotube
XRD	X-ray diffraction

ABSTRACT

Author: Aliahmad, Nojan. PhD
Institution: Purdue University
Degree Received: August 2019
Title: Polymer Electrolytes and Paper-based Current Collectors for Flexible Lithium Ion Battery Applications
Committee Chair: Kody Varahramyan, Edward Delp

Paper-based flexible devices represent a new frontier in electronics technology. The research has focused on the fabrication of the lightweight, and flexible paper-based lithium ion batteries. A lithium ion battery relies on the interplay of multiple components. These components themselves, as well as the processes used to create them, need to be adjusted and modified in order to achieve a fully flexible lithium ion battery. These components include the electrode current collector, active material, and electrolyte. By modifying these components to be fully flexible and resistant to damages caused by deformation, a fully flexible battery can be achieved.

Herein, the paper-based platform utilized is key to provide flexibility for the battery components. The goal of this work not only focused on the creation of a paper-based flexible battery to be used as an integrable energy storage system for flexible devices, but also on developing methodologies and processes that can advance the emerging area of paper-based electronics, where different functional units must be fabricated within a single paper substrate. The key to make effective paper-based batteries, is to achieve a highly conductive paper structure as the base. In this work, conductive nanomaterials including carbon nanotubes (CNT) and graphene were used to fabricate conductive paper, where wood microfibers were coated with layers of these nanomaterials via layer-by-layer nanoassembly. These fibers were then combined into paper sheets. The resulting paper offers a conductive and porous base for electronic devices that utilized only small quantities of CNT or reduced graphene oxide (rGO) to provide length resistances of 468 Ω/cm and 74.6 Ω/cm, respectively for each fabricated conductive paper.

Flexible lithium ion batteries were then made by using CNT paper-based electrodes and a solid polymer gel electrolyte. The electrodes were made by deposition of lithium active materials over the conductive paper and where shown to be flexible, durable, and light weight. With respect to

the electrolyte, a new type of gel electrolyte based on PVDF-HFP was fabricated to overcome problems related to the use of liquid electrolytes in flexible batteries. This gel, which provides a high electrolyte uptake (450% by weight), was made by infusing both liquid and ceramic electrolytes inside a polymer gel structure and demonstrated conductivity up to 10^{-4} S/cm. The paper-based battery developed with these new materials has a comparable capacity to commercial batteries and represents a flexible and light weight alternative. The use of ultra-high capacity lithium compounds as cathode materials, such as vanadium pentoxide (with theoretical capacities of 440 mAh/g) in conjunction with rGO-paper as a stand-alone electrode (with a reversible capacity 546 mAh/g) were also explored and results will be discussed.

This research has led to the development of a novel method of making a fully flexible lithium ion batteries, using paper-based current collectors, leak proof polymer gel electrolytes and ultra-high capacity lithium ion active materials. Thus, flexible high conductive paper-based current collectors, polymer-gel electrolytes, vanadium based ultra-high capacity cathode electrodes, and graphene-based stand-alone paper-based anodes have been developed and tested.

CHAPTER 1. INTRODUCTION

1.1 Motivation

Current literature demonstrates a critical need for flexible electronics, from textiles to smart labels, and having a flexible lithium ion battery could overcome key limitations in the energy storage technologies needed. However, fabrication of such a fully flexible lithium ion battery remains a challenge. The main goal of this research was to make a completely flexible and paper-based energy storage unit that be integrated with other paper-based devices. The lithium-ion configuration was chosen as the energy storage device building block of this project as it can provide enough energy for integrated systems and it is also rechargeable. Although there are different approaches to make lithium ion batteries, a solid lithium ion battery is the best choice for making flexible batteries. As has been reported, liquid-based cells have some limitations such as leakage and complex packaging. This limits the usage of liquid cells for flexible batteries [1]. In this case, the fabrication of a reliable and highly stable solid electrolyte is one of the main parts of this project. In addition, the commercial metallic electrodes are not flexible, sensitive to forces and where the active material would crack after bending.

To overcome these issues, paper-based electrodes were developed. Paper-based electrode made by CNT-microfiber paper can provide flexibility to the lithium ion battery. Different materials such as LTO, LCO, LMO, and V_2O_5 were tested to check the performance of the paper-based batteries for different applications [2-6]. In addition, the CNT-microfiber paper must be improved to increase the cyclability of the lithium ion batteries in the future. The conductivity of the CNT-microfiber paper can be increased by applying functionalized CNT nanomaterials to reduce the usage of polymer layers. The final battery will also need a packaging which is flexible and compatible with lithium ion batteries. Importantly, the methodologies developed here in not only pertain to energy storage, the developed strategies to create CNT-microfiber paper can be utilized for other applications as well, where CNT-microfiber paper coated with a variety of other materials for use in an array of potential applications.

1.2 Background

During the past decades, lithium ion batteries have been significantly improved to achieve higher capacities and life cycle. However, recent advancements in electronic devices have increased the necessity of also developing thin lithium ion batteries with flexible properties and recently there has been a shift in research toward creating light weight, thin and flexible battery technologies. Development of safer, cheaper, and durable batteries, with advanced materials is the key challenge of novel lithium ion batteries [7, 8]. Here different modern battery researches with a brief discussion on the chemistry and fabrication methods, is reported.

Lithium ion batteries can be a sustainable energy source to replace fossil fuels. With the limitation of fossil fuel sources and emissions are main concerns of modern civilizations, having a clean and durable energy source is a significant research topic these days. A lithium ion battery is made of electrochemical units providing current and voltage. To achieve smaller and lighter batteries, higher current density materials have been developed. In addition, to increase the output current, larger active surface area of electrodes is an alternative to provide higher recurrent densities. Here, using nano materials can increase the active surface area and provide a higher current/capacity for lithium ion batteries [9-11].

The early lithium ion batteries were developed by Sony around 30 years ago to achieve lighter and more powerful energy source for portable devices. In that era, formation of oil crisis, shifting towards renewable energy, fabrication of small-scale electronics, and higher demands of high power applications, increased research in batteries (mainly lithium ion batteries). Lithium is the most reactive material with the lowest atomic number and density. The measurement of electromotive force also revealed that this material has the maximum electromotility and can provide the highest voltages compare to other materials such as sodium or potassium [12]. Because of this high electrode potential, lithium has been used as the active material for voltaic pills since 19^{th} century. In the late 1960s lithium again became a topic of interest manly to make primary lithium ion batteries. The first generation of lithium metal cells were fabricated using a lithium foil anode, and a propylene carbonate- sodium hexafluorophosphate electrolyte. Although lithium was a good choice, the first generation of lithium ion batteries were based on a primary battery setup and were therefore not safe or easy to fabricate. To achieve enhanced safety and durability,

secondary batteries were developed using metals such as lithium. nickel and lead. While most other secondary batteries were not promising, lithium ion secondary batteries had great potential due to the high-power density and voltage range [1].

To achieve high energy lithium ion batteries, the anode and cathode materials must be made of lithium active materials as lithium has smallest atomic weight, high capacity and very low reduction voltage compared to other elements [1, 13]. This high capacity is due to the high columbic efficiency of the oxidation process. Compared to some other elements, the energy density of lithium is lower, but because it only has one oxidation state it is more stable and has better cycle life. Having different charge states make ions less mobilized in mediums and provide more permanent, non-reversible bonds. In addition, the chance of reaction with electrolyte is higher in metals with more than one charge state. This also reduces the diffusion coefficient of the ions inside the cell. The energy of a battery can be found by multiplication of voltage and capacity. The actual voltage of a battery is the difference between the voltage level of anode and cathode, and capacity represents the total parallel capacity of anode and cathode. In this case, all electrodes and electrolytes must have a lithium base in order to achieve maximum efficiency and high power density [14, 15].

First generation lithium ion anodes and cathodes were based on the formation of crystals with a lithium metal structure [1, 16]. Titanium disulfide and tungsten disulfide were the basic materials used for these cathodes. The layer structure of these compounds could be used to store lithium ions and provide good recyclability and lithium transfer [17]. Later, lithium was also added to the titanium disulfide structure further improve the capacity. These cathodes were used in primary lithium ion batteries mainly due to their high capacity of 240 mAh/g. The negative side of this cell resulted from using lithium metal anodes. This could reduce the voltage by around 2 volts and came with additional safety issues [15]. To replace lithium foil used in these lithium metal anodes, different lithium alloys were developed and tested. However, developing material for the anode was more challenging, as it was hard to find other materials to replace lithium by still providing high capacity and cycle life. Aluminum, silicon, and tin were some of the alloys that were used as alternatives in these lithium ion batteries, but they have been discarded due to their non-reversibility and low cycle life that results from the high volume expansion and contraction in each

charge and discharge cycle. Among these alloys propitiated tungsten oxide was introduced in early 80s as a very durable anode material for lithium ion cells [15, 16, 18].

Cathode materials for secondary lithium ion cells, are categorized by one (olivine), two (layered) or three (spinel) dimensional crystal structure to provide enough lithium ion mobility [19]. The one-dimension cathodes have lower ion mobility due to their 1D structure, but recently through the development of new nanomaterials, high capacity one-dimension crystals have been created; lithium iron phosphate is among one of the best examples of 1D cathodes and can provide a working voltage of 3.4 volts and a capacity of 170 mAh/g [20].

In comparison, 2D lithium compounds produce more energy density and have increased durability, which have made them widely used in lithium ion batteries. Lithium cobalt oxide was fabricated to overcome the limitations of the cathodes designed around 30 years ago. This material has a similar structure to lithium titanium disulfide, but provides significantly higher voltage (around 4 volts) and capacity (274 mAh/g) [21].

The 3D crystals were later developed to enable higher lithium diffusion and provide better cycle life, although the capacity of these materials are slightly lower than 2D crystals [20]. The spinel lithium manganese oxide is generally known as a reliable, robust, and common cathode material of lithium ion batteries. These materials are still widely in use for many commercial lithium ion batteries today. Other 3D materials based on phosphates have also been developed. However, these materials are still in the research phase, but have proven to be a solution to achieving higher capacities [22].

The major early anode materials for secondary lithium ion batteries were carbon and graphite-based materials, and some of them are still widely in use. Some of these materials still in use include forms of graphene and graphite due to their low fabrication costs and stable discharge plateau. While graphene is the most inexpensive material, its high reactivity to the electrolyte limits the usage of this material in some types of lithium ion batteries [19]. One of the early anode materials used in these battery types was lithium carbide. It was developed to overcome the limits of lithium alloy anodes such as solid electrolyte formation. Its solid electrolyte layer reduces the

columbic efficiency and cycle life of the lithium ion battery by forming a layer of lithium on the anode surface. However, this can damage the separator layer and make short circuits inside the cell [23]. By developing the lithium carbide and then graphite, higher charge rate, temperatures, and capacity were achieved. The capacity of these cathodes can reach up to 372 mAh/g, although they have lower cycle life compare to other cathodes. To improve the weaknesses of graphene-based electrodes, other lithium compounds have been developed. Using nanotechnology to form nanostructures and carbon composites helped to eliminate the limits of raw graphene in lithium ion batteries. Further, materials based on copper, silicon, and titanium have been developed to be used in anodes. Lithium titanite, later developed to provide less capacity compared to metal alloys at around 170 mAh/g, has better stability and cycle life [23].

Many cathode materials have been tested to qualify their electron conductivity and energy capacity, yet they all have issues in some way or another. Issues like thermal stability, structure stability and energy capacity are what have kept some materials from being used in batteries. For this reason, most materials have to be modified in some way and increase their capabilities. Graphene and metal oxides cathodes have been gaining attraction for their great mechanical and chemical properties [16, 18]. The addition of active materials enhances the properties of these batteries, improving lithium ion diffusion as well as conductivity, meaning less resistance and more lithium ions pass through.

Lithium batteries provides an alternative to petroleum or gasoline [24]. However, there are many things we need to take into consideration when making lithium ion batteries, such as being environmentally friendly, reliable, and reducing fabrication costs. There are now many ways to approach making a reliable lithium ion battery, incorporating methods under hydrothermal conditions and electrospinning among others. Li-ion batteries have the potential to become an alternative source of energy and could be incorporated in not just electronics but also vehicles. While they may have some problems to deal with, there are innovative ways to improve their deficiencies in order to make high quality lithium-ion batterie [16]. Some new ways include working being done to improve current collectors.

Cu and Al have been utilized as current collectors because of their honeycomb structure, but they have poor adhesion due to low contact area. To overcome this issue, an etching process was used to increase its surface area of the electrodes to achieve higher capacity and cycle life. Specifically, the cathodes used $LiNi_{0.75}$, $Co_{0.57}$, $Mn_{0.11}$ and O_2 (BNMC) as Ni-based cathodes [16]. Their structure is well defined, and it does not have any impurity peaks. It is very important that cathodes do not contain impurities because it slows ion diffusion and creates viscosity when used with a BNMC. The etching process was done to reduce pattern dimensions, which increase the amount surface area which in turn enhances the mechanical flexibility for bendable electrodes. Achieving mechanical flexibility with the current collector and active materials is very important for a high performance battery, with high lithium diffusion so in this case silicon was used [16]. For comparison, if a non-patterned structure were used, the surface area would be 1.7 times less than that of a honey-comb patterned one. In addition, the pattern creates spots where active materials can adhere, and where bending won't cause significant problems. Thus, a coating method was used where NH_3VO_3 powder acts a precursor because the VO_3- can bond with Li-ion with LiOH and $LiCo_2$ on the surface. This creates a uniform layer. However, when tested the main problem that occurred was that Ni-based cathodes are containing impurities, which in turn decreases Li-ion diffusion. Consequently, with LiV_2O_5 reduced the pH and increased the rate capabilities. An amorphous V_2O_5 with cathode layers of the previous materials mentioned was made [16, 25].

Graphene is an interesting material because it is has a 2D structure characterized by great mechanical and chemical properties [26]. Lithium can be bound with graphene-based electrodes and more efficiently store Li-ions. While studies done on graphene initially showed that it had good capabilities (in this case the graphene was chemically prepared), recently it has been shown that it has irreversible capacity when used as an anode material. However, graphene used with conjunction with metal oxides nanoparticles reduces the irreversible capacity and enhances the cycle life; the integration of these nanoparticles works to prevent graphene from turning into graphite. It is important to note that materials as anodes or cathodes is important [27, 28]. By using graphene as an anode material initially, it exhibited in the first cycle 1233 and 672 mAh/g. After 30 cycles it exhibited a reverse capacity of 502 mAh/g, but it had low Coulombic efficiency at 55%. Now by using with the metal oxide, in this case, SiO_2 it showed a reverse capacity of 810 mAh/g. After 30 cycles it maintained capacity retention of Li-ions at 70%. These results can be

explained by a couple of reasons: 1) the amount of Li-ion they can receive, 2) the increased conductivity between particles, 3) the flexibility in keeping the volume expansion at a minimum, and 4) the metal oxides keep the graphene from restacking and it maintains the large surface area which is what the Li-ions need [29, 30].

Aside from graphene, other materials have been explored for their potential use. Tin and silicon are interesting options to look at [31]. The most important reason for this is that they can bind with Lithium and offer much higher capacity values than graphite. However, there is a big problem in that these materials have a large volume expansion and contraction that can potentially lose the electrodes. Reducing the size to a nanometric particle greatly enhances the performance of the electrode. By doing it this way it can facilitate Li-ion diffusion. However, nanostructured electrodes are not very good because of their high surface area. Thankfully methods have been achieved to help with this issue by designing carbon metal composites, which help to maintain stability and mitigate volume expansion [30].

Making tin and silicon alloys with lithium as electrode materials is promising to develop stable lithium ion batteries. By doing this a long and stable cycle life with high efficiency close to 100% has been achieved. LiSi displayed higher capacity with 990 mAh/g versus LiSn with the capacity of 500 mAh/g. LiSi also has higher potential than LiSn because of the high theoretical capacity. Both still display good capabilities as good buffers for volume expansion and contraction in the cell. Recently, carbon composites made Si and Tin good materials for use by having a stable capacity of 800 mAh/g [31]. These results bring good light in the fabrication of lithium batteries.

Sulfur and lithium sulfide (Li_2S) has been explored as well. One reason is its theoretical capacity of 1675 mAh/g, which is in the ultra-high range. It does have some drawbacks though, including low conductivity and a low vaporization temperature that induces sulfur loss [16]. A big problem that some of these materials have is the volume expansion with lithium insertion; as an example sulfur has a volume expansion of 80%. To mitigate this, active material was put into an expandable capsule with a hollow structure made with carbon, TiO_2 and polyvinyl pyrrolidone polymer capsules with thermal and chemical precipitation. A better method that was used is electrolyte modification for mitigating polysulfide dissolution [16].

Now for a safer method to mitigate volume expansion, Li_2S has been used instead. Li_2S has a high melting point, but is highly soluble in solvents like ethanol. This, in turn, can be used to make Li_2S nanocomposites. These have shown a cycle life of around 400, where no changes were observed in the Li_2S nanocomposite, demonstrating its stability. Carbon-based nanocomposites enhanced and helped make Li_2S a good choice for a lithium battery [31].

Another challenge in making lithium ion batteries has been to develop a sustainable electrolyte solution. Early lithium cells used a lithium chloride pyridine solution. Although the cell voltage was high, the low solubility of the lithium salt in pyridine solution reduced the columbic efficiency of the cell significantly [32]. This low columbic efficiency was the main reason for the low cycle life seen in early lithium ion batteries. Later, organic liquid electrolytes had been developed to overcome the capacity fade of lithium ion batteries. The basic liquid electrolyte for a lithium ion battery consisted of a lithium salt and a mixture or organic solvents such as alkyl carbonate and a chain carbonate mixture to provide maximum solubility [33]. Lithium hexafluorophosphate is one of the most widely available lithium salts for liquid electrolytes. This material, developed in 1960s, can be dissolved in organic solvents in conjunction with a polymer separator to make an electrolyte with high ionic conductivity for lithium ion cells. Due to its high stability and working voltage (around 5 volts) this material is widely in used for many applications, although solvents have been changed over the years to provide more stability and safety. As was noted before, having a high conductivity liquid electrolyte can be achieved using a stable lithium salt and proper organic solvents. The ionic conductivity of the liquid electrolyte is based on the lithium ion mobility and the number of free ions in the electrolyte solution. Therefore, having a less viscous organic solvent and higher dielectric constant can help lithium diffusion in liquid electrolytes and in turn simultaneously increase the capacity of the cells. There are also some high viscous solvents that are desired for specific electrolyte applications due to their decreased reactivity towards lithium. These solvents can provide a free path for ions and surge the diffusion coefficient of the lithium ion electrolyte. Mixing different types of solvents can be more helpful. Ethylene carbonate, dimethyl carbonate, diethyl carbonate, dimethyl sulfoxide and propylene carbonate are some of these solvents [8].

Recently, research in electrolytes have been devoted to replacing liquid electrolytes with high ionic conductive gel polymer electrolytes. This can eliminate the need of a polymer separator by combining that layer with the electrolyte. This method can reduce fabrication costs while increasing the safety and durability of the lithium ion batteries. In addition, having a gel electrolyte can give rise to the fabrication of fully flexible batteries. Early primary lithium ion batteries used polyethylene oxide infused with lithium salts as electrolytes, but the low ionic conductivity of them was a bottleneck of applying them in making secondary batteries. This is in addition to their low ionic conductivity, high operation temperature and low chemical stability of the polymer electrolytes which were further limiting factors to using them [8]. Today, recent developments in polymer fabrication could provide high ionic conductive materials for gel electrolytes.

Today, flexible and wearable electronics have become more and more prominent. Among the candidates, Li-ion batteries have promising properties for use in these applications. Yet, it is important to take into consideration possible limitations for their use, both in the materials and the methods utilized to make them. There have been novel advancements in making flexible electrodes for lithium ion batteries, including, using nanomaterials, developing nanostructures, and the development of carbon materials, graphene, and 3-dimensional (3D) nonmetallic current collectors [30]. Carbon-based materials are well desired to achieve flexible lithium ion batteries because of their high electrical conductivity and high mechanical flexibility [34].

The electrolyte is a key component in designing flexible lithium ion batteries. Liquid electrolytes are not a desired choice for pouch-type flexible batteries due to safety factors such as leakage and low mechanical stability [23]. Solid electrolytes are more stable and safe to be used in flexible batteries, but they provide less ionic conductivity compared to the liquid electrolytes, thereby resulting in less electrochemical performance and power density [35]. Gel electrolytes have been in development to achieve high conductivities compared to liquid electrolytes. Various polymers have been used but none have worked, primarily due to reactive, volatile and flammable solvents. Ionic liquids have been used instead because they fix the issues previously mentioned but at the same time exhibit poor cycling and power performance. To achieve high ionic conductivity, a well-delocalized charged ionic solution is needed on the cathode and anode sides of a cell, so ionic liquid polymer electrolyte film with solid-like features has been developed [35].

To develop a fully flexible cell, the previous cell manufacturing issues have been resolved by the development of flexible fabrication processes such as roll to roll printing, electrospinning, multistep spray painting, and screen printing. However, all of these methods are based on liquid electrolytes and therefore still require seal proof cells [34]. A new efficient method was devised to solve these issues by printing solid-state batteries (PRISS). The major components of PRISS cells are printed over arbitrary substances through a stencil process and ultraviolet sintering for the cross linking of polymer binders. The developed process will help to overcome the design issues for flexible batteries. Here the printable slurry is a composition of UV-curable ethoxylated trimethylolpropane triacrylate and a high boiling point electrolyte, such as lithium hexafluoride in ethylene carbonate propylene carbonate. This, mixed with active materials such as $LiFePO_4$ (LFP, cathode) or $Li_4Ti_5O_{12}$ (LTO, anode) and highly conductive carbon-based materials such as carbon black, was directly printed over an aluminum sheet [34]. In comparison with a conventional electrode slurry, it displayed higher viscosity and shear-thinning behavior. However, with higher amounts of solid content, particles start to agglomerate, so the amounts introduced are very important. The current collector was subjected to repeated bending tests and showed no appreciable deformation between it and the active materials, as well as no change in the electrical resistance. When analyzed at room temperature, it showed cycles 1.0 and 2.5 V with 90% capacity retention while maintaining structural stability. The ratio used for carbon-based materials improves conductivity by reducing electrical resistance. This showed a facile and efficient method for making flexible batteries [34].

1.3 Objectives

The main limit of using these flexible materials is the cell assembly process still relies on using liquid electrolytes, nonflexible metallic current collectors, and separator membranes. In this thesis, a new approach to make flexible paper-based lithium ion batteries has been developed using paper-based flexible electrodes, polymer gel electrolytes and ultra-high capacity lithium ion active materials.

Conventional metallic-based electrodes for lithium ion batteries are not flexible, which represented a significant challenge in the creation of the fully flexible electrode developed in this research. Previously reported methods to make flexible electrodes are based on making flexible structures

such as polymer sheets or highly conductive composite structures. These methods are highly complex and expensive compared to conventional metallic current collectors. Paper-based electrodes were previously designed as a less complex alternative. Although the paper was a better option, it still required high amounts of nano materials to make the paper conductive. Moreover, the creation of the conductive layer on the paper structure was based on the chemical deposition, ink deposition or direct growing of materials over the paper structure. Due to the complexity, these methods are simply not feasible to make commercial flexible lithium ion batteries.

To address these issues, a highly conductive CNT-microfiber paper was developed to be used as a flexible current collector to provide flexibility and stability in lithium ion electrodes. Later a reduced graphene microfiber paper was also developed to be used as a stand-alone anode for lithium ion batteries. This paper is a combination of current collector and active material (graphene) and can be used to eliminate the need of having a separate metallic current collector. This reduces fabrication complexity. Another challenge in making flexible lithium ion batteries is to keep the integrity and safety of the cells during bending. Having a liquid electrolyte and a standalone separator limit flexibility and stability of the batteries. Therefore, a polymer gel electrolyte made by Poly(vinylidene fluoride-co-hexafluoropropylene) was been developed to make a fully flexible leak-proof electrolyte. While previously reported gel electrolytes were providing acceptable ionic conductivity and flexibility, in this work the polymer structure is well developed to maximize electrolyte uptake and stability. In addition, the fabricated gel structure has been modified using lithium ceramic to achieve higher ionic conductivity compared to other gel electrolytes. Finally, to make the paper-based batteries more suitable for commercial applications having lighter and higher capacities are desired. Several strategies were explored to make the flexible cells lighter and to increase their power density, but most of this research was focused on making thinner current collectors or using highly complex methods to make thin films. As an alternative, having ultra-high capacity lithium active materials can address the weight issues. Here to achieve higher capacities, a novel vanadium pentoxide graphene combination was been used and was modified as active material in conjunction with paper-based current collectors in order to develop ultra-high capacity flexible lithium ion batteries.

1.4 Contribution

The main contribution of this dissertation to flexible batteries, are the development of flexible novel current collectors, gel electrolytes, vanadium-based high capacity cathode electrodes and graphene-based standalone paper-based anodes.

The fully flexible CNT-microfiber paper has been made using the layer-by-layer self-assembly of highly conductive CNT and polymers, such as PEDOT, over individual paper fibers. The coated fibers then formed a fully flexible and conductive paper sheet with the resistance of 468 Ω/cm with only 0.4% wt CNT utilization. This paper sheet can be used as the current collector in lithium ion batteries. While the oxidation voltage of CNT is below one volt, this conductive paper can be coated with many commercially available active materials to make flexible electrodes.

Another main component for any flexible lithium ion battery is the electrolyte. While the conventional liquid electrolytes are not flexible due to capacity loss and safety issues. Moreover, the liquid cells need a separator layer between the anode and cathode to make an electrically isolated barrier between them. Thus, any bend or deformation can lead to leaks or damages to this layer. Therefore, a novel polymer gel electrode is needed to make flexible lithium ion batteries a reality. In polymer gel cells, the electrolyte and separator are integrated into a single gel-like structure, which reduces failure and damage resulting from deformation processes (i.e. bending). While these available polymer-gel electrolytes do not have acceptable capacity, compared with liquid electrolytes, a PVDF-HFP based polymer gel electrolyte has been developed by trapping LiTFSI liquid-based and LATP ceramic electrolytes. An ionic conductivity of 2.1×10^{-3} S/cm and 86% stability after bending tests has been achieved. This electrolyte has also been used with paper-based LTO/LCO electrodes to make bendable lithium ion batteries with minimal capacity fade after bending, and no presence or leak of any toxic material.

Since the paper-based electrodes have a slightly higher internal resistance, higher capacity lithium active materials are needed to make durable and long-lasting flexible lithium ion batteries. In this research vanadium pentoxide xyrogel with graphene was used as an ultra-high capacity lithium ion active material for paper-based electrodes. While the vanadium pentoxide capacity is high, the cycle life of this material is still limited. Here, the presence of graphene in the vanadium pentoxide

structure improved the electrical conductivity and cycle life of this material, making it suitable for flexible battery applications. The capacity of the flexible paper-based batteries made by this material could reach 396 mAh/g with a voltage range of 0 to 4 volts.

Later, to have a compatible anode for vanadium-based cells, reduced graphene microfiber paper was developed. Here, a rGO paper was created using rGO coated paper fibers. The paper fibers were coated with graphene oxide, using layer-by-layer self-assembly, followed by a microwave thermal reduction to form a rGO layer. The rGO layer acts as a conductive current collector and lithium electrode at the same time, eliminating the need of separate current collector and providing capacities up to 546 mAh/g in half-cell configuration and a length resistance of 74.6 Ω/cm.

.

CHAPTER 2. REVIEW OF LITERATURE

2.1 Carbon Nanomaterials

Broad applications of flexible electronics devices have led to vast research and development of paper-based electronics [36-38]. These devices are made by Paper-based parts such as energy storage unit, sensors and other electronics [39-41]. Applying paper-based material can improve the flexibility of these devices, while reducing the weight and fabrication costs. One approach to integrating the paper-based parts inside the electronic devices is to make conductive papers. One method to make conductive paper is to apply conductive materials over the paper fibers [42]. Due to its high conductivity and stability, CNT is one of the best candidates to make conductive papers-based substrates due to its high conductivity and stability [43-45]. CNT has unique electrical characteristics due to its special structure. This material can be in the form of metallic or semiconducting according to its structure, so it can be used to make conductive and semiconducting substrates for different electronic devices.

Among carbon compounds, graphene also has excessive properties such as high conductivity, mechanical reliability, and thermal stability. Graphene is a 2D sheet of carbon in a honeycomb structure, and it can be used as a plane, role to 1D nanotubes or be stacked and form 3D graphite sheets [46]. Graphene also has high electron affinity and ionization voltage (4.6 eV) thus, it can be used as a reducing or oxidizing agent. This property and high conductivity make it a good candidate for lithium ion battery electrodes [47]. Figure 2-1 shows the structure of graphene and CNT rods from carbon atoms.

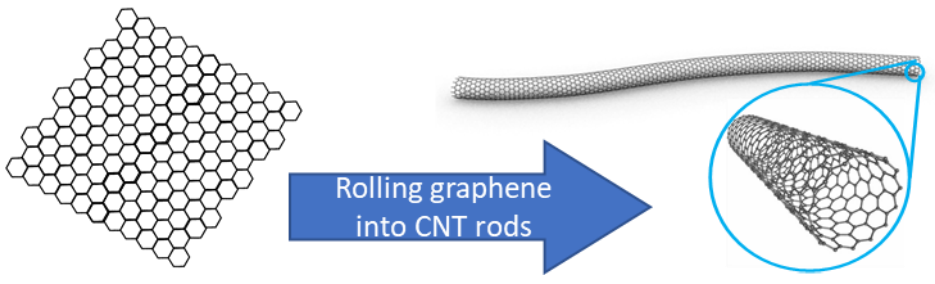

Figure 2-1 2D graphene and 3D CNT structures

Graphene, in different forms, can also be used as a great martial with outstanding properties in lithium ion batteries [48]. There are multiple methods of making graphene such as chemical vapor deposition, mechanical exfoliation, and organic synthesis but using graphene oxide is one of the most reliable and fast techniques. As it was reported, in this method an aqueous solution of graphene or graphite oxide will be reduced to graphene by Hammers method. In this case, the layer of graphene will be stacked and dispersed in water. Later other reduction methods such as thermal reduction, chemical reagent reduction, photocatalyst reduction, solvothermal reduction, and microwave reduction have been developed to reduce the aggregates and form a single layer highly conductive layer of graphene [49].

2.2 CNT-Microfiber Paper

Thin carbon nanotube films (Bucky papers), conductive CNT-based inks and a thin film of CNT coated over the paper are some of the CNT-based flexible substrate replacing traditionally used materials in electronic devices such as aluminum and copper [50, 51]. The negative side of using CNT to make these conductive papers is fabrication costs and complexity. As it was reported by Hu et al. CNT paper can be used for a flexible energy storage device, such as supercapacitors and batteries [8, 50, 52]. The CNT paper can be made by using conductive inks. To reach a minimum conductivity CNT must be dissolved in a solvent with a polymer binder to make a conductive ink. Here the CNT utilization is around 2%, which is higher than other reported methods like evaporation or filtering [53]. In another approach, multiwall carbon nanotubes (MWNT) were grown over the silicon substrate. MWNT then mixed with cellulose fibers using 1-butyl,3-methylimidazolium chloride and filtered to make conductive papers. The fibers fixed using dry ice to form sheets and then baked to removes the residues [54]. Although this method has limited steps, removing solvents is a very hard process form the fibers and CNT utilization is significant. In another approach, the conductive paper is made by filtration of CNT and polystyrene solution. This paper then used in making vanadium oxide and manganese oxide cells. The reported energy density is in the range of 100W/kg and 851 W/kg respectively. In this method, having a polymer inside the CNT sheet is a limiting factor for making highly conductive materials [55, 56]. The CNT sheet also can be made using spray-on method. In this method, the films were made over a pre-casted polyethylene terephthalate films to make a highly conductive flexible substrate. The highly conductive interconnected layers of CNT ink provide a uniform layer which is electrically

conductive. This highly conductive film then can be used in making flexible energy storage devices such as lithium ion batteries, and flexible electronics [57].

Having a commercially adaptable CNT-based conductive paper needs a further reduction in CNT utilization. Devices presented here are using CNT-microfiber paper, which only contains around 0.2% (wt) of CNT [45]. CNT-microfiber paper is made by coating individual wood fibers with conductive materials such as CNT through a Layer-by-Layer (LbL) self nanoassembly. This technique allows the precisely controlled formation of multilayers of materials in nanoscale around the wood microfibers, though he alternate deposition of oppositely charged nanomaterials. The individually coated wood fibers then form a single sheet of CNT-microfiber paper which has the resistance up to 1.92 kΩ·cm. Using LbL process also keeps the other characteristics of the paper, such as high binding with other materials and surface area. The CNT-microfiber paper can be used as the current collector for paper-based batteries, a conductive and flexible substrate for electronic devices or a paper-based sensing device [36, 43, 45].

One of the applications of the fabricated CNT-microfiber is to be used in flexible lithium ion batteries. The main goal of this section is to make flexible batteries, by implying the flexible properties of the paper-based electrodes. As it was shown before, the CNT-microfiber paper can be used as a flexible current collector for flexible lithium ion batteries. Flexible lithium ion batteries have been developed using different configurations such as micro-batteries, polymer batteries, printable batteries, origami cells, paper-based batteries, and stretchable batteries [51, 58, 59]. Recent advancements in material sciences and flexible electronics have exposed a huge potential in the development of flexible batteries. One of the promising methods of making a commercially feasible flexible electronic device is to use paper-based structures. The paper-based devices also need a paper-based energy storage unit that can be based on lithium ion technology. Despite all the improvements, the development of a fully flexible paper-based lithium ion battery is still a challenge [45, 60].

2.3 Reduced Graphene Microfiber Paper

Graphene is also another option to make flexible paper-based batteries. It has high conductivity and energy density suitable for lithium ion battery applications [29]. Graphene has novel mechanical and electrical characteristics, and it can be used to make conductive structures. Graphene can be deposited using chemical vapor deposition, epitaxial growth, or micromechanical exfoliation. All of these methods are complicated and costly. An alternative method is to deposit graphene directly using cross-ionic LbL self-assembly, but graphene itself does not have a zeta potential. On the other hand, graphene oxide (GO) has a negative zeta potential, so it is suitable for LbL deposition over paper substrates to make conductive paper [61]. The conductive paper then is finished by reduction of GO to rGO by either a chemical process or a thermal treatment. Chemical reduction processes, however, also dissolve the cellulose and change the characteristics of the paper fibers. Conventional thermal reduction of GO in a furnace is not feasible because there, samples need to be heated up to 800°C, but the paper will be carbonized around 250°C in an argon environment and will burn in an oxygen environment. However, microwaving coated fibers in the presence of an organic solvent leads to the rapid reduction of GO to rGO [26].

This alternative method increases the surface energy of the coated fibers and reduces the GO to rGO without destroying the paper fibers. Here the organic solvent works as the temperature limiter (the boiling point of the solvent) and prevents the aggregation of graphene after the reduction step. In this case, the unique properties of the paper fibers will be saved, and the conductive graphene layer will be formed around the fibers. The fabricated graphene microfiber paper can act as an active electrode for flexible and paper-based lithium ion batteries while eliminating the usage of current collectors.

2.4 Lithium Ion Batteries

There are several different types of rechargeable batteries available for different applications, but among all of them currently, there is a huge demand for lithium ion batteries. Lithium ion batteries are working like any other batteries by the migration of ions from inside and electrons from outside of the cells between electrodes through the charge and discharge process. During the discharge by draining the electrons from the battery, lithium ions are released from the negative electrode and

migrate to the positive electrode by an ion exchange process inside the electrolyte. In the charging cycle by injecting the electrons back to the battery, these ions also move back from positive electrode to negative electrode [7, 14]. In this case the lithium ion passes the electrolyte/separator by diffusion mechanism using electrolyte and separator act as an isolating barrier between electrodes to prevent short circuits.

Lithium ions can provide higher specific power and energy compare to other materials such as nickel bases, silver based or lead acid-based batteries [62-64]. In addition, higher current density and more stability are other benefits of using lithium ion batteries. The lithium ion batteries providing more capacity with smaller weight and size are best choices of energy source in electronic and high-power applications. As it is reported in Table 2.1, the lithium ion batteries can be the best candidate for portable and light applications while their energy density is much higher than other available rechargeable batteries and their cycle life is also greater [65, 66]. In addition, the maximum nominal voltage of these batteries is as high as twice of other types of cells.

Table 2-1 Comparison study between different types of rechargeable batteries

Type of the battery	**Energy density**	**Cycle life**	**Nominal Voltage**	**Cost**	**Operation temperature**
Lead Acid	30-80 Wh/kg	400-600	2V	Cheap	-20 to 60 ^{o}C
Nickel Cadmium	50-80 Wh/kg	500-1000	1.2 V	Moderate	-20 to 60 ^{o}C
Alkaline	50-120 Wh/kg	300-500	1.2 V	Cheap	-18 to 55 ^{o}C
Lithium ion	100-180 Wh/kg	500-1000	3.7 V	Expensive	10 to 60 ^{o}C

The huge demand of having high capacity lithium ion batteries, with high cycle life and flat voltage plateau has been maintained the development of high capacity active materials for lithium ion batteries. While the charge/discharge cycles of the batteries are specially related to the depth of discharge, having stable materials for high current applications is a must for having stable lithium ion batteries. To achieve the maximum efficiency, the constant current rate of lithium ion batteries is in the range of 0.2 to 0.5 C which is high compared to the other conventional batteries. Although there is still a high research to increase the C rate of the cells for fast charging applications such as electric cars and handheld devices. In addition to the capacity, the stability of the batteries is

another important factor. Lithium ion batteries now have high shelf life and very low self-degradation, but still the market standards are set to have less capacity and charge fade for these batteries. Further, the safety of the battery is another issue, for high current application of lithium ion batteries [1, 67].

2.5 Flexible Lithium Ion Batteries

Flexible cells have been developed using many materials and multiple approaches to meet the needs of flexible electronics. As it was reported, the conventional metallic current collectors are not suitable for making flexible lithium ion batteries, due to the weak adhesion of active material layer over the metallic surfaces. While there is no chemical bonding between the active material layer and metallic surface, the active material layer is not flawlessly bonded to the metallic layer [53, 68]. One of the key challenges of making a flexible battery is to make a highly conductive porous structure to be comparable with metallic current collectors such as aluminum and copper films. In this case, polymer sheets or cellulose based current collectors are better options while they can make chemical bonding to the active material layer and provide stability [35, 69].

Polymer-based current collectors have been developed using conductive polymer or highly conductive nanomaterials embedded into polymer structures. Conductive polymers for this current collectors can be materials such as polypyrole, poly(3,4-ethylendiocythiophene) (PEDOT) or polyaniline. The conductive nanomaterials such as carbon nanotubes also mixed with polymers such as polyethylene, Poly(methyl methacrylate) or polyethylene terephthalate, in shape of ink or direct mix to make flexible current collectors. One of the easiest methods of making this deposition is to make conductive ink. As it was reported carbon nanotubes mixed with polymer binders can make a highly conductive ink with the sheet resistance of 5 Ω/cm^2 [53]. This ink is deposited over the polymer sheets and then coated with an active material layer to make flexible electrodes. Besides, making inks, the direct deposition methods such as hot press, imprinting, and nanocoating have been tested using carbon nanotube-based inks to make flexible conductive current collectors. Although this technique can produce flexible electrodes for lithium ion battery, it needs loads of nanomaterials and it is not an efficient way of making flexible batteries.

To overcome the limits of carbon nanotubes, cheaper nanomaterials also have been added to the conductive inks, such as silver, silicon, and zinc [70-72]. As it was reported the CNT-silver ink has been developed to make flexible lithium ion batteries. The fabricated current collector has a sheet resistance of 1 Ω/cm^2, and batteries have been made using this current collector with capacities up to 108 mWh/g. In another method CNT-Si nanoparticles have been used to make batteries [56]. In this case, the chemical vapor deposition has been used to make a layer of CNT. Here the CNT-Si can act as a current collector, and active material at the same time with capacity of 1000 mAh/g but the cycle life is limited to 35 cycle and the fabrication costs are so high. Another material to make flexible current collectors is graphene. Highly conductive graphene coatings using spray, chemical bath, sputtering, and filtrations have been developed [73]. These methods can provide high conductivity flexible current collectors, more efficiently. As it was reported [74], the reduced graphene oxide was combined with a solvent/metallic nanoparticle mix, then filtered following by annealing. This mix then dried and formed a flexible electrode for lithium ion batteries. Although all the above methods reduce the carbon nanotube utilization, the fabrication method of these current collectors are still a challenge and the stability of them in lithium ion environment is still a question. In addition to usage of nanomaterials polymers are not environmentally friendly and they are not that porous to keep high bending and deformations. Having a fully flexible highly porous current collector with less usage of nanomaterials is still a challenge to make flexible lithium ion batteries [25, 34, 53, 56].

2.6 Paper-Based Lithium Ion Batteries

One of the main challenges to achieving flexible paper-based batteries is the difficulty to develop a paper-like structure, compatible with lithium ion current collector standards such as high conductivity and stability. CNT has been studied to overcome these challenges. Improvements in flexibility and stability have been made using this material in paper-based electrode structure such as reported capacities up to 153.5 mAh/g and columbic efficiency up to 90.6% [51, 75, 76]. Despite these improvements in flexibility, these devices are still using liquid electrolytes and very sophisticated CNT-based current collector fabrication processes. Here to achieve a less complex and integrable CNT-based current collector, a highly conductive paper-based current collector has been developed from CNT-coated paper microfibers (CNT-microfiber paper) [36, 43, 45]. The CNT-microfiber paper preserves the porous structure, making it suitable for flexible applications.

The developed microfiber paper has the CNT mass loading of 10.1 µg/cm^2 and the length resistance 1.92 kΩ·cm for 50 µm thickness. This research also shows the implementation of a fully flexible paper-based battery with a leak-proof PVDF-HFP polymer gel electrolyte using the CNT-microfiber paper electrodes. To also check the quality of the polymer gel electrolyte, both (i) standard cells with metallic current collectors and (ii) CNT-microfiber paper current collectors have been made and tested. Figure 2-2 shows the schematic of the flexible microfiber paper electrodes, assembly of the cell, and a flexible pouch cell made by paper-based electrodes.

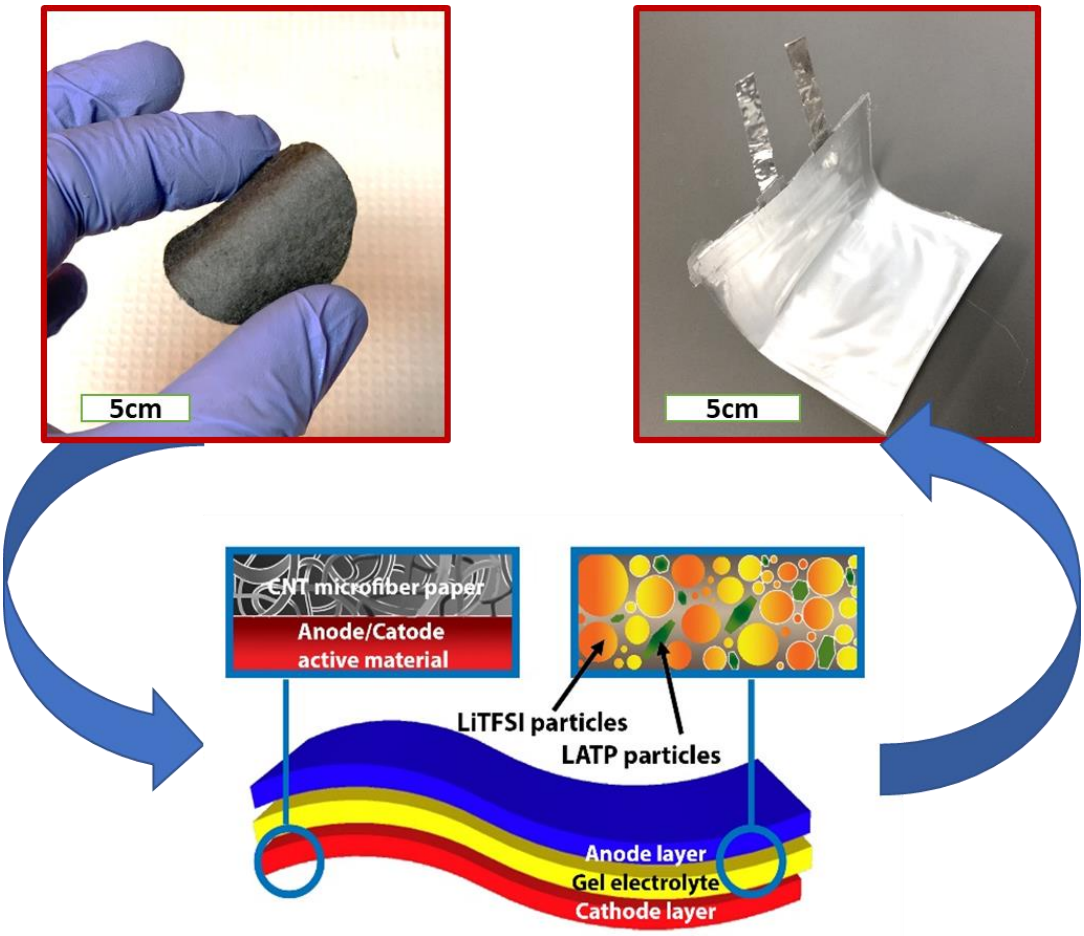

Figure 2-2 The CNT-microfiber paper, schematics of a paper-based battery with polymer-gel electrolyte, and pouch cell made by paper-based electrodes

The CNT can also be used directly as the cathode/current collector of the lithium ion batteries, and improves the properties such as capacity, and flexibility while reducing the weight of the battery by eliminating the use of metallic current collectors [2, 6]. The CNT sheets have been used in

lithium ion half cells and provide the capacities up to 1600 mAh/g [2]. This capacity is much higher than other reported capacities from other anode materials such as graphene, which has a similar chemical structure compared to CNT [7, 8]. The CNT films can be used as the stand-alone electrode in lithium ion batteries in the form of CNT papers, freestanding sheets, bulky papers and CNT composites with other materials such as silicon or lithium salts are used in lithium ion batteries [1, 4, 7, 9]. The CNT-microfiber paper can be a solution to reduce the CNT utilization, while keeping the both characteristic of the CNT and paper such as high capacity and flexibility. As it was mentioned before, the CNT covers the individual cellulose microfibers with the thicknesses up to 40 nm [11, 12] and makes a uniform coating around it. The CNT-microfiber paper utilizes less amount of CNT compared to other reported CNT-based electrodes. [10] Half cells with CNT-microfiber paper anodes have made and tested.

In conjunction with the CNT-microfiber paper, to overcome the resistivity limits, an ultra-high capacity lithium salt is also needed. Different metal oxides such as $LiNi_{1/3}Mn_{1/3}Co_{1/3}O_2$ (160 mAh/g) [77], $LiFePO_4$ (170 mAh/g) [20], and $LiMn_2O_4$ (120 mAh/g) [78] have been previously fabricated to achieve the high and ultra-high capacities [79, 80]. As an example, the nickel manganese cobalt alloy in spherical shape can be used as a lithium nest, to produce capacities in the range of 164 mAh/g and voltages in the range of 2.8 to 4.3V. This can be an acceptable material for high voltage applications, but the capacity is moderate. In addition the fabrication costs are higher compared to regular conventional lithium salts [77]. $LiFePO_4$ is another candidate for high capacity lithium ion batteries. The capacity of this material is limited to 170 mAh/g which is 20-25% higher than conventional lithium salts. Although this material has durability, the voltage plateau is limited to 3.4 volts. Another challenge in using this material is the fabrication steps. Complex synthesis is one of the main limiting factors of using this lithium salt in conventional lithium ion batteries. In addition, the oxidation states also must be done in controled temperature to prevent chemical changes. In this case a simpler fabrication method is needed to make high capacity active material suitable for commercial applications. $LiMn_2O_4$ is another active material for lithium ion batteries. This material is in form of nano spinel and crystals and can provide capacities up to 150 mAh/g. This material can produce high voltages in range of 3.5-4.3 volts and in spinel form the capacity fade is also limited so can be cycled up to 200 cycles. In addition to the high capacity and durability the fabrication is easier compared to other nanomaterials for lithium

ion batteries. The only limiting factor of using this material is its high sensitivity to high C rate charge/discharge cycles. Here, the voltage plateau of the cell drops and the capacity becomes lower by 30% which makes it not suitable for high current applications or using with fast chargers.

The materials discussed can provide the necessary capacity and cycle life for flexible lithium ion batteries, although their theoretical capacity is still not sufficient enough for the needs of next generation electronic devices and high power applications such as portable devices and electric cars. To achieve higher specific capacity/energy, new ultra-high capacity lithium salts are needed. In this case, vanadium oxides are good candidates to be used as the lithium ion cathode active materials due to their multi-valence change during the charge/discharge process providing high capacities [16]. Vanadium is also a very accessible and cheap metal and can be found and developed. In addition, the oxide or the sol-gel of this material can be used as an active material for lithium ion batteries while they are producing nests for lithium ions in their crystal structure. This structure is shown in Figure 2-3 [81].

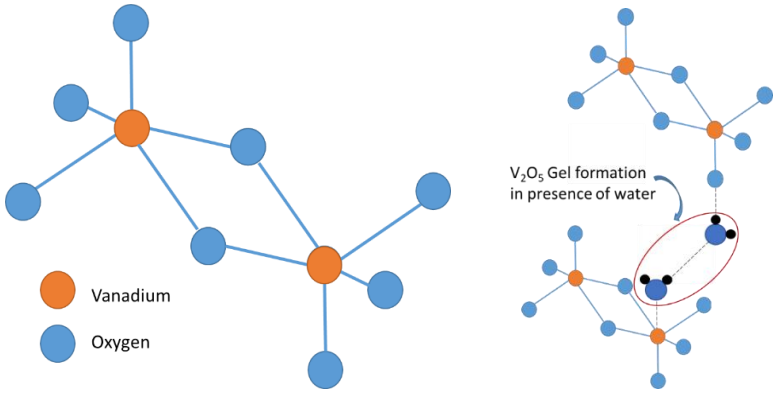

Figure 2-3 Vanadium Pentoxide chemical structure and gel formation

Vanadium pentoxide (V_2O_5) can intercalate with three lithium ions and provides a voltage plateau of 2.75 V. The theoretical capacity of 443 mAh/g and specific energy of 1218 Wh/kg can be achieved using this material. The challenges for realizing a high specific capacity/energy in practical LIB applications [82-88] lies in these three issues: (1) low electron conductivity of V_2O_5 nanoribbons, (2) slow lithium-ion diffusion rate due to the crystal structures, and (3) irreversible phase transitions upon deep discharging of V_2O_5. Recently, we have developed a nanostructured hybrid V_2O_5 material by adding graphene (1-2 wt.%) to incorporate a layer of this material between

V_2O_5 nanoribbons [89]. Such a developed V_2O_5/graphene (V_2O_5/G) hybrid nanostructure solved the issues, mentioned before by (1) providing the intra-electronic conductive paths between the V_2O_5 nanoribbons, (2) enhancing the lithium ion diffusion by having smaller V_2O_5 nanoribbons, and (3) improving integrity of the vanadium structure due to the graphene sheets which can hold the V_2O_5 nanoribbons. This hybrid V_2O_5/G structure exhibits the high cycleability and rate performance while achieving the actual vanadium pentoxide theoretical capacity.

2.7 Solid Gel Electrolytes

The use of liquid electrolyte in flexible lithium ion batteries is still the main challenge. This is a limiting factor of making many flexible batteries such as paper-based batteries due to the safety issues and capacity fade [60]. Solid electrolytes can be made in the form of polymer and ceramic-based materials [90, 91].The limiting factors of liquid or ceramic electrolytes led to the fabrication of gel electrolyte for flexible battery applications. These electrolytes can provide high ionic conductivities up to 10^{-3} S/cm or high at room temperature with a wide potential window without any side reactions. In addition, gel electrolytes have high thermal stability and mechanical properties.

The main goal of this work is to create a highly ionic conductive polymer gel electrolyte structure by mixing polymer and ceramic electrolytes for paper-based applications. Polymer gel electrolytes have presented the potential of being mechanically flexible, durable, safe, light-weight, and long-lasting [92]. Polymers such as PVDF-HFP, thermoplastic polyurethane (TPU) and polyethylene oxide (PEO) have been previously reported to be used as the solid electrolytes due to their high ionic conductivity and stability a lithium ion environment [93-96].

Early solid batteries were made of the PEO separator films as the host polymer for ionic conduction. The amorphous phase of PEO is the main conductive region for ionic conduction. Having a more crystalline PEO structure reduces the ionic conduction, and this is the main limiting factor of using PEO as the solid electrolyte. The temperature is also effective for ionic conductivity of PEO while the chemical structure of this polymer changes by temperature. PEO is mostly in crystalline form in room temperature, and it has a structure that is more amorphous in higher temperatures. To form an amorphous structure, fillers are added to the PEO structure. Silicon oxide and titanium oxide

are some candidates to make amorphous PEO [97]. Polyurethane is another candidate to be used as a solid electrolyte. There were many reports about using polyurethane to make ionic conductive films [96]. Polyurethane can provide a high mobility ion exchange membrane due to the high solving ratio and mobility of the charged carriers. The polymer matrix can absorb ionic liquids and form a gel-like structure. To also increase the mechanical strength of polyurethane other blends like PEO or PEG added to the polymer. The TPU matrix can absorb most of the lithium ionic solution such as LiTFSI or $LiClO_4$. The LiTFSI is one of the best candidates to make a very good gel electrolyte in conjunction with TPU [98, 99]. This lithium salt has high stability and a large working voltage window. The TPU can also absorb many organic solvents, but finding a stable solvent is still a challenge. While the flexible gel electrolyte is required to make a paper-based solid cell, the TPU gel also might be stable in conjunction with water or air [100].

Solid-state lithium ion batteries using polymer-gel electrolytes have been recently reported as a successful pathway to achieve flexible batteries, due to their high safety, and stability toward bending. However, the development of solid-state batteries is still in a primary stage due to the low ionic conductivity of the polymer gel electrolyte (in the range of 10^{-6} to 10^{-3} S/cm). Recently, higher ionic conductive gel-polymer electrolytes have been developed to overcome the issues of solid electrolytes for lithium ion batteries [101, 102]. Dual-ion batteries (DIB) are one of the newly designed batteries, using gel electrolytes. This type of battery is an interesting option because of their high working voltage, low cost being environmentally friendly. For DIB, both anode and cathode are involved in charging/discharging process, which is different from traditional LIBs that are based on a single lithium ion reaction process. A big problem with DIB batteries is their poor cyclic stability due to carbon electrolyte decomposition. Several methods have been utilized to counteract this issue, but it is still not enough. A method was devised to counteract this issue by making a DIB battery on a copolymer via weak hydrogen bonds. PVDF-HPF have high conductivity and mechanical stability for the polymer matrix for gel polymer electrolyte. Having a mixture of PVDF-HFP with PEO will improve connectivity between the pores, porosity and porosity. Adding graphene oxide to this membrane will also improve the mechanical and thermal properties. Here, 5% wt PEO and 1% GO will be used in the PVDF-HFP matrix. This, in turn, will develop a 3D porous network which will improve the ionic conductivity and cyclic stability.

Here, ionic conductivity reached to a value of 2.1 KS/cm with 1% GO in comparison to a liquid electrolyte. It was due to the presence of an oxygen termination on the GO flakes, which can interrelate with the polymers such as PVDF-HFP and PEO to make a highly amorphous porous structure. Thus, high ionic conductivity can be achieved by using this membrane with liPF_6 -based electrolytes due to its PF_6 intercalation kinetics. Excessive amounts of GO will affect the properties previously mentioned. For comparison, it was compared to PVDF-HPF. It showed good capacity while the PVDF-HDF showed a decay. It maintained high capacity retention of 92% after 200 cycles while the latter dropped quickly after 630 cycles. No changes in morphology were observed, indicating as well as good structural stability [35, 102].

EMIMDCA ionic liquid polymer electrolyte was another attempt to make flexible leak-proof electrolyte. In this material, the weight ratios of the gel electrolyte components consist of 30% PVDF-HDF, 60% EMIMDCA (ionic liquid) and 10% $LiCLO_4$ (salt). $LiClO_4$ salt has been used mainly because of the stability, better tolerance to moisture, and lower cost. Maintaining adequate contact between the layers is essential for developing a high-performance flexible lithium ion battery. It was tested in bent and flat positions and for 200 cycles it can deliver 300 $\mu Ah/cm^2$ for 20 cycles in a flat position. In a bent position, the resistance observed dropped. However, the performance dropped, possibly due to impurities, moisture penetration, among other things. It can generate 2.1 V and it is a safe battery that can be built upon [103].

The ionic conductivity of a PVDF-HFP alkali salt composite, and PVDF-HFP polymer gel made by soaking in and ionic solution was reported to be in the range of 10^{-3} S cm^{-1} [104-106]. Infusing an alkali salt in a cross-linking polymer results in a formation of an ionic conductive membrane. While, the PVDF-HFP is a polar polymer and has a semi-crystalline structure with amorphous domains with high porosity, it can absorb the ionic solutions and alkali salts to transport free ions [107]. The porous structure in PVDF-HFP films is the place that gel formation happens, so here adding a plasticizer such as represents a simple method of preventing over crosslinking and improving porosity. In the presented work, LATP and LiTFSI alkali salts, in form of crystal and ionic solution in ethylene carbonate (EC) and diethyl carbonate (DEC) respectively, have been added to the PVDF-HFP membranes, to provide gel polymer electrolytes ionic conductivity, high working voltage window (up to 4 V), and lithium ion reaction stability [108-110]. It has also been

shown that the creation of porous structures in electrolyte membranes increases ionic liquid uptake, thereby increasing the ionic conductivity [110]. Here, a highly porous PVDF-HFP gel electrolyte with the combination of ceramic and polymer electrolyte has been developed to provide maximum ionic conductivity for flexible battery applications.

2.8 Integration of Paper-Based Battery with other Paper-Based Electronics

The paper-based flexible substrate can also be used as a base for other electronic devices. As an example, this paper-structure can be used to make sensors due to its high surface area, and absorption. The paper-based devices are chipper than the solid-state sensors while the fabrication is easier and less costly. In addition, paper can provide flexibility, and being disposable for electronic devices. These devices can be integrated into other paper-based applications like cards, boxes and packaging materials. This approach can be used to make devices such as RFID tags, displays, sensors, electroluminescence devices, and solar cells [111-113]. Different sensors have been developed over the paper using carbon nanotube to measure different parameters such as humidity, pressure, biomarkers, and different gases [113]. As it was reported by Han et al., CNT can be used to make paper-based humidity sensors. In this case, the single wall CNT was used to make resistor type, humidity sensors. In their approach, the CNT deposited over the filter paper to provide a conductive layer over the fiber. Then another layer of CNT-COOH is added to increase the sensitivity of the device while carboxylic acid (COOH) group is hydrophilic, adding this layer can increase the response of the sensor to humidity. The CNT will react with H_2O atoms while a voltage is applied. The voltage makes H+ and OH- ions over the paper and changes the electron movement side the CNT layer [113, 114]. In this case, the conductance decreases by increasing the humidity up to 75%. Another CNT based sensor is made by depositing CNT over Fe coated alumina substrate. The CNT has a thickness of 10 microns and can detect gases such as CO_2 (0.2%), CH_4 (0.7%), H_2 (1%), NH_3 (0.1%), CO (0.1%) and NO_2 (10ppm) [114]. The presented resistive sensors can detect gases, but the response of the sensor is not significant. In this case, to increase the selectivity and response, CNT rods in this project were also decorated with different metal nanoparticles such as Ag, Ru, and Pt. This can increase the conductivity of the CNT rods and improve the sensitivity of the fabricated sensors [114]. Although adding metallic particles to CNT can increase the sensitivity, the fabrication cost and complexity also increases. Having functionalized CNT is a better approach while it can reduce the complexity of the sensor and

improve the selectivity. As it was reported by Kong et al, the electron withdrawing or electron donating molecules like (NO2 or NH3) can affect the charge transfer in carbon nanotubes. While CNT has a semiconducting property, adding these molecules can make it more conductive and it can increase the sensitivity of the CNT-based sensors. While adding metallic nanoparticles to the CNT rods can increase the sensitivity of the sensors to gases like hydrogen and carbon monoxide, the functionalized groups can increase the sensitivity and reduce the memory effect of the sensors to detect gases like carbon dioxide and nitrogen oxides [115].

Among the reported gases that were detected by CNT, CO_2 is one of the desired gases. While the paper-based devices can be used in packaging, detecting CO_2 and NO_2 can be helpful to identify the opening of the package and the freshness of the products. CNT is used to detect CO_2 and NO_2 in resistive and transistor based devices [116, 117]. While the paper-based system does not have enough space to have a logic section, the resistive sensor is the better option. As it was reported by Kuffman et al, CNT used to identify NO_2. The CNT can detect NO_2 in the range of 1 to 1000 ppm. CNT can also be used to detect CO_2. CNT at levels above 5% becomes toxic for humans. In this case CNT can be used to detect CO_2 in different temperatures and concentrations. Recent development also shows that the CNT-SiO_2 compound can detect CO_2 in the range of 0 to 100% [118]. The only problem of detecting gases with CNT is the lack of selectivity. The CNT based sensors response of many gases and is shard to identify the source of the changes in resistance of the CNT in presence of different gases.

The cellulose fibers are highly attractive for sensor applications due to their high hydrophilic structure. The hydrophilic structure of the paper can also improve the sensitivity by eliminating the need of external sources like pumps. Furthermore, the lower fabrication costs and high versatility of the paper-based sensors are other benefits of using these devices. The paper-based sensors are a very good candidate for portable and flexible sensors applications such as medical, packaging, and environmental devices. Electrical conductivity change in presence of a chemical compound is a simple and low power method of sensing. Using conductive paper with other chemical materials, the paper-based sensors can be made. Meanwhile the paper can be used as a base for gas sensors, nanomaterials can be used in conjunction with the paper structure to make very sensitive detectors. The high surface to volume ratio of the nanomaterials is the advantage of

using them to make gas sensor. This property of the nanomaterials can increase the sensitivity of the sensor, makes it ideal for gas molecules adsorption and storage. Among the nanomaterials, CNT is one of the options that can be used as a sensing material [119].While CNT is applied to the paper-structure to form the CNT-microfiber paper, this approach can also be used to make paper-based sensors. As it was mentioned above, CNT is a good candidate for making these paper-based sensors due to its high conductivity and reaction to certain elements. The paper-based sensors can be made by CNT-microfiber paper to provide a durable and cost-effective method for gas sensing. The electrical properties of the CNT rods can be changed when they are exposed to different chemicals. This can change the doping of the CNT and change the charge transfer characteristic of the CNT rods. This property of the CNT can be used to develop gas sensors. In addition, adding functionalized groups to CNT rods can increase the gas sensitivity of the rods by improving the chemical sensitivity and reversibility. The plain CNT has not enough sensitivity due to the low adsorption energy and electron affinity [120].

2.9 Theoretical Analysis

Nowadays, most of the research in lithium ion batteries is based on the experiments but there is also a need for theoretical analyses to check the feasibility and to design the optimum research plan. In this case the lithium ion redux reactions are the basics of the calculations to derive the charge and discharge voltage levels, current densities and predict the possible capacity. Further this analysis can provide the voltage level for the electrolyte helping to find the efficient electrode/electrolyte systems for lithium ion batteries. In addition, the safety and durability of the cells can be determined. Energy balance equation can be used to determine the ion concentrations and capacity of the batteries. Knowing the diffusion rate and particle concentration can also be used in conjunction with ohms low to identify the current densities of the batteries. Further, the thermal analysis can also be done to check the stability of the cell. One of the challenges in making batteries is overheating and thermal runaway, so to address this issue its desired to use proper modeling before developing a cell to check the stability of the electrodes, and the heat dissipation.

In each cycle, a redox reaction as it is shown in Figure 2-4, happens in lithium ion cells. In each charge cycle the lithium ion leaves the cathode active material, while electrons leave the cathode from the outer circuit. The free ions pass the electrolyte and stabilized in anode active layer. In a

discharge, ions move back to cathode side. In oxidation, the lithium active material breaks generate free lithium ions and extra electrons. The free ions pass through the separator using electrolyte and reach to the other electrode using the electric field. Free lithium ions react with electrons and stabilized inside the crystal structure by a reduction process [7]. The total electrochemical reaction can be summarized as a redox reaction as it is shown in equations 1 to 3. Here the Li+ is the free lithium ions and *n* is the number of generated or used electrons in the redox reactions.

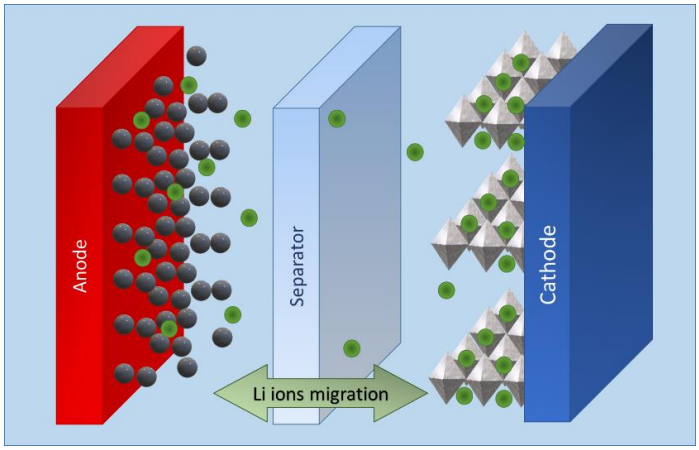

Figure 2-4 Lithium migration due to redux reaction inside a lithium ion battery

$$Li\ X \rightarrow Li_{-n}X + nLi^{+} + ne^{-}\ (oxidation) \quad (2\text{-}1)$$

$$Li_{-n}Y + nLi^{+} + ne^{-} \rightarrow LiY\ (reduction) \quad (2\text{-}2)$$

$$Li\ X \rightarrow Li_{-n}X + nLi^{+} + ne^{-} + Li_{-n}Y \rightarrow LiY\ (redox) \quad (2\text{-}3)$$

This electrochemical reaction always generates voltage, current density and heat. By having these parameters, a lithium ion battery can be simulated.

The energy balance equation is the fundamental equation to simulate any lithium ion battery [121, 122]. The heat generated in electrochemical reaction is the driving force of the ion migration and provides free ions to move. From energy balance the ion concentration (C) can be calculated based on irreversible and reversible heat generated in the cell [123]. Equation 2-4 is the general equation that can be used to determine the ion concentrations based on the change in temperature inside the battery and reversible and irreversible heat (Qr_{ev} and Q_{irv}) inside the cell. Here the reversible heat

is generated by change in potential inside the cell as it is shown in equation 2-5. The reversible heat (equation 2-6) is made of the both ohmic and reaction heats, related to the thermal changes inside the cell which is mostly related to the electron transport and chemical reactions.

$$\rho C \frac{\partial T}{\partial t} = k \frac{\partial^2 T}{\partial x^2} + Q_{rev} + Q_{irv} \tag{2-4}$$

$$Q_{rev} = -ajT \frac{\partial \mathrm{U}}{\partial t} \tag{2-5}$$

$$Q_{irv} = Q_{ohmic} + Q_{reaction} \tag{2-6}$$

$$Q_{reaction} = aj(\Phi_{1i} - \Phi_{2i} - U) \tag{2-7}$$

$$Q_{ohmic} = a_+ \frac{\nabla \Phi_+{}^2}{R_+} + a_- \frac{\nabla \Phi_+{}^2}{R_-} \tag{2-8}$$

Here the a is area of positive and negative electrodes, Φ is charge, U is open circuit voltage of cell, T is temperature in kelvins and R is resistance.

The mathematical model of a lithium ion movement inside the battery can be designed using Fick's second law. Here the concentration of the ions can be determined in spherical coordinates using the radius of particle and diffusion coefficient of ions. In undersection flow with no steady state condition it will be written as equation 2-9. When there is no drift force, Ions always move form high concentration to low concentration. In this case by considering the atoms of lithium salts as the lithium ion nests in 1D, the change of the ion concentration for each atom versus time (rate of change) is related to the diffusion coeffect of the material and the change of ions around the core of that material [124, 125]. Here the one-dimensional model has been obtained based on a constant diffusion coefficient and the accusation of change of ion concentration versus distance from the core.

$$\frac{\partial C_s}{\partial t} = -D\left(\frac{\partial^2 C_s}{\partial x^2}\right) \tag{2-9}$$

Here C is the concentration and D is diffusion coefficient. Considering the atoms of materials in lithium ion batteries are spherical it can be also written as equation 2-10 [122].This is a spherical model based on the spherical dimensions of atoms derived from equation 2-9.

$$\frac{\partial C_s}{\partial t} = -D\frac{1}{r^2}\left(\frac{\partial}{\partial r}\ (r^2\frac{\partial C_s}{\partial r})\right) \tag{2-10}$$

In this case r is the distance of the ion from the center of particles as it is shown in Figure 2-5 a. To solve the differential equation the boundary conditions also needs to be considered. At the core of particle, the diffusion is zero and at the surface of the particles the initial condition will be defined by equation 2-11.

$$-D\left(\frac{\partial C_s}{\partial x}\right) = J_r \tag{2-11}$$

Where J_r is the diffusion flux of ions and radius is the distance between the core surfaces of the particle. The diffusion coefficient D also can be calculated using multiplication of diffusivity of salt times porosity of electrolyte. This number for lithium hexafluorophosphate can be calculated as it was reported previously [126]. In that case, we consider the battery as a one-dimensional system as it is shown in the following Figure. Here, as shown below in Figure 2-5 b, the boundary conditions are both zero while the ions will not leave the material.

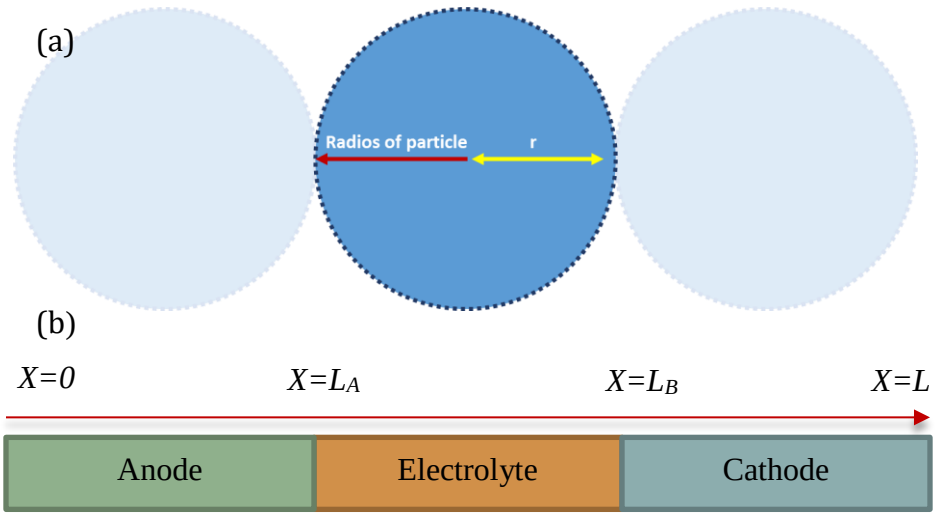

Figure 2-5 (a) Particle modeling using 1-dimensional circular coordination and (b) 1-dimensional model of lithium ion battery

$$C = -D\left(\frac{\partial C_s}{\partial x}\right)_{x=0} = -D\left(\frac{\partial C_s}{\partial x}\right)_{x=l} = 0\,, C_{LA+} = C_{LA-}, C_{LB+} = C_{LB+} \tag{2-12}$$

In this case the conductivity also can be found by ohms law, while the i_s=$I_{applied}$ at x=0 and there is no current at points x=L_A and L_B. Thus, the current passes inside the cell is defined by the change of the electric potential ($\frac{\partial \Phi}{\partial x}$) and conductivity of the electrolyte (σ_{eff}) based on the ohms law.

$$i_s = -\sigma_{eff}\frac{\partial \Phi}{\partial x} \tag{2-13}$$

While we used a liquid electrolyte, the charge balance can be derived based on Ohm's law [123] so do to the conservation of current and mass the ion concentration can be identified. The charge balanced can be determined by ohms law shown in equation 2-14 can be used in this case, to determine the charge transfer inside the gel electrolytes using the change of electric field inside the cell structure. This model is based on the change of potential ($\frac{\partial \Phi}{\partial x}$) , and change of charge concentration ($\frac{\partial \ln C}{\partial x}$) inside the cell to generate the ion transport and *t* is the transport number. In this equation *F* is the Faraday constant, *J* is the charge density and *a* is the area. This equation can be modified in format of equation 2-15 to determine the current of the cell. In this case the change of current inside the cell is considered to be constant and because of that the change of current between electrodes is the actual current generated inside the cell. This equation can also be used to determine the actual current generated by having the activity coefficient of lithium salts (*f*). The modified equation 2-15 considering the ∂x as length of the active region of battery, has been used to find the current generated throughout the length of the battery.

$$-\frac{\partial}{\partial x}\left(k_{eff}\frac{\partial \Phi}{\partial x}\right) + \frac{2RT(1-t_+)}{F}\frac{\partial}{\partial x}\left(k_{eff}\frac{\partial \ln C}{\partial x}\right) = aFJ \tag{2-14}$$

$$\left(-k_{eff}\frac{\partial \Phi}{\partial x}\right) + \frac{2kRT(1-t_+)}{F}\left(1+\frac{\partial \ln f}{\partial \ln C}\right)\frac{\partial \ln C}{\partial x} = i \tag{2-15}$$

Here the k is ionic conductivity, T is temperature R is gas constant of 8.3145 J/mol K and F is Faraday constant of 96487 C/eq. Using this result in Butler-Volmer equation the total flux then can be determined, and it will be replaced in the energy balance for next iteration. This equation

(2-16) is based on the charge transfer in electrochemical reactions [122]. Thus, the electric charge transfer and ion transport inside the lithium ion cells can be modeled with that. This model in conjunction with ohms low can predict the state of charge and capacity of the cell. In this case while the ion concentration of electrodes will be changed in electrochemical reactions, to have the exact voltage level and current density of the cells, the change of the ion concentrations must be determined and then used to calculate the total charge transfer and capacity of batteries, throughout the time for both charge and discharge process [122]. As it is shown in equation 2-17 the parameters for equation 2-16 can be determine using charge concentration and initial current of cell. Here, the η is the difference between initial difference in voltage levels of cathode and anode (Φ_{1i} and Φ_{2i}) and the equilibrium potential of cell (U_i).

$$i = i_0(\exp\left(\frac{a_n F \eta_i}{RT}\right) - \exp\left(-\frac{a_c F \eta_i}{RT}\right)) \tag{2-16}$$

$$a = 0.5\,, i_0 = k\left(C_{i\,max} - C_{i\,surf}\right)^{0.5} C_{i\,surf}^{0.5} C_i^{0.5}, \tag{2-17}$$

$$\eta = \Phi_{1i} - \Phi_{2i} - U_i \tag{2-18}$$

The internal resistance of the batteries can also be model by Warburg model [127]. In this model the total capacity of the cell is the number of charges that will move between anode and cathode in each cycle. In this model the state of charge (SOC) can be defined using equation 2-20 as which z is the derivative of impedance over time and q is the charge (equation 2-19) [128, 129]. Efficiency which is the assumed percentage of charge or discharge is also considered in the following formula as ρ.

$$z = -\frac{i(t)}{Q} \tag{2-19}$$

$$SOC = \frac{dz}{dt} = -\frac{i(t)}{Q}\rho \tag{2-20}$$

Where z is the SOC, Q is capacity and i is current. Beside that the diffusion of ions inside the cell generated a voltage which can be calculated form ohm law by having the resistance of the cell. In

this case measuring the voltage and current of the cell can show the impedance of cell. In addition, while the electrochemical reactions provide capacitance, like polarization, the total impedance of the cell must be considered. Figure 2-6 shows schematics of an ideal lithium cell model by Warburg method.

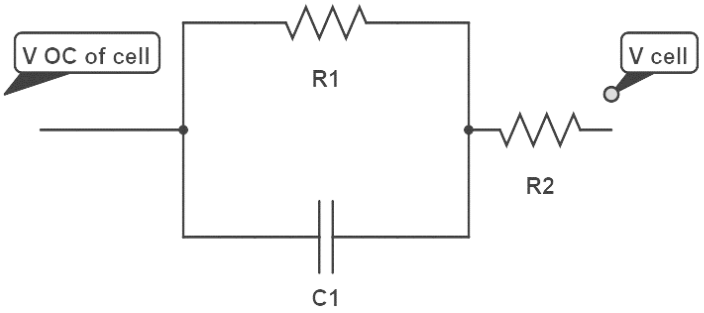

Figure 2-6 Schematic of internal impedance of a lithium ion battery based on Warburg model

Here the voltage of the cell can be modeled using R_1 as electrolyte resistance, R_2 as the charge transfer resistance, and C_1 as the capacitance between the electrode surface and the electrolyte as it is shown in equation 2-21 to 2-23.

$$v(t) = V_{oc} - i_{R1}(t)(R_1) - i(t)R_2 \tag{2-21}$$

$$i_{R1}(t) + d\frac{C_1 v_{C1}}{dt} = i(t) \tag{2-22}$$

$$\frac{di_{R1}}{dt} = -\frac{1}{R_1 C_1} i_{R1}(t) + \frac{1}{R_1 C_1} i(t) \tag{2-23}$$

Using this model [129], by changing the frequency of applied current, the impedance of the cell can be determined. Detailed results have been reported in Chapter 4 of this thesis. At very low frequency, the capacitance is acting as an open circuit, so the total impedance of the cell can be determined, while at very high frequency, the capacitor acts as a short circuit, such that R_2, which is the charge transfer resistance and related to electrode material, can be determined.

CHAPTER 3. RESEARCH METHODOLOGY

3.1 CNT-Microfiber Paper

The CNT-microfiber paper has been made by wood microfibers, individually coated with conductive nano materials such as CNT through a layer-by-layer (LbL) nanoassembly process, described in detail elsewhere [45, 60]. The LbL nanoassembly technique allows the formation of a multilayer coating at with nanoscale thicknesses around the fibers, by deposition of oppositely charged nano materials and polymers. To begin, an aqueous dispersion of each material has been made. Here, the poly(3,4-ethylenedioxythiophene)-poly(styrenesulfonate) (PEDOT-PSS) as a conductive polymer (3 mg ml^{-1}) and carbon nanotubes (25 μg ml^{-1}) as a conductive nanomaterial has been used as the anionic solutions. The poly-(ethyleneimine) (PEI) (3 mg ml^{-1}) was also used as a cationic solution to make alternate positive and negative nanolayers around the fiber surface. Thus, covering the surface of microfibers with bi-layers of PEI/CNT and PEI/PEDOT-PSS leads to provide a conductive shell around the fibers. The formation of layers using LbL has been demonstrated in Figure 3-1. Following the LbL process, the coated wood microfibers were assembled into standalone sheets (CNT-microfiber paper) and used as current collectors in lithium ion batteries. While the surface of the fibers is negatively charged, two positively (PEI) and negatively charged (PSS, PEDOT-PSS, and CNT) aquatic solutions have been made and deposited over the fibers. Thus, fibers first were soaked in PEI and then PSS solution twice followed by proper washing and rinsing to make a double layer buffer layer. Due to the zeta potential of solutions the materials will be deposited over the fiber structure. These initial layers help to form a uniformly charged surface for the deposition of highly conductive materials. Later, fibers were soaked in PEI and PEDOT-PSS and CNT solutions alternatively to make form a conductive layer around the microfibers. In this method particles stick to the surface and the next layer is stabilized using the alternate charge of the previous layer around the fibers. A proper washing after deposition of each step is needed to remove the residues and prevent non-uniform formation of layers. CNT-microfiber paper provides conductivity to the paper sheets while preserving the original properties of the paper, such as flexibility and porous structure, while limits the CNT utilization to 0.2% by weight [45, 60].

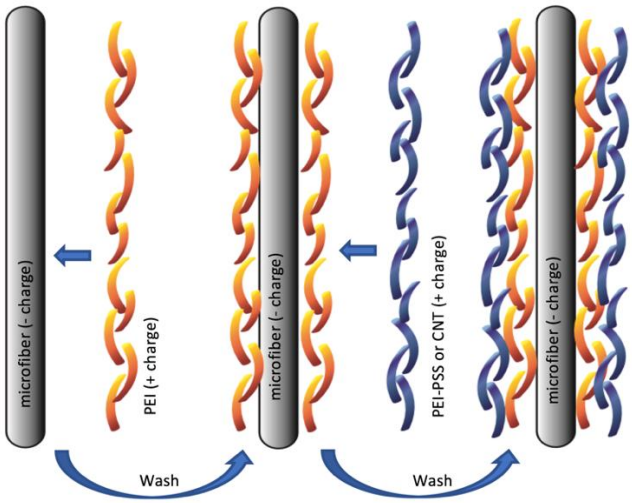

Figure 3-1 Schematic of the LbL process of depositing oppositely charged polyelectrolytes to coat paper microfibers

The fabricated sheets from coated fibers are made by a homemade setup (meeting the standard of Technical Association of Pulp and Paper (TAAPI) T 205T) and dried overnight in a 80 ˚C oven to be used as the current collector. The conductivity of the CNT-microfiber paper was measured using a Keithley 4200 IV probing station (Tektronix USA) and the formation of CNT over the fibers was investigated by using Emission Scanning Electron Microscope (FESEM) (JEOL, Japan) and X-Ray Diffraction (XRD) (Bruker USA).

3.2 Reduced Graphene Microfiber Paper

3.2.1 Graphene oxide

Graphene oxide (GO) was prepared using pre-oxidized graphite [130]. In this process, 2 g of graphite was allowed mixed with 1 g of sodium nitrate and 46 mL of sulfuric acid for 30 minutes, before adding 6 g of Potassium permanganate. This was mixed for 3 hours at 35 ˚C. Next, 100 mL of Milli-Q water was added and the mixture was brought 100 ˚C. A solution of water:hydrogen peroxide (15:1 wt) was used to dilute the hot mixture, which was then removed from heat. Nanoparticle samples were washed using a centrifuge (Thermo Legend X1) at 10000 rpm for 20 minutes. The supernatant was then removed and the graphene at the bottom was redistributed in fresh deionized water. This washing process was continued until the solution reached a pH of 7.

Next, the solution was sonicated using a bath sonicator to provide a uniform dispersion of GO flakes in the water. All the chemicals have been supplied by Sigma-Aldrich.

3.2.2 Graphene microfiber paper

The graphene microfiber paper has been made using bleached Kraft softwood microfibers (99% cellulose, 1% lignin) (Bastrop, Louisiana). The microfibers were soaked in aqueous dispersions of while poly(ethyleneimine) (PEI) (3 mg/mL) and graphene oxide (250 μg/ml) alternatively followed by washes in Milli-Q water for the LbL coating of the layers. The microfibers were coated with 2 bilayers of PEI/GO. The thickness of the deposited layers has been measured using a quartz crystal microbalance (QCM, 9 MHz, USI-System, Japan). In addition, the quality of the fibers was examined using Emission Scanning Electron Microscope (FESEM) (JEOL, Japan) images. The fabricated fibers were washed with Milli-Q water to remove residues from the LbL process. The washed microfibers then were mixed with dimethylacetamide (DMAc) (100mg/ml) and reduced using microwave digestion system (MDS2000) in 630 watts for 5 minutes under an inert gas such as nitrogen. The reduced GO microfiber then was collected and washed again to remove excess solvents. The microfibers were then formed into a single sheet of a graphene microfiber paper using an in-house setup based on the Technical Association of Pulp and Paper (TAAPI) T 205 T standard. The formation of graphene was identified using Raman Spectroscopy and X-ray Diffraction using and Discover X-Ray Diffraction (XRD) (Bruker, USA) respectively.

3.3 Solid and Polymer Gel Electrolytes

3.3.1 PEO Films

PEO was mixed with acetonitrile with a ratio of 10% wt. The polymer mixture was stirred overnight to form a uniform solution. The LiTFSI and $LiCLO_4$ lithium salts then were added to the solution and stirred for another 6 hours. The mix then casted using doctor blade coating method and dried inside the glovebox. The films made with this technique were used as the solid electrolyte inside the cells [131-133]. To check the quality of these films, the samples have been made and hot-pressed between LTO/LCO electrodes and tested.

3.3.2 PVDF Gels

PVDF- gels have been made by fabrication of PVDF membranes as the main part of gel electrolyte. PVDF and PVDF-HFP has been added to the N-Methyl-2-pyrrolidone (NMP) with ratios of 2 to 10% and mixed overnight. The solution then casted with different thicknesses from 10 to 200 microns and dried the quality, mechanical stability, porosity and structure of the films then have been tested.

3.3.3 LATP/LiTFSI Electrolyte in Gels

PVDF-HFP, glycerol, and NMP solution was made by adding 2-5% LATP (by weight of PVDF-HFP) and mixed overnight in normal atmospheric conditions to form a uniform solution. Lather the solution was casted to make a PVDF-HFP/LATP polymer gel membranes followed by a drying process in air and controlled moisture environment. After setting up, the membranes also dried in a vacuum oven at 50°C. The fully dried polymer membranes were soaked ionic solution such as LiTFSI liquid electrolyte to form polymer gel electrolyte. The LiTFSI solution is made by mixing one mole of LiTFSI in 1 liter of a 1:1 volume ratio solution of EC:DEC or TEGDME. The membranes then dried and stored in an argon filled glove box. All procedures for membrane fabrication were conducted at room temperature unless noted otherwise [45, 60, 134, 135] .

3.4 Paper-Based Battery

3.4.1 LTO/LCO Electrodes

To make electrodes, LTO, and LCO active materials (Sigma Aldrich) mixed with carbon Black KS6 and super P lithium (Timcal) and PVDF-HFP and dissolved in NMP to form a thick solution. Here, the PVDF-HFP is the binder and carbon black is the highly electric conductive material. The electrode active material solutions then were deposited over the paper-based or metallic current collectors, using a spraying method followed by a drying process in a vacuum oven overnight. The thickness of the active material for each electrode was reached to 25 microns after the deposition of five to six layers and the mass loading for active materials (LTO and LCO) were 8-9 mg/cm^2.

Two types of current collectors have been investigated for this part. The conventional metallic (aluminum and copper) and the flexible CNT-microfiber paper have been used. The CNT-

microfiber paper current collector is highly conductive, has porous structures, and shows more flexibility compared to the metallic current collectors. Figure 2-1 also reveals the simple assembly with of a flexible paper-based battery made out of CNT-microfiber current collector. In this setup the anode and cathode are on top and bottom while the middle layer is a gel electrolyte. The LATP/LiTFSI gel electrolytes have been chosen to be used as a highly ionic conductive and flexible gel electrolyte for flexible batteries. The left inset of the Figure 2-1 also shows a cross section representation of a paper-based electrode with CNT-microfiber and the right inset represents a schematic of PVDF-HFP polymer gel electrolyte. The cells were made in the form of coin cell, pouch cell, laminated packages and PDMS casing. In addition to check the quality of the electrodes half cells also have been made and tested. All battery fabrication steps, as well as electrolytes encapsulation for impedance measurements, were conducted in an argon filled glovebox. In addition to the fabrication of the cells, the simulations have been conducted using COMSOL to check the capacity and thermal analysis of the fabricated cells.

3.4.2 Simulation of LTO/LCO Battery

The cells have been designed to check the safety and durability of the LTO/LCO system. The electrochemical model of the lithium ion reaction is based on the migration of lithium ion inside the gel electrolyte structure. Here the cell voltage, electrochemical reaction rate and conductivity of the electrolyte are depending on the temperature of the reaction. In this case in each iteration, the temperature of the cell can be used to determine other parameters and the simulation continues.

Many of the previously designed models were just on the 1D models or 1D/2D models. In 1D modeling, the temperature distribution inside the cell is considered to be negligible although using non-thermal conductive materials such as paper-based structures and lithium active martials in conjunction with polymer electrolyte has increased the need of having a 2D or 3D models to determine the exact temperature inside the cell. Further, 1D model cannot be used to determine the temperature of the large size electrodes and battery packages. Later a 1D/2D models were developed to overcome the limits of the 1D models to consider the heat difference between the electrodes. This model could provide better accuracy while it could determine the heat generated inside the cell although the accuracy was not enough.

In this case the model of the lithium ion battery is based on a 1D/3D model. While the electrochemistry can be done in a 1D model the 3D model can be developed for thermal analyses of the system. LTO, LCO, and graphene electrodes have been simulated. Figure 3-2 shows the schematic of modeling cells using a 1D/3D modeling. In 1D, cathode, anode and liquid electrolyte were considered while in 1D the current collectors and packaging also added. Table 3-1 shows the parameters and results of each part. In this case, the electrochemistry happens in nanoscale and a 1D model should be enough to simulate the reactions. In addition, the 3D model is needed to model the heat formation and eat fellow inside the battery cells. As it was mentioned, the heat generated in the cell can be used for ion movement inside the cell and this can lead to more electrochemical reactions so having the heat formed inside the cell, the capacity and voltage of the cell can be predicted precisely.

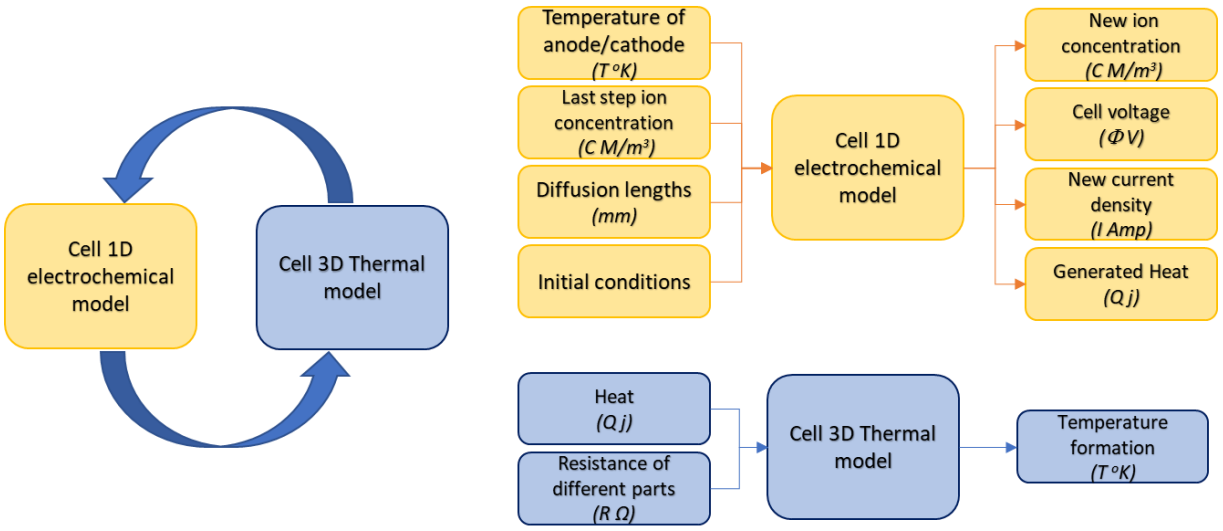

Figure 3-2 Coupling of the 1D model with the 3D model

Table 3-1 Simulation parameters for lithium ion modeling

	Takes	**Calculation Based of**	**Gives**
Cell Model, 1D	Average Temp, T	C_s = Concentration(mol/m3) of solid Electrode material φ_s = Electric Potential of the Electrode C_l = Concentration(mol/m3) of solid Electrolyte material Φ_l = Electric Potential of the Electrolyte	Average Heat Generated, Q_h
Thermal Model, 3D	Average Heat Generated, Q_h	T = Temperature of the cell at any given time. v = velocity of the flow air.	Average Temp, T

In this case, the electrodes first were developed with the actual size of 25mm×25mm×25µm. Not the whole weight or volume is the active materials in each electrode. As it was measured, almost 20% is conductive carbon materials and binder. This volume can be as low as 8% due to the shrinkage of the binder. This increases room for the electrolyte (as porosity) or more mass can be loaded. In addition to make the model more accurate, the porosity of the active material also was added. In real life, not all the lithium ions can be released in each charge and discharge cycles, while the electrolyte cannot reach all areas. In this case the porosity of the electrode is very important. In this case almost 40% of the active material is only accessible and this was considered in the model. Here for LTO or LCO electrodes size can be same but for LCO/graphene cells the dimensions were increased at least one millimeter from all side. In the case of the thickness, we would maintain the same, owing to the fact that the reaction rate (travel rate) of the Li^+ through the material thickness would be same on the positive as well as the negative side. Figure 3-3 shows the actual model made using electrodes and packaging for simulation. All the simulation is based on the mathematical multi-scale model, developed and simulated by COMSOL Multiphysics using electrochemistry and thermal modeling packages.

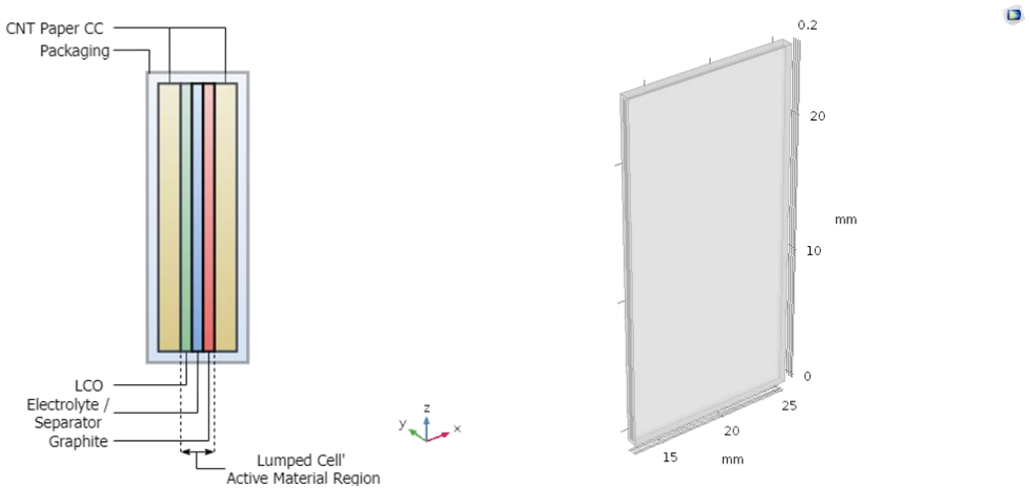

Figure 3-3 3D modeling of a lithium ion battery in pouch cell packaging

Further, the stacking of multiple layers inside the core of a pouch cell has been also tested. In real life, the cells are made by stacking multiple layers of electrodes and this can change the heat generation inside the cell and reduce the safety of fabricated cells. Figure 3-4 shows a design for a 10 layers cell system. Simulation and analysis based on the developed model have been reported in Chapter 4 of this thesis.

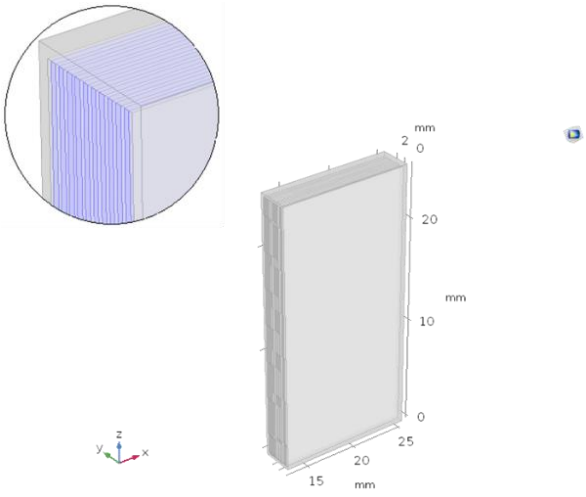

Figure 3-4 3D modeling of a 10 layers lithium ion battery in pouch cell packaging

3.4.3 V_2O_5/G Electrodes

V_2O_5/G was synthesized by the novel and simple method of incorporating graphene sheets into the nanostructure of V_2O_5 xerogel via a sol–gel process and forming a graphene-modified V_2O_5 hybrid with a stabilized layered structure. While the previously reported vanadium pentoxide materials did not provide enough cycle life, using xerogel can be a solution to achieve high capacity and high columbic efficiency while achieving higher cycle life for lithium ion batteries [28]. The vanadium pentoxide xyrogel has been made by ion exchange process of a 0.1 mol sodium metavanadate aqueous solution in polystyrene sulfonate resin (mesh size 100-200 microns). In this process the gel forms by removal of sodium atoms from the salt. The graphene oxide then was added to the xyrogel and rested for at least 15 days to achieve a uniform structure. Later the xyrogel was freeze-dried and baked in 500 °C in presence of nitrogen to make V_2O_5/G flakes.

To make the electrodes, the V_2O_5/G, Super P Li (TIMCAL), and PVDF (Kynar) were dissolved in NMP solvent with ratios of 85:10:5 by weight. The solution then sprayed over the paper-based and metallic current collectors to make electrodes. The active material mass loading for vanadium-based electrodes (V_2O_5/G) is 0.4 mg/cm^2. The fabricated electrodes were rested in a 90 °C vacuum oven overnight and later stored in an argon-filled glovebox. The pouch cells (electrode dimension: 3 cm by 5 cm, cell capacity: 2.4 mAh) and coin cells (electrode geometric area: 2 cm^2, cell capacity: 0.8 mAh) were made using half-cell configuration with lithium foil and V_2O_5/G electrodes. The Celgard 2400 film was also used as separators with only 90 µL of lithium phosphorous fluoride ($LiPF_6$) liquid electrolyte. The electrolyte is a 1.0 M $LiPF_6$ solution in ethylene carbonate/diethyl carbonate (EC/DEC) mixture (1:1 by volume). After making the cell, they were rested overnight to reach to achieve and stable state for testing. The fabricated devices were tested using an Arbin BT2000 battery testing system. The composition study and morphology of the electrodes made by the CNT-microfiber paper current collectors and the damages/deformations of the electrolyte layer after bending test were analyzed by JEOL 7800F Field Emission Scanning Electron Microscope (FESEM) (JEOL Japan) images.

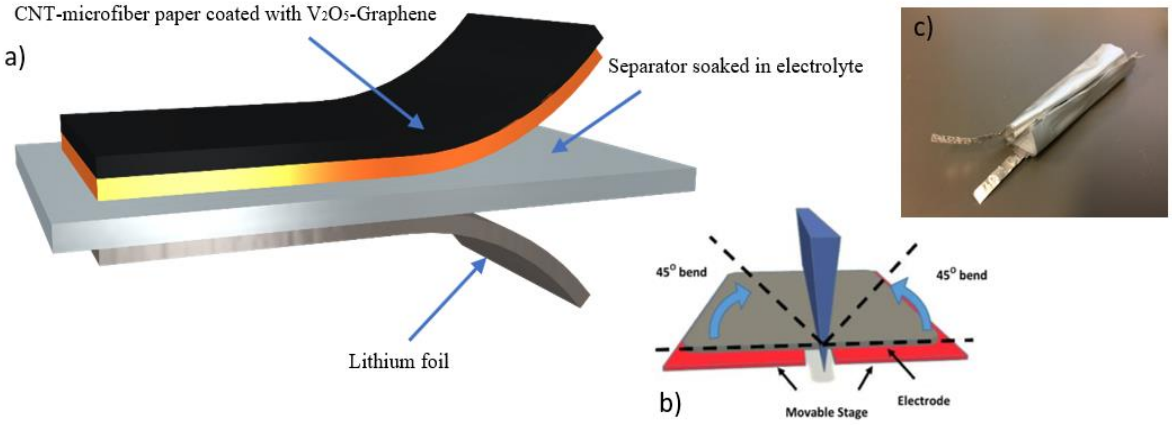

Figure 3-5 (a) Illustration of the paper-based V_2O_5/G battery layers, (b) the bending test set-up, and (c) a bendable pouch cell made by paper-based electrodes

3.4.4 Graphene cells

The fabricated graphene microfiber paper was dried in the vacuum oven overnight and then transferred to an argon-filled glovebox. The coin cells were made with lithium foil and a Celgard 2400 separator. A 1.0 M lithium phosphorous fluoride ($LiPF_6$) liquid electrolyte solution in ethylene carbonate/diethyl carbonate (EC/DEC) mixture (1:1 by volume) was then added to the cell. The assembled cells were tested after 24 hours of rest using an Arbin BT2000 battery testing system. The cyclic voltammetry of the cells was investigated using a 1470E multistate (Solarton Analytical, UK) with the voltage range of 0.2 to 3 Volts vs Li/Li+ and the scan rate of 5 mV/s. Finally, electrochemical impedance spectroscopy of the graphene microfiber paper cells was conducted to characterize the internal impedance of the cells, using a 1287A/1260A potentiostat (Solarton Analytical, UK) with a frequency range of 0.01 Hz to 1 MHz.

3.5 Packaging of the Paper-based Battery

Packing of the lithium ion battery was made with different methods. The basic cells were made in the form of coin cells using CR2032 standard. In addition, pouch cells, and laminated cells were made to check the flexibility of the batteries. While pouch cells cannot provide enough internal force to run solid batteries, PDMS encapsulation and lamination method were chosen. The thermal lamination films are made by Polyethylene Terephthalate (PET) plastic, which is not reactive with organic solvents, used inside the lithium ion battery electrolyte. Ethylene-Vinyl Acetate (EVA) as

the thermos-active adhesive also makes the inner layer. Hot rolling the polymer films around the battery layers did thermal lamination. The other approach of paper-based battery encapsulation was to use PDMS. The PDMS sheets were made with different thicknesses and used to wrap the batteries. The PDMS sheets adhered together using PDMS glues such as ARclear Optically clear adhesive 8154, and oxygen plasma bonding.

3.6 Testing of the batteries

3.6.1 Cyclic Voltammogram (CV) test

To check the electrochemical stability of the CNT-microfiber paper in lithium ion environment, a CV test has been conducted. Thus both metallic and paper-based V_2O_5/G electrodes (Al foil and CNT paper) were used as the working electrodes. The counter electrode and reference electrodes for both samples was lithium foils. The potential window for CV test was set in the range of 1.5 V to 4.0 V (vs. Li/Li^+) which is the typical voltage range of cycling any V_2O_5 active material, with a scan rate of 5.0 mV/s using a 1470E Multistat (Solartron Analytic, UK). Lather to check the stability of the CNT-microfiber paper a new CV experiment was carried out with the range of 0.0 V to 4.0 V (vs. Li/Li^+) and a scan rate of 5.0 mV/s to estimate the electrochemical stability of developed paper-based current collector in harsh conditions such as deep discharge.

3.6.2 Electrochemical Impedance Spectroscopy (EIS)

EIS was also conducted to identify the changes of internal impedance for both metallic and paper-based V_2O_5/G electrodes after different tests such as bending and cycling, respectively. A Solartron 1287A/1260A Potentiostat/Impedance System (Solartron Analytical, England, UK) was engaged to check the AC impedance of different V_2O_5/G paper-based and metallic cells with the frequency range of 0.01 Hz–1 MHz and 5 volts amplitude.

CHAPTER 4. RESULTS AND DISCUSSION

4.1 CNT-Microfiber Paper

While the resistance of the fiber changes after CNT deposition, the formation of each conductive layers over the paper microfibers was investigated by checking the change of resistance. Here through the LbL process, the resistance of coated microfibers were measured after the deposition of every bi-layer. Later the size (length) and coating of the fibers also checked using a Keithley CV measurement with a microprobe station. Figure 4-1 a shows the average, minimum, and maximum length resistance (resistance/ length of the microfibers) of coated fiber. To perform this experiment, 20 random microfibers have been chosen and measured. The results proved that after applying the PEI/PEDOT-PSS or PEI/CNT bilayer, the resistance of the microfibers have been significantly decreases. While the thickness of each coating, which was measured by QCM is around 5 nm, this layer is enough to provide a conductive layer surrounding the microfibers and reduce the resistivity exponentially. Figure 4-1 b shows the thickness and resistant changes of every deposited LbL layers around the microfibers. The total thickness of the deposited bi-layers was measured to be in the range of 100 to 110 nm. This layer is not comparable with the actual thickness of the microfibers while the average diameter of the wood microfibers is between 35 µm to 50 µm. It was observed that the thickness of the coating is only limited to 2 - 3% of the actual thickness of each microfibers. This can preserve the unique properties of the fibers such as porosity, absorption, and flexibility. The conductive path around the microfibers has been made of a uniformly deposited and continues networks of highly conductive CNT nano rods on top of a highly conductive polymer layer made by PEDOT-PSS. Here the presence of PEDOT-PSS improves the conductivity of the CNT-microfibers, while the CNT coating on top layers limits the chance of oxidation and conductivity reduction of the PEDOT-PSS. The final length resistance of CNT-microfiber after adding 8 bilayers of PEI/CNT was measured to be 0.468 kΩ/cm. The fabricated CNT-microfiber papers had a thickness of 100 to 200 microns and densities of 0.23 g/cm^3 and 0.46 g/cm^3 respectively. The resistance degradation of these sheets is also limited to a 10% or less drop in 6 months. In addition, the CNT mass loading of the fabricated paper-based current collectors is about 10.1 $\mu g/cm^2$ and the PEDOT:PSS mass loading in such a current collector is 100 $\mu g/cm^2$.

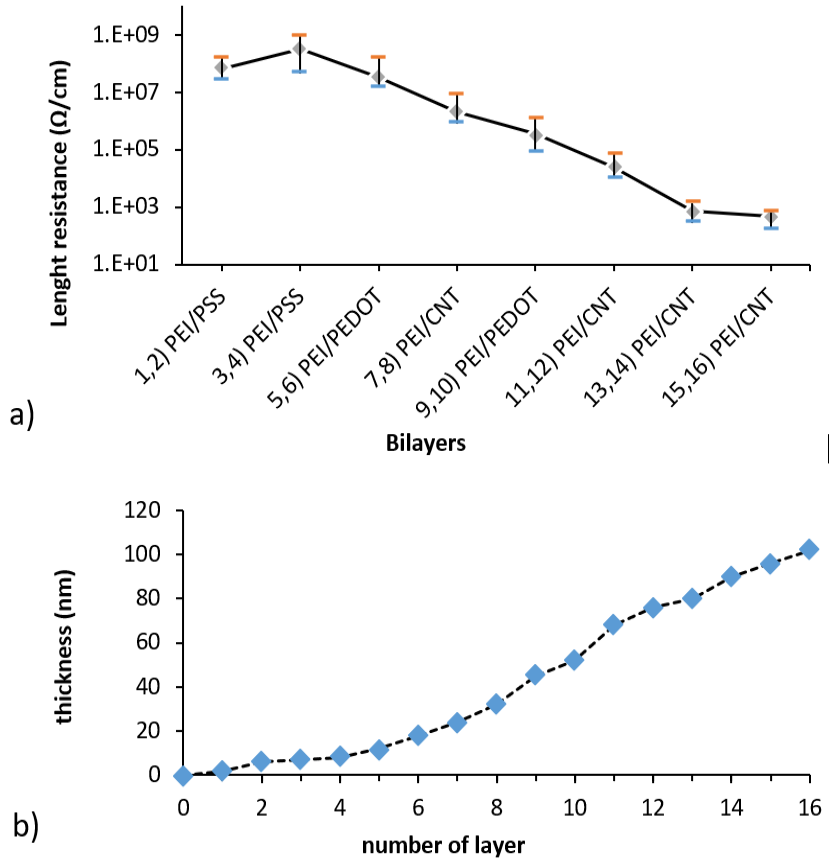

Order of the deposited layers over paper fibers

Layers	Material
1	PEI
2	PSS
3	PEI
4	PSS
5	PEI
6	PEDOT:PSS
7	PEI
8	CNT
9	PEI
10	PEDOT:PSS
11	PEI
12	CNT
13	PEI
14	CNT
15	PEI
16	CNT

Figure 4-1 (a) Length resistance of the wood microfibers after layer-by-layer assembly of PEDOT or CNT bilayers. Here the error bars show the minimum and maximum resistivity of microfibers, and data points show the average, and (b) QCM analysis of coated microfiber to specify the thickness of each coated layer

The X-ray diffraction analysis of the CNT-microfiber paper has been reported in Figure 4-2. As is was showed the diffraction results of CNT-microfiber paper proofs the formation of a uniform layer of CNT over the microfibers. In addition, the peak at 24º is related to the anisotropy of the 002 plane of the CNTs. This strong peak is visible in CNT-microfiber paper and the CNT:PSS drop cast sample, representing the formation of a uniform and stable layer of CNT:PSS around the paper microfibers [75].

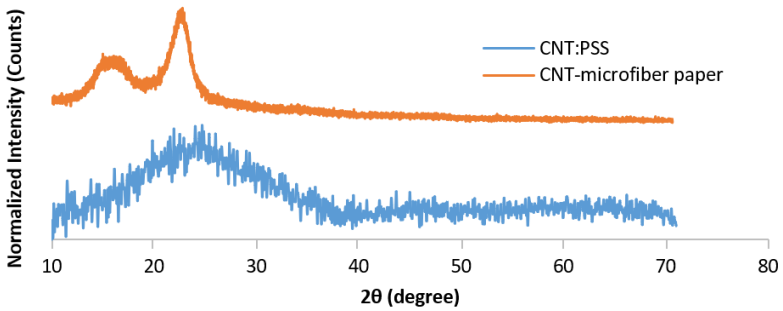

Figure 4-2 XRD pattern of the CNT-microfiber paper and drop casted CNT film over the glass slide. Here the intensity is normalized

4.2 Solid and Polymer Gel Electrolytes

The characterization results of the fabricated PVDF-HFP polymer gel electrolyte with LATP such as morphology, composite formation, electrolyte uptake, and ionic conductivity have been presented and discussed. A precisely controlled formation of similar size pores was attained by applying glycerol as a plasticizer in the polymer structure. Further the residual at a constant temperature and moderate moisture level (60%-70%) could also help the uniformity of the polymer membranes. Addition of glycerol helped the crosslinking process thus increased the viscosity of the polymer solution and it also reduces the crystallization of PVDF-HFP and separating polymer from the solvents uniformly. The reduction of crystallization and uniformly drying while the membrane is still wet, resulted in the formation of a uniform porous membrane [136, 137]. Figure 4-3 shows the FESEM images of the (a) cross-section and (b) surface of the PVDF-HFP membranes made by glycerol and residual drying, to be used as the gel electrolyte. The cross-sectional discloses a uniform porous formation inside the PVDF-HFP structure with an average diameter of ~ 1 µm. The FESEM images of the surface of this membrane (Figure 4-3 c) also revealed the uniformity of the casted films, accurate surface roughness and even distribution of the lithium salts. Even though some non-uniform peaks have been reported on the surface of the membrane, fractures, cracks, holes or other evidence of damage were not observed. However, these small non-uniformities on the surface of each membrane may contribute to a small increase in the final internal resistance of the cells made by this polymer gel electrode and also and may contribute to a capacity fade due to the changes in the contact and lithium diffusion length inside the polymer structure [60].

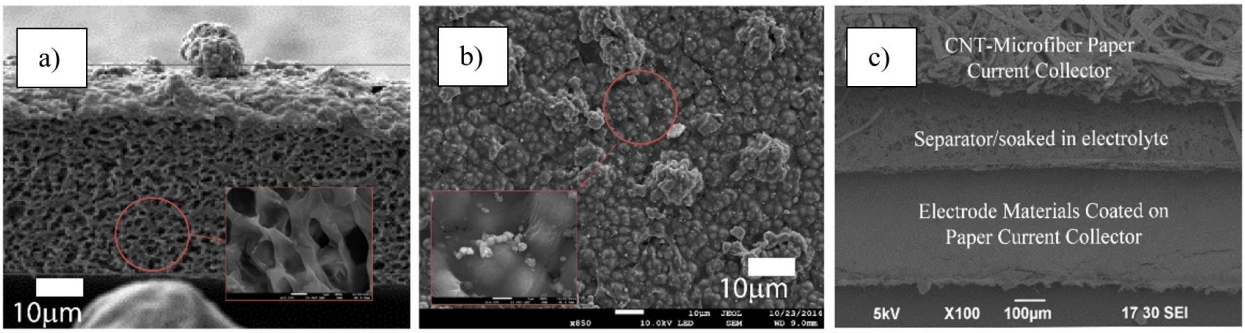

Figure 4-3 FESEM images of (a) the cross-section and (b) the surface area of a casted ~70 µm thick PVDF-HFP, and (c) the three layers assembly of the paper-based LTO/LCO PVDF-HFP gel electrolyte cell

Dispersion of LATP and LiTFSI salts inside the electrolyte membrane was observed using energy-dispersive X-ray spectroscopy (EDS). Figure 4-10, from the cross-section part of the PVDF-HFP membrane with LATP and soaked in LiTFSI ionic solution, provides the traces of uniform dispersion of sulfur which was related to the LiTFSI (yellow sections) and phosphorus which was related to LATP (green sections). Although PVDF-HFP also has phosphorus in it the amount that is not comparable with LATP crystals, so all bright green objects and their random distribution are only indicating the LATP. Figure 4-4 a shows a trace for LiTFSI (sulfur, yellow) while Figure 4-4 b shows a trace for LATP (phosphorous, green). In this case, the presence of LATP particles can reduce the over-crystallization of the PVDF-HFP and this can lead to achieving higher ionic conductivity for polymer gel electrolytes. Further, LATP is a polar filler inside the PVDF-HFP structure and lowers the crystallinity of the casted membranes. This can also improve the ionic conductivity and reduce the lithium ion resistivity of the gel electrolyte. The XRD results of the PVDF-HFP films with 0, 0.3% and 0.5% weight of LATP are also reported in Figure 4-4 c. Here, the peaks at 18.4° and 20° represent the crystalline phase of the PVDF-HFP, 14.7° and 21° are attributed to the LATP [99, 138]. It was observed that by adding glycerol to the PVDF-HFP the peak at 20° became wider, which means the crystalline phase was lowered inside the membrane. By adding the LATP to the PVDF-HFP structure the peaks at 14.7° and 21° became sharper and again the both 18.4° and 20° peaks became broader. This shows that the crystalline structure of the PVDF-HFP has been reduced after adding both glycerol and LATP and more amorphous structure has been developed. Further, the ion transfer inside the PVDF-HFP membrane takes place due to

the aggregation of lithium ions from LiTFSI and LATP in the polymer membrane [139]. By using polar ceramics particles such as LATP. A polar medium forms inside the PVDF-HFP structure and this led to a reduction of the crystalline (non-polar) phase of the fabricated films makes it more ionic conductive [99, 138].

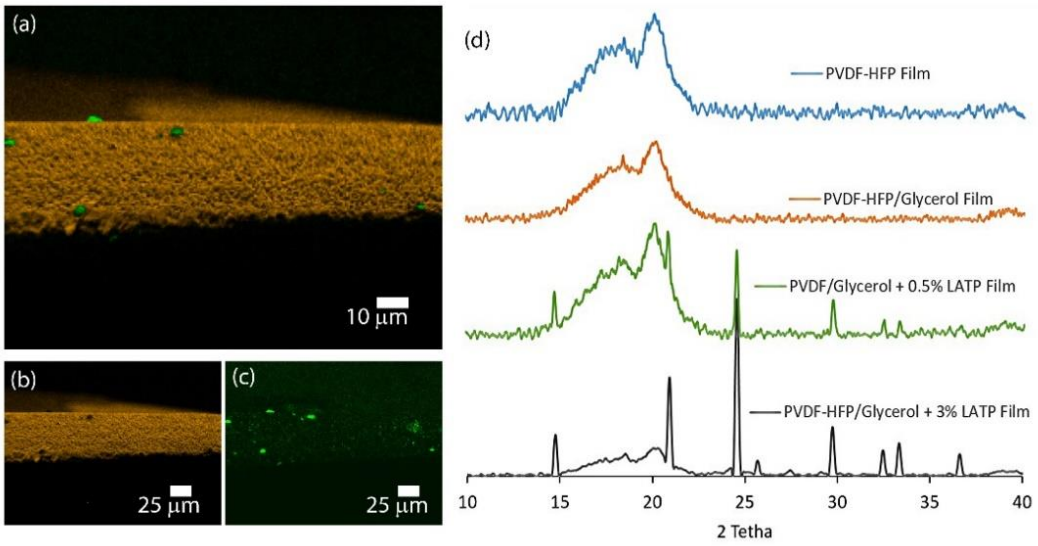

Figure 4-4 EDS of the PVDF-HFP gel electrolyte cross-section: (a) Trace of electrolyte materials, (b) Yellow pixels represent the trace of sulfur for LiTFSI detection, and (c) Green pixels represent the trace of phosphorus for LATP detection, and (d) normalized XRD results to identify the amorphous polymer gel formation by adding LATP in PVDF-HFP structure

PVDF-HFP membranes with 0.5%, 1%, 2%, and 3% by weight concentration of LATP have been made and tested for the electrolyte uptake. Here, films with a specific size of 1 cm^2 were prepared and soaked in a LiTFSI/EC/DEC solution (1 mol, 1:1 by weight) for 24 hours. No significant change in electrolyte uptake has been observed, and all of the samples maintained absorption of (450±30)% by weight. The ionic conductivity test of these samples also showed that the LATP concentration of 3%, improved the ionic conduction inside the membrane by 20% while increasing the LATP concentration to values higher than that leads to a reduction in ionic conductivity.

FTIR results for (a) PVDF-HFP, (b) PVDF-HFP/LATP, and (c) PVDF-HFP/LATP/LITFSI have been reported in presented in Figure 4-5. Here the peak at 2750-3000 cm^{-1} and 840-880 cm^{-1}, which occur in all three samples (marked "1" in Figure 4-5), proves the polar form of PVDF-HFP after all steps [99]. The peak at 1200-1300 cm^{-1} in (a) is related to the C-F bonding in PVDF-HFP. This

polar section is in charge of the segmental movements inside the polymer structure and directly is related to form ionic conductive paths inside the membrane [106, 109]. Sharp peaks of LATP are visible at 500-700 cm^{-1} (marked "2" in plots (b) and (c)). Another peak of LATP is the 980 cm^{-1}, is related to P-O bonding (marked "2" in plots (b) and (c)) [140]. Peaks for LiTFSI, at 1140 cm^{-1} and 1490 cm^{-1} (marked as "3" in plot (c)), shows the uniform desolation of LiTFSI inside the membrane [141, 142]. The peaks at 1600-1700 cm^{-1} (marked "4" in plot (c)) revealed the formation of ionic liquid traps inside the polymer gel structure [141, 142]. Bands 879 and 841 cm^{-1} visible on both (b) and (c) identify the β and γ phases of the PVDF-HFP, related to the amorphous structure of membrane. The symmetric and asymmetric out of plane deformations of SO_2 group in LiTFSI structure are also visible at 1138 and 617 cm^{-1} bands respectively and revealed the uniform mixing and formation of a gel. A C=O vibration peak is identified at 1734 cm^{-1} while a C-H stretching, at 1420-1440 cm^{-1}. These two peaks show the aggregation of lithium compound inside the polymer gel structure [99, 136].

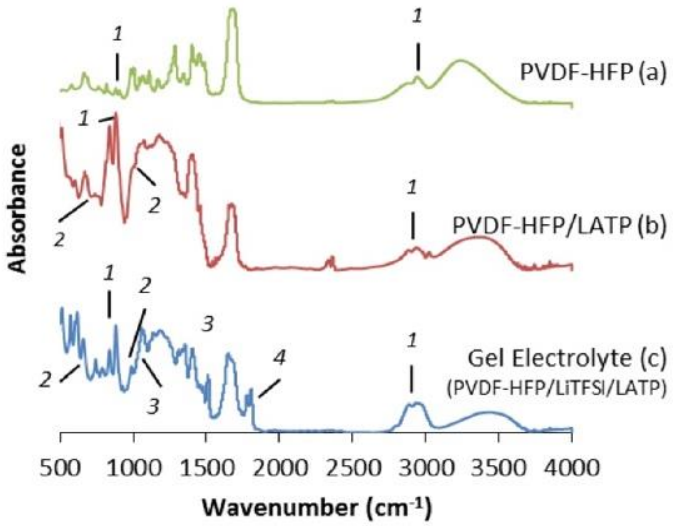

Figure 4-5 FTIR of casted (a) PVDF-HFP, (b) PVDF-HFT/LATP, and (c) PVDF-HFP/LATP/LiTFSI membranes.

The electrical impedance spectroscopy (EIS, Solarton Galvanostat) of the electrolyte was conducted using stainless steel counter electrodes. The DC potential for this measurement was 0.5 mV and frequency range was between 100 mHz to 1 MHz. The ionic conductivity of the PVDF-

HFP polymer gel electrolyte was 2.1×10^{-3} S cm^{-1} and 2.8×10^{-3} S cm^{-1} for 100 µm and 280 µm thick membranes respectively. The lithium transference number of the electrolyte, measured using stainless steel and lithium electrodes, was observed to be 0.967. Figure 4-13 also displays the ionic conductivity of the gel polymer membranes with different thicknesses and cycles. The bending test was performed for these samples to check the ionic conductivity fade after deformation of these samples. The conductivity of the electrolyte was reduced by 14% after performing the bending test. This is due to surface deformation of the electrolyte, and migration of the ionic liquid inside the gel structure form the damaged areas. Further, shallow surface fractures on the polymer were formed around the damaged areas that could also lead to capacity fade and drop of ionic conductivity [136].

In conclusion, high ionic conductive PVDF-HFP polymer gel electrolyte has been fabricated to be used in paper-based batteries consisting of CNT-microfiber paper current collectors. This electrolyte is based on a highly porous and amorphous PVDF-HFP structure enhanced with LATP and LiTFSI. The ionic conductivity of 2.1×10^{-3} S cm^{-1} was achieved using 3%of LATP in the polymer structure. Here, by combination of LATP ceramics and PVDF-HFP polymer, a stable and flexible gel electrolyte with high ionic conductivity has been developed. This can also be used in conjunction of paper-based batteries and enable the advancements in making flexible lithium ion batteries. The polymer gel electrolyte was applied in metallic and paper-based cells using conventional lithium active materials such as LTO and LCO to oversee the performance of these electrolytes. Capacities up to 123 mAh/g and 99.5 mAh/g have been achieved for LTO/LCO metallic and paper-cells respectively. Here the charge/discharge plateau of the paper-based is lower than the metallic cells due to the difference impedance. This is related to the structure of electrodes while in metallic cells more surface area is internally connected to the polymer gel surface while in the paper-based electrodes some of the active material is trapped in the inner layer of the paper and cannot be exposed to the polymer gel electrolyte. Further, the second cycle of the paper-based battery has lower performance due to this higher internal. This the solid-state and flexible paper-based lithium ion battery indicates new potentials in low power applications such as RFID tags, handheld devices, electrochromic displays, and paper-based sensors.

4.3 Paper-Based Battery

4.3.1 Simulation

The LTO/LCO cell also has been simulated using a 1D/3D model, presented in Chapter 3, to check the safety and durability of the paper-based battery. In this case a 1D electrochemical and a 3D thermal model have been developed. To achieve the maximum persistence, the LTO and LCO states of charge have been added directly as it is shown below. As it is shown in the simulation parameters in Chapter 3, the capacity of the lithium ion batteries has been predicted for different C rates. In this case, the parameters are the size of the electrodes, materials, and state of charge. The state of charge for these simulations have been imported from actual tests of the CNT-based half cells and then imported to the simulations. The Figure 4-6 shows the state of charge for LTO and LCO paper-based electrodes. This can be later transferred to the number of ions and provide the capacity of the cells. In addition, the room temperature also was set to 25 ˚C for all the simulations.

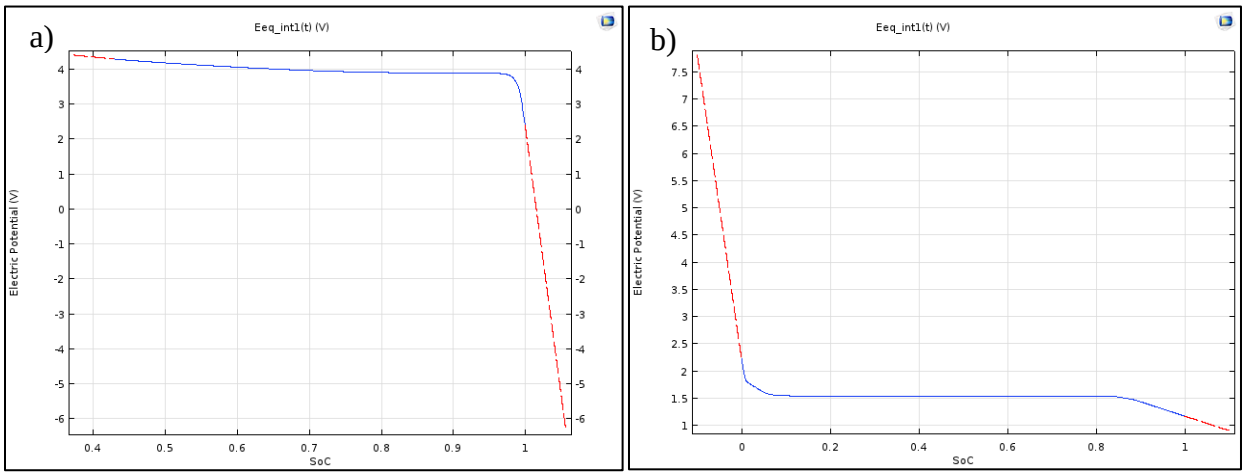

Figure 4-6 State of charge for (a) LCO and (b) LTO electrodes

In the first try, the LCO/Graphene cells have been simulated. The graphene has been chosen as the unlimited lithium nest, so the simulation will be predicting a half-cell LCO electrode. LCO has a very higher thermal generation, less stability and higher voltages. Here, LCO cells have been developed, and the capacity and heat generation of these cells have been tested. In this case the capacity of the LCO and its fade was measured and also the heat generated. Figure 14-7 shows the results of this simulation. The results are comparable with experiments although in real life the

capacity is limited to the 75% of the simulated results due to solid electrolyte interface formation, the internal resistances, and inconsistency of the electrochemical reactions.

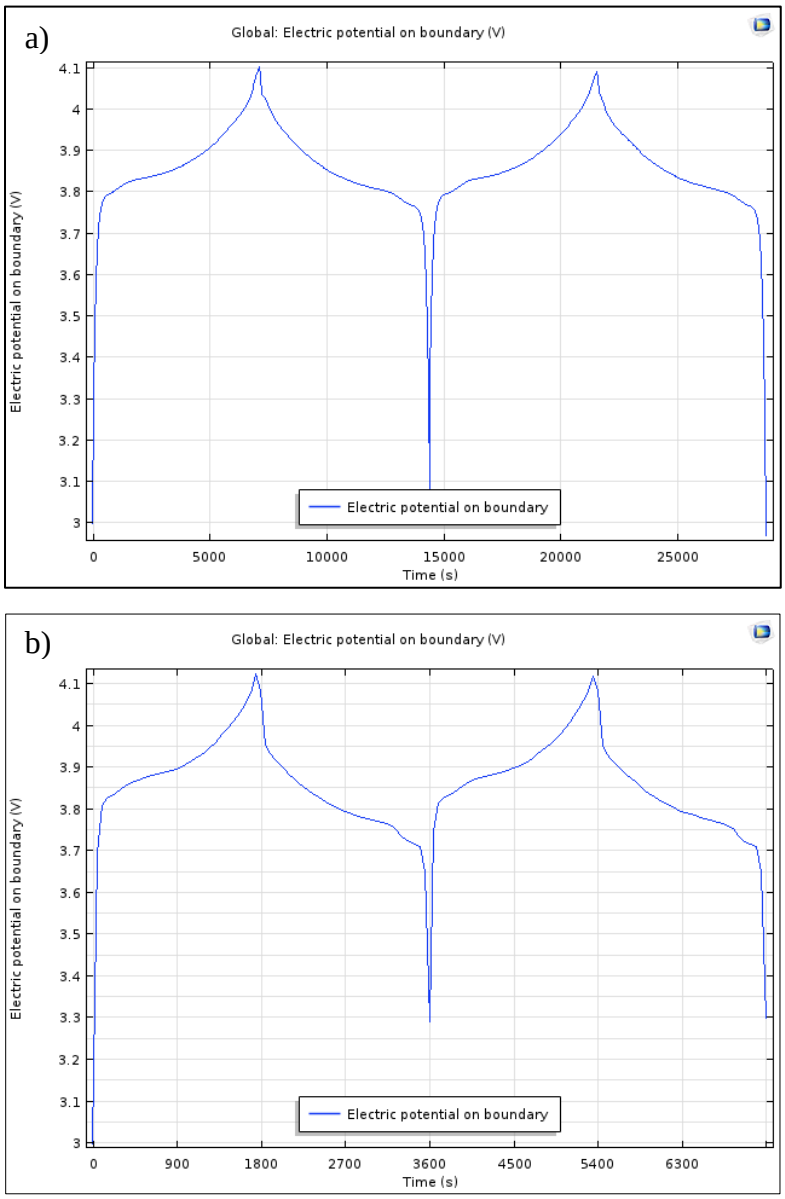

Figure 4-7 Simulated charge/discharge cycle of a LCO/Graphene cell with (a) 0.5 C rate and (b) 2 C rate current

Further the difference in the state of charge versus voltage of LTO and LCO were used to predict the open circuit voltage of the LTO/LCO cell. The concentration of Li-Ion in each cycle decreases on anode side to generate free ions and electrons thus the generated lithium ions must

accommodate themselves to the cathode electrode in each run. So, by the migration of the lithium ions from one electrode to the other one the OCVs of the difference between the electric potential of the cathode and of the anode will be predicted. The voltage of the LTO/LCO cell has been reported in Figure 4-8 with 0.5 C and 0.8885 Ah current.

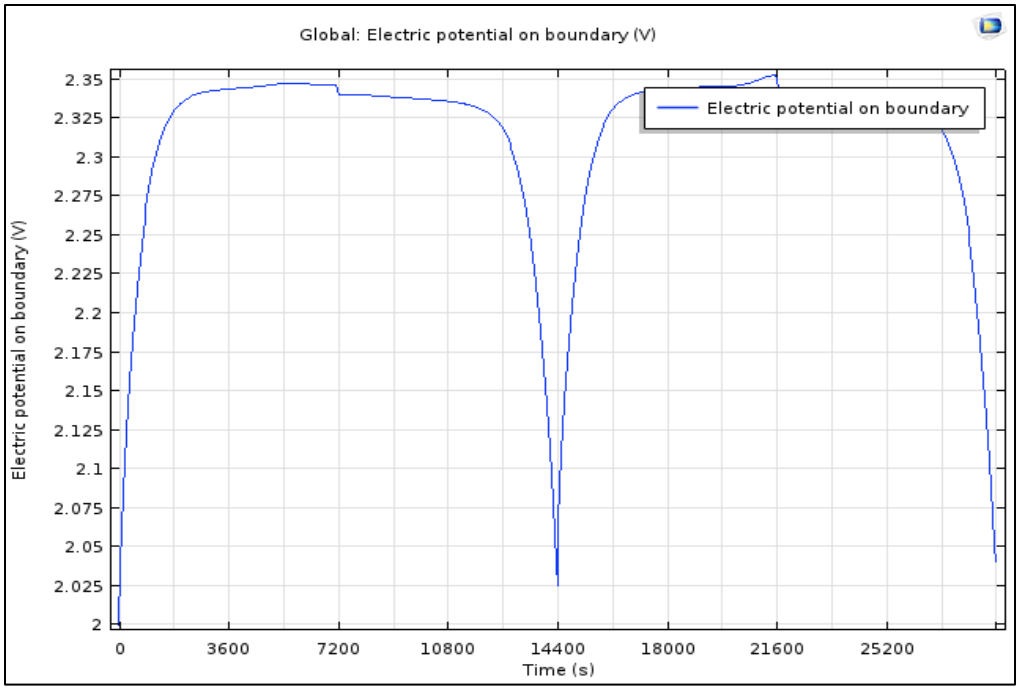

Figure 4-8 Simulated charge/discharge cycle of a LTO/LCO cell with 0.5 C rate current

The lithium ion concentration of the electrodes also has been calculated and modeled. In this case the concentration of ions at the beginning and 1st cycle has been modeled. The ions are generated uniformly inside the LTO electrode in each charge cycle. This also shows that not 100% of the LTO or LCO ions are released in each cycle. Our simulation also shows that this is limited to 10-15% due to the internal resistance of the active material layer and limits of electrochemical reactions.

In addition to the capacity, the heat generation of cells also has been reported. As it is shown in Figure 4-10, the cells start to warm up after each cycle although as it was reported a portion of this heat will be used for next cycle. Thus, the heat in the core only changes in a couple of degrees.

Here, LCO electrode has been tested while maximum heat is generated in LCO electrode and LTO electrochemical reaction doesn't generate too much of irreversible heat.

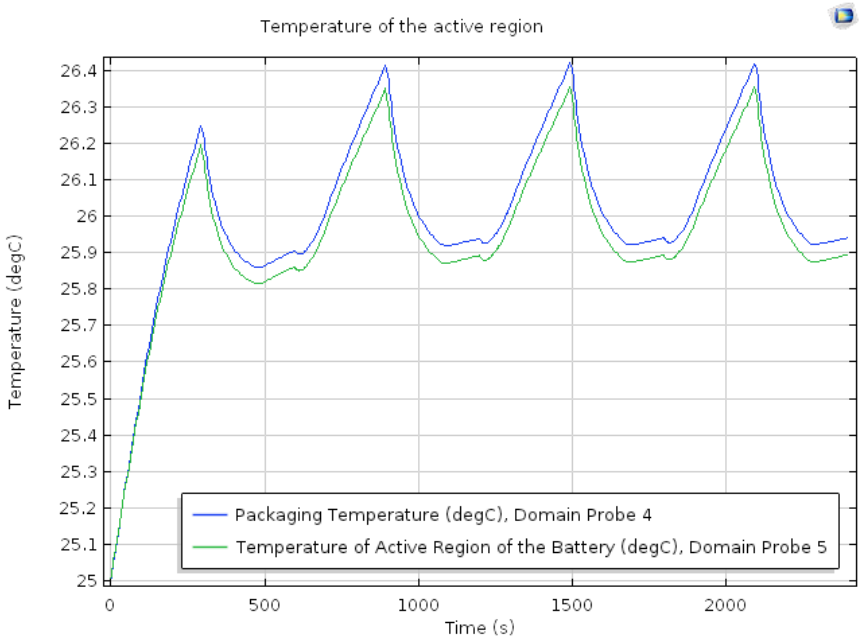

Figure 4-9 Single layer cell (LCO/G) temperature change after charge discharge cycles

In reality the core temperature of the cell will be changed though the pouch cells. Figure 4-10 also reveals the head generation inside a pouch cell. As it is reported the core has higher temperature compared to the sides, although it is still well below the burning temperature of the paper.

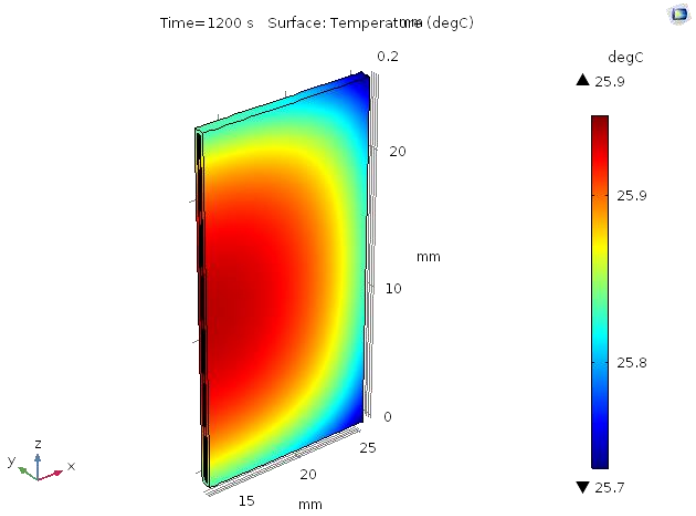

Figure 4-10 Heat generation after 2 cycles in a LCO/G cell

While the stacking in pouch cells is also a very common method, the samples have been made by 10 layers of cells inside the same pouch. In this case, the change in temperature again measured and reported. As it is reported in Figure 4-11 the temperate goes up to 10 degrees higher than room temperature but it is still less than the igniting temperature of paper.

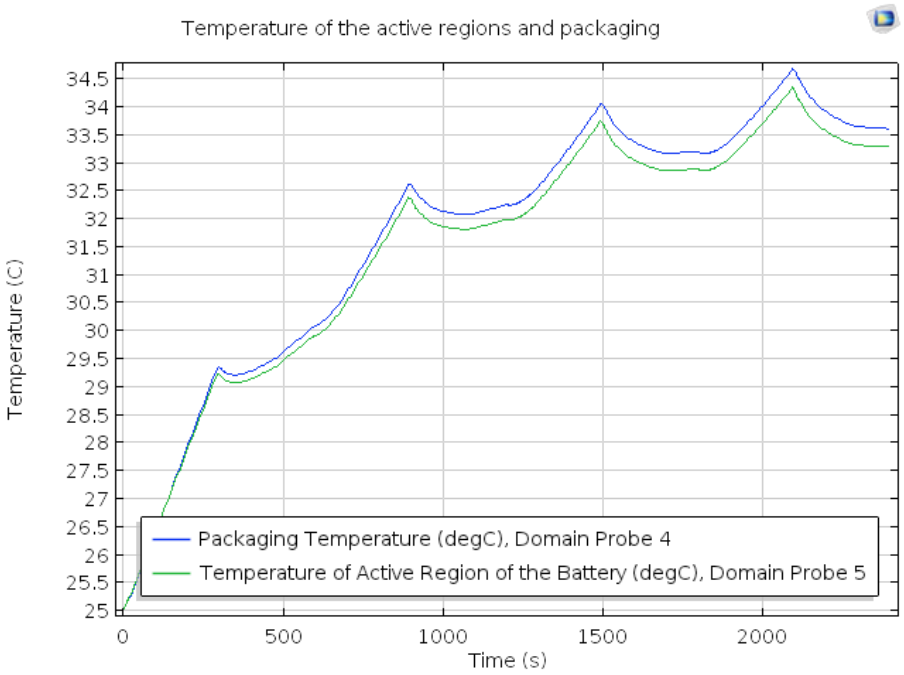

Figure 4-11 A 10 layer cell (LCO/G) temperature change after charge discharge cycles

The core temperature of the pouch cell also compared with side or surface temperate and it is reported in Figure 4-12. As it is reported, the temperature difference is in the range of 2-3 degrees and still acceptable and safe.

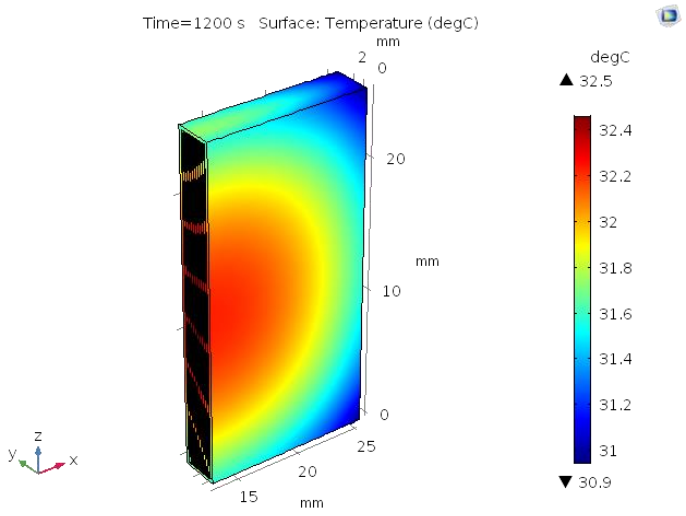

Figure 4-12 Heat generation after 2 cycles in a 10 layer LCO/G cell

Further, the presence of the CNT-microfiber paper current collector also has been simulated. In this case a heat core with temperatures up to 45 was designed between two aluminum and paper sheets with the same thickens of conventional metallic, and CNT-microfiber paper current collectors. As it was measured the final temperature around the metallic cell was in the range of 28 to 35 °C while the paper-based cell was reached to 20 to 30 °C. This shows that the heat dissipation in slightly lower in paper-based cells, but it is not that effective for the performance or safety of the produced cells.

4.3.2 LTO/LCO Polymer Gel Cells

The ionic conductivity of the LTO/LCO paper-based and metallic lithium ion batteries, using PVDF-HFP gel electrolyte have been checked. Here, Warburg model was implied to find the resistances of the cell. Here the ohmic resistance (R_s) and charge-transfer resistance (R_{ct}) of the cell have been reported to check the conductivity of the electrodes and electrolyte simultaneously. Figure 4-13 shows the ionic conductivity of metallic and paper-based LTO/LCO cells. Here, the inset of Figure 4-13 is the Warburg model of equivalent circuit related to the electrochemical reaction inside the cells. These batteries for this experiment has been made by a 100 µm thick polymer gel electrolytes. The R_s and R_{ct} are 0.15 Ω and 5.78 Ω, and 7.92 Ω and 40 Ω for metallic and paper-based batteries, respectively. The higher value of R_s for CNT-microfiber paper electrode

is ascribed by the higher dielectric constant of the CNT-microfiber paper and non-uniform contact surface between the electrodes and electrolyte. It was also noted that the roughness of the paper-based electrodes could lower the contacting surface between the polymer gel electrolyte and active material, resulting in lower lithium diffusion inside the electrode.

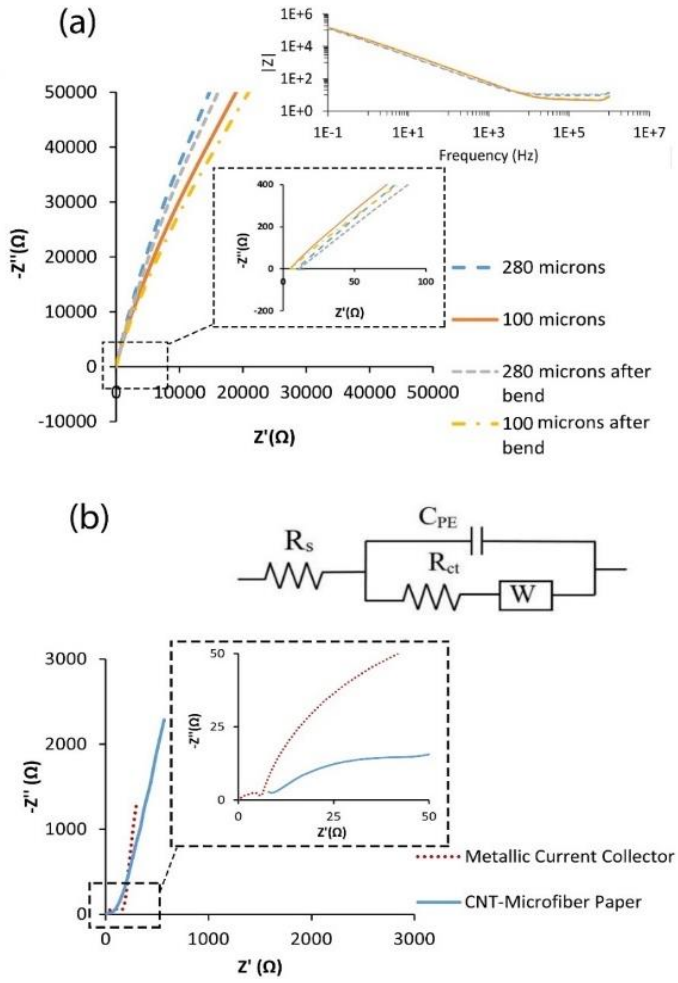

Figure 4-13 (a) Impedance analysis of the PVDF-HFP polymer gel electrolyte for different thicknesses and (b) The internal resistance of a LTO/LCO cell made by PVDF-HFP gel electrolyte. Here inset shows the Warburg equivalent circuit of the cell

LTO/LCO full cells were fabricated using metallic (copper and aluminum) and PVDF-HFP polymer gel electrolyte and tested between 0.8 to 2.5 V with C/5 rate. The voltage profile these cells for both 1st and 10th cycles are 123 mAh/g and 85 mAh/g respectively and have been reported in Figure 4-20 a. These capacities are comparable to the commercially available and previously

published LTO/LCO batteries [45, 60]. The 18% capacity fade from the 1st to 2nd cycle also have been observed. Yet, the capacity fade after the 2nd cycle in consecutive cycles was limited to a maximum of 4%. The capacity fade between 1st to 3rd and 1st to 5th cycles were 21.4% and 28.1%, respectively, while the capacity fade from 2nd to 10th cycle was only 24%. The capacity fade is attributed to the loss of ionic conductivity, due to the non-reversible lithium migrations and the extraction lithium from the polymer gel electrolyte. In addition, a solid electrolyte interface (SEI) layer formation on the electrode/electrolyte interface, unbalanced capacity between anode and cathode, and trapping ions inside the active material structure in both cathode and anode, may also contribute to the capacity drop [136, 143].

LTO/LCO cells using CNT-microfiber current collectors and PVDF-HFP polymer gel electrolyte were fabricated and tested using similar metallic cell parameters. The FESEM of the fabricated paper-based cell with CNT-microfiber current collectors sprayed active material layer and polymer gel electrolyte is shown in Figure 4-3 c. It was observed that the active materials have been evenly deposited over the CNT-microfiber paper. This provides perfect adhesion and stability between the active material and paper surface, due to the porous nature of the CNT-microfiber paper. The charge/discharge capacity plateau for the metallic and paper-based cell are reported in Figure 4-14 a and 4-14 b respectively. Here the 1st cycle charge and discharge capacities are 99.5 mAh/g and 75.6 mAh/g, respectively. This 1st cycle charge capacity is 24% lower than the previously reported capacity of metallic cells. This is due to the higher internal resistance of the cell which was discussed above, and slightly lower voltage observed in the CNT-microfiber current collector cells as compared with the metallic current collector cells.

As it was reported, the surface roughness of the paper-based electrode is higher than metallic cells. This provides an imperfect contact area between the electrode and electrolyte, and reduces the ionic conductive pathways, which also contributes to a reduction in the overall capacity [52]. The reported capacity of the paper-based reported here suing polymer gel is still comparable with the previously reported LTO/LCO paper-based batteries using liquid electrolytes. As it was reported in Figure 4-14 c similar capacity drop between cycles has been observed in both metallic and paper-based batteries. Here, the capacity fade of 13% from 1st to 2nd cycle and 19% from 2nd to 10th cycles were observed in the paper-based batteries. These numbers are lower than the capacity

fade in the metallic cells. As it was described, the metallic cells are less resistive to SEI formation, material stabilization, and variations in electrode mass loadings due to the spray method are attributed for these capacity drops. In addition, for the 1st cycle, having the CNT in the electrodes increases the chance of the SEI formation int 1st charge cycle using any electrolyte made by EC and DEC solvents [52]. Figure 4-20 c show the capacity for the first 15 cycles of both paper-based a metallic LTO/LCO cells. Here the capacity drops sharply at first due to the SEI and lithium dendrite formation but stays stable through the 15th cycle [144, 145]. Here mode advancement is needed to improve the cycle life of the cells. It should also need to identify that the active material over CNT-microfiber current collectors provides better flexibility and stability compared to the conventional aluminum and copper electrodes. Most importantly, using flexible and stable CNT-microfiber current collectors and a polymer gel electrolyte are breakthrough to achieve fully flexible and integrable paper-based lithium ion battery to develop paper-based or flexible electronics.

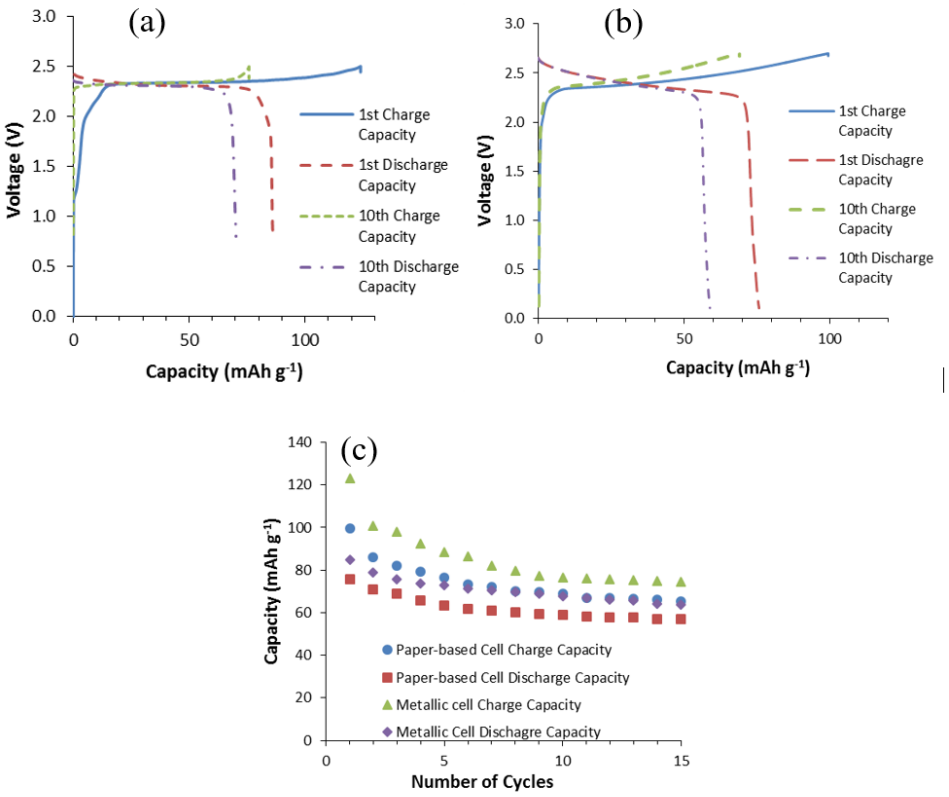

Figure 4-14 1st and 10th charge/discharge cycles of PVDF-HFP gel electrolyte and LTO/LCO electrodes for (a) metallic current collector and (b) paper-based current collectors, and (c) The cycle life of the polymer gel electrolyte cells

4.3.3 V_2O_5/G electrodes

To check the stability of the V_2O_5/G through bending and deformations, both paper-based and metallic electrodes were made and tested through different bending tests. Thus, the CNT-microfiber paper and aluminum foil were coated using a spray method with a V_2O_5/G active material layer and for bending test, each electrode was bent to 90º for 20 times. To prevent any movements, the electrode was fixed using a stage and just bent in one direction for 90º. The damages, crack formation, fractures, peelings, and deformations of the active material over both substrates have been examined using FESEM. The morphology of each electrode was examined using FESEM and energy dissipative spectroscopy (EDS) before and after the bending test to have detailed trace of crack formation and development of damages toward the electrode after conducting a bending test. The results of these experiments have been reported in Figure 4-15 (top view) and Figure 4-16 (cross-section). Here, the EDS data is based on the traces of the sulfur for coated CNT-microfiber paper, aluminum for metallic current collectors and vanadium for V_2O_5/G layer of active material over the current collector surface. As was observed, for the metallic electrode, some portion of the coated V_2O_5/G layers was completely peeled, detached, and removed from the center core of the formed fracture over the surface of metallic current collector. The V_2O_5/G layer was less intact over the paper-based current collector and had fewer fractures. Additionally, a part of V_2O_5/G layer was seen to get completely detached from the surface of the metallic current collector. It is anticipated that the air gaps and cracks in the conventional electrode after bending will result in a significant drop of the capacity and lower cycle life and rate performance of the cell due to the increased internal resistance of the electrodes up to 300%. The paper-based electrodes are less intact after bending, while only small portions of the active material over the core of fracture show some cracks and no significant detachment of the V_2O_5/G layer was observed. The internal resistance changes of the paper-based electrodes after the bending test was observed to be less than 20%. Such good active material integrity over the paper-based current collectors must be attributed to the porosity of the paper-based current collectors that improves the adhesion between the active material layer and the fibers of the CNT-microfiber paper. In addition, the V_2O_5/G particles entangle with the fabrics of the paper current collector to form an integrated layer with strong bonding between the layers, which, in turn, leads to improved stability and performance of the electrode as well as improved flexibility.

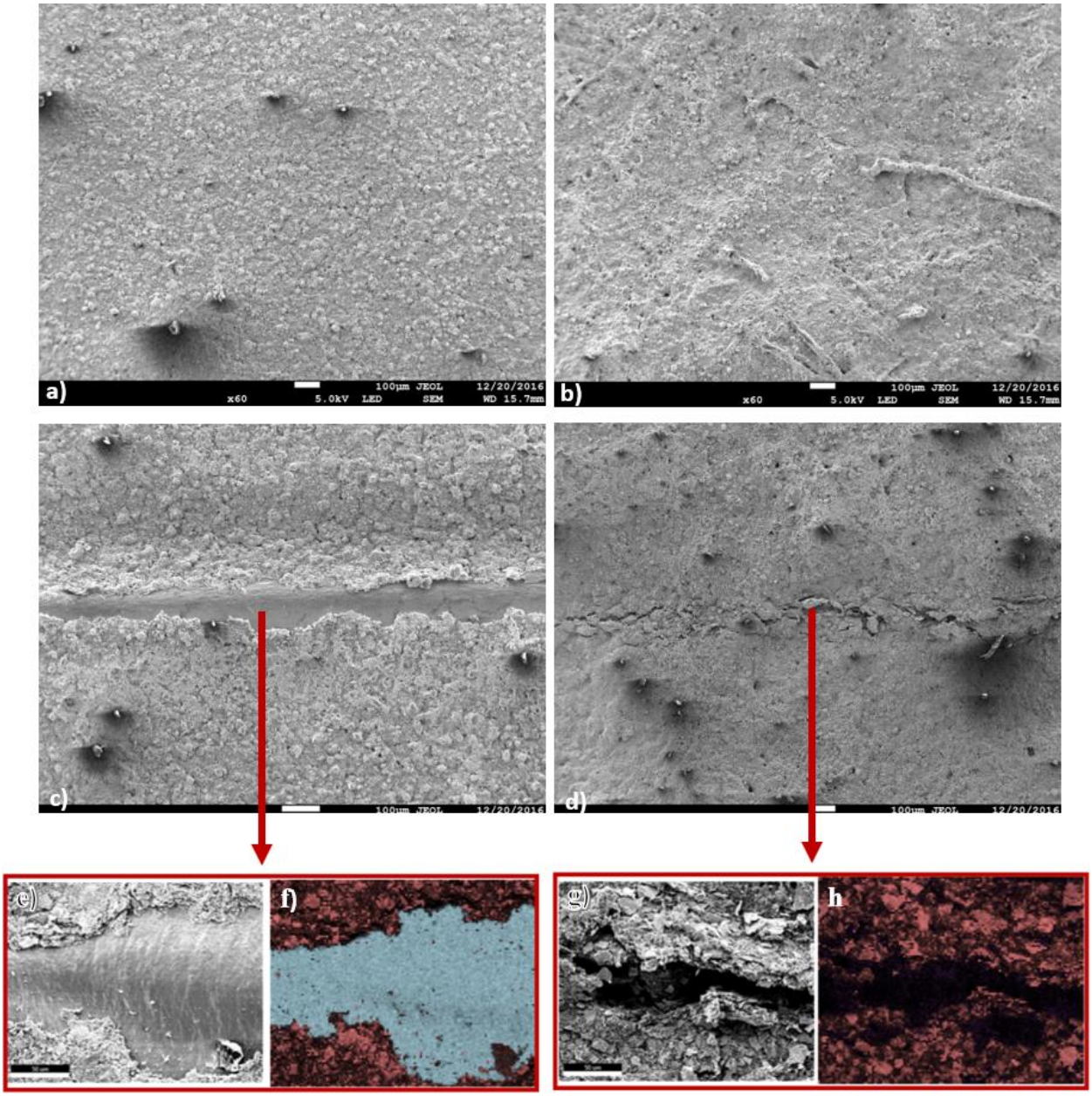

Figure 4-15 FESEM images of surface of (a) metallic and (b) paper-based electrodes, and (c) metallic and (d) paper-based electrodes after bending test. (e) FESEM, and (f) EDS of the crack formation over metallic electrodes after bending test. (g) FESEM and (h) EDS of the crack formation over the paper-based electrodes after bending test. The EDS images show the trace of aluminum with blue color, and sulfur with pink color for CNT-microfiber paper and Vanadium with red color to detect the aluminum current collector, paper current collector and electrode layers respectively

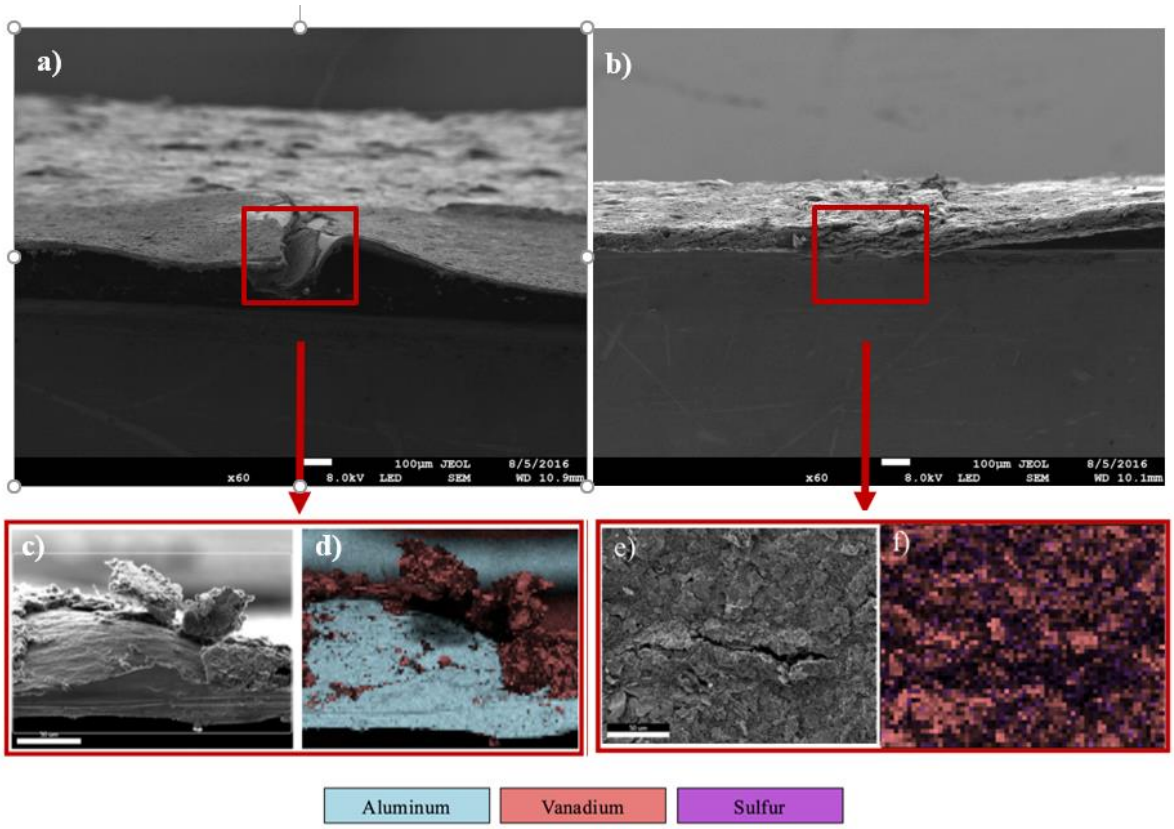

Figure 4-16 FESEM images of the cross section of (a) metallic and (b) paper-based electrodes, and (c) metallic and (d) paper-based electrodes after bending test. (e) FESEM, and (f) EDS of the crack formation over metallic electrodes after bending test. (g) FESEM and (h) EDS of the crack formation over the paper-based electrodes after bending test. The EDS images show the trace of aluminum with blue color, and sulfur with pink color for CNT-microfiber paper and Vanadium with red color to detect the aluminum current collector, paper current collector and electrode layers respectively

The morphology of the paper-based electrodes was examined using FESEM. Figure 4-17 shows the structures of a non-coated cellulose microfiber, a CNT-coated microfiber, and a CNT-coated microfiber with a layer of sprayed V_2O_5/G active material. Figure 4-17 a shows the detailed image of the surface of a blunt cellulose microfiber with no coating. The inset of this figure (Figure 4-17 d) also reveals the high surface porosity of the fiber and its structure. These fibers can be coated with many high conductive nanomaterials such as the CNTs, through the LbL process and provide a highly conductive and stable nanolayer. As can be seen in Figure 4-17 b, the pores of the microfibers have been coated with the conductive CNT layer to provide a highly conductive nanocoating on the surface. Here the CNT-coated microfiber has been coated with PEDOT-PSS

and CNT conductive bilayers. The formation of a multilayer conductive and polymer layers surrounding the microfibers is completely visible in Figure 4-17 e and 4-17 c also shows a single CNT-coated microfiber coated with a layer of V_2O_5/G active material. Here the V_2O_5/G crystals entangle with the fabrics using the polymer binder in the active material mixture and cover the of the surface of CNT-microfiber paper current collector forming an integrated layer. Here graphene sheets provide a highly conductive layer surrounding the V_2O_5 crystals and additionally the CNT layer around microfibers can provide high conductive paths form outer circuits to active material layer. As it is shown in Fig 4-17 f, the electrodes are formed by the formation of a V_2O_5/G layer over the CNT coated microfibers. As it is observed a thin layer of V_2O_5/G composite layer has been deposited uniformly over the microfiber surface, thus the graphene particles provide a very short and high conductive pathway between the V_2O_5 particles and the conductive CNT coated microfibers. The high porosity of the microfibers as it is observed also helps to provide a very rigid and mechanically stable active material layer embedded over the surface of the CNT-coated microfibers.

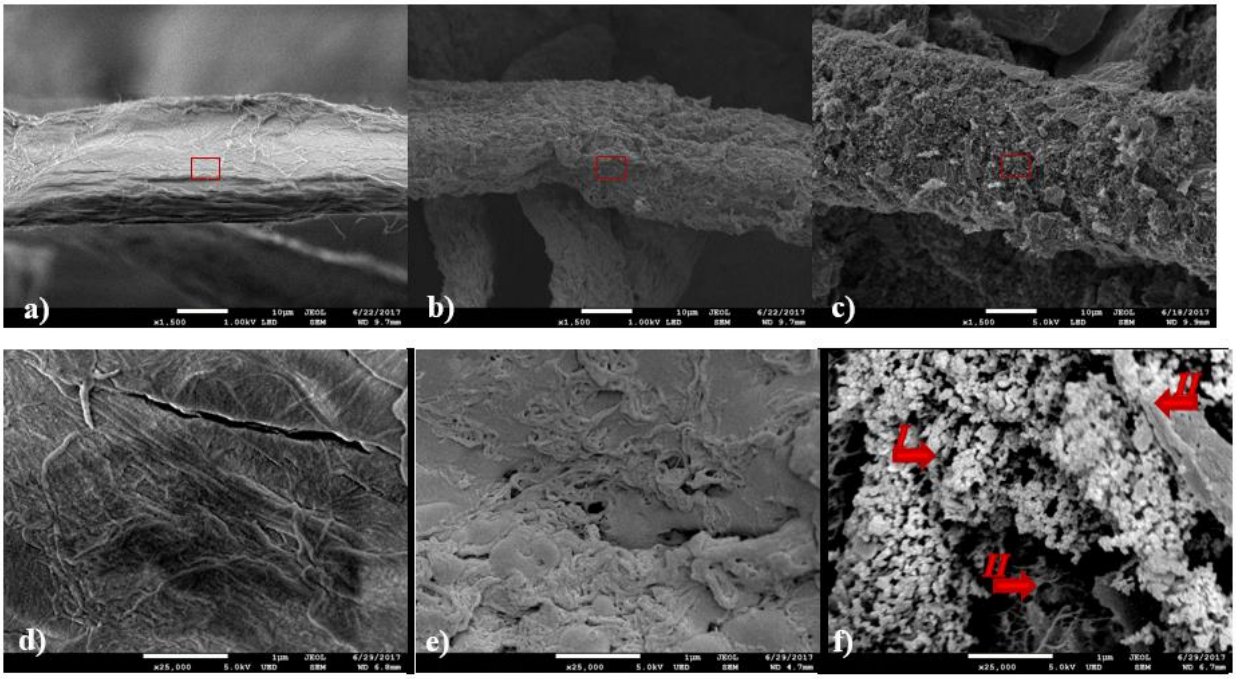

Figure 4-17 FESEM images of the cellulose microfibers: (a) blunt, (b) CNT-coated and (c) V_2O_5/G-coated CNT-microfiber. Higher magnification of the formed layer (the red box in the top row images) of (d) blunt, (e) CNT-coated and (f) V_2O_5/G-coated microfiber where I) shows the V_2O_5/G layer, II) shows surface of the paper microfiber III) shows the CNT coating

The electrochemical stability of the CNT-microfiber paper and metallic current collectors (aluminum sheet) in the liquid $LiPF_6$ electrolyte was investigated by cyclic voltammetry, as shown in Figure 4-24. The potential range for the experiment was set from 1.5 to 4.0 V (*vs*. Li/Li^+) to demonstrate the typical potential range of V_2O_5 cathode materials [89]. As it is shown in Fig. 4-18 a, no obvious redox reactions were observed for the CNT-microfiber paper current collector in the potential range of 1.5–4.0 V (*vs*. Li/Li^+). There was only a shuttle-shaped pattern was observed, which is related to the double-layer capacitance of this current collector. The aluminum foil was also stable in the potential range, but it is starting to show some increment in current when the potential reached 1.5 V (*vs*. Li/Li^+), which may correspond to redox reaction on the aluminum surface and the alloying process by lithium ions (Figure 4-18 a). Here it was concluded that the CNT-paper showed better electrochemical stability compared with the conventional aluminum current collector. In some harsh conditions, such as over-discharge of a lithium ion battery, the potential of each electrode might be required to go below the 1.00 V (*vs*. Li/Li^+) or even reaching to 0 V (*vs*. Li/Li^+) which can lead to the aluminum corrosion [146, 147]. Thus, the electrochemical stability of CNT-paper under over-discharge condition is also reported. A CV scan from 0.0 to 4.0 V (*vs*. Li/Li^+) was conducted for both aluminum and CNT-microfiber paper. It is known that a Li-Al alloying process would happen in a low voltage around 0 V (*vs*. Li/Li^+) [148, 149], and the CV scan result in potential low discharge condition with the range of 0 ~ 4.0 V (*vs*. Li/Li^+) also showed an obvious redox peaks around 0.5 V and 2.5 V (*vs*. Li/Li^+) (as appointed by arrows in Figure 4-28 b). As it is reported for the CNT-microfiber paper (Figure 4-24b), there were no redox peaks observed during the wide potential range, suggesting that the CNT paper has much higher electrochemical stability for cathode under extreme conditions. Moreover, the CNT paper can be used as the current collector instead of conventional copper foils for the anode while the typical potential range for anode material is typically in the range of 0 to 2.5 V (*vs*. Li/Li^+), which perfectly lies in the stable voltage range of the CNT-microfiber paper (0~4.0 V *vs*. Li/Li^+).

Electrochemical impedance spectroscopy was also employed to characterize the resistance of the V_2O_5/G electrode on CNT-microfiber paper and conventional aluminum current collectors. As it is shown in Figure 4-18 c, the CNT-microfiber paper has a relatively higher but comparable resistance compared to the aluminum sheet. An equivalent Warburg model shown in the inset of the figure was used to identify the impedance values. Here R_0, which is the total ohmic resistance

of the cell containing the electrodes, the electrolyte, the current collectors, the separator, and the connections between them. This value can be found by the interception of the high frequency loop and the *x* axis of impedance curves. The R_{SEI} and C_{SEI} which are the electrical resistance and capacitance of the solid electrolyte interface over the electrodes, for which the high frequency stands. The R_{ct} and C_{dl} are also representing the charge-transfer resistance and the double-layer capacitance of the electrode structure, which correspond to the average (mean) frequency area, and σ is the Warburg diffusion impedance, which also can provide the lithium diffusion coefficient inside the electrode according to the 45º point in the second arc [150]. The impedance results shown in Figure 4-18 d were fitted with this equivalent circuit [151, 152]. The V_2O_5/G electrodes on CNT paper showed relatively higher Ohmic resistance and charge transfer resistance, which might be due to the extremely low loading of the CNT fibers

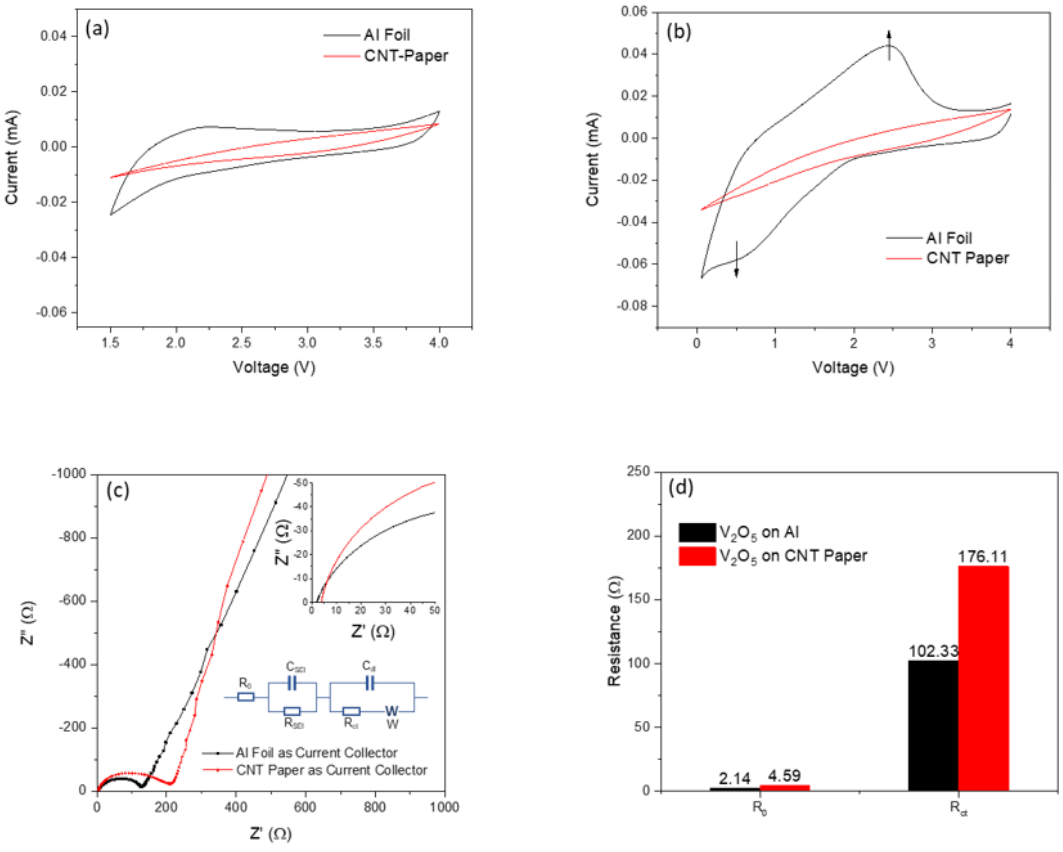

Figure 4-18 Comparison of the electrochemical stability of CNT-microfiber paper and aluminum foil current collectors at a scan range of (a) 1.5 ~ 4.0 V and (b) 0 ~ 4.0 V, and (c) Comparison of the V_2O_5/G electrodes resistance on CNT-microfiber paper and aluminum foil, and (d) Ohmic resistivity comparison of V_2O_5/G electrodes

In our previous work [89], by adding a small amount of graphene into the V_2O_5 xyrogel structure, the reversible capacity of 438mAh/g has been achieved, which almost meet reported theoretical specific capacity (443 mAh/g) of V_2O_5 and shows a greatly enhanced cycle life. This achieved capacity is much larger than other available cathode active materials, such as $LiFePO_4$ (165 mAh/g) [153], $LiCoO_2$ (148 mAh/g) [154], $LiNi_{0.33}Mn_{0.33}Co_{0.33}O_2$ (160 mAh/g) [155], and $LiMn_2O_4$ (120 mAh/g) [78]. Figure 4-19 a shows the voltage profiles of the first charge and discharge cycles of V_2O_5/G on metallic and paper-based current collectors. Here the capacity of 396 mAh/g has been achieved for the V_2O_5/G on CNT paper, compared with 406 mAh/g for V_2O_5/G on Al foil at 0.1 C rate. While the amount of the coated CNT over the paper fibers is negligible (0.2%wt) compared to the deposited V2O5/G, the CNT rods are not effective on the charge/discharge capacity of the fabricated paper-based cells.

The paper-based V_2O_5/G cell also shows a stable cycle life with capacity retention at 1 C rate. The capacity retention results are shown in Figure 4-19 b, and the results reveal that the metallic V_2O_5/G has less cyclic performance compared to the paper-based cells (81.2% for CNT vs. 72.6% for Al). This proves that the CNT-microfiber paper is a promising substitute for metallic current collector material of lithium-ion electrodes. The Coulombic efficiency of paper-based electrodes made by V_2O_5/G is also around 100%, which is comparable with metallic cells. Figure 4-19 c shows the cell performance after a bending test of 180º for three times using the reported setup in the previous chapter. Here the initial capacity loss of the paper-based electrode after the test was only 9.8 mAh/g (3.3% capacity loss), while the capacity loss of metallic electrodes after the bending test was 119.9 mAh/g, (37.9% capacity loss). These results are similar to the FESEM observation which proves the capacity loss in flexible cells is a result of active material layer detachment from the current collector.

The longer cycle life test for both paper-based and metallic cells also revealed that after 100 cycles the capacity of the paper-based cell was 1.66 times higher than the metallic cells. The average coulombic efficiency of the CNT-microfiber paper electrode during this test after 100 cycles was 97.93% which is also slightly higher than the reported value for metallic electrodes which was 95.92%. It was observed that through the bending test, the CNT-microfiber paper holds the active material layer better compare to the metallic current collectors. This can also reduce the drop in

electrical conductivity of electrodes after bending tests. The rate performances of V_2O_5/G electrode on CNT-microfiber paper and metallic current collectors are shown in Figure 4-19 d. The paper-based electrodes have a comparable specific capacity at lower C rates compared with metallic current collectors although, at higher C rates (5 C and 10 C) paper-based electrode has a relatively higher specific capacity (5.6% higher at 5 C, and 14.0% higher at 10 C). After bending, the electrode on CNT-microfiber paper still retains a high capacity compared to the metallic cells. Table 4-1 and Figure 4-19 d show the results of the bending test for different C rates

Table 4-1 Capacity compaction after the bending test of paper-based and metallic cells using different C rates

C rate	0.1 C	0.2 C	0.5 C	1 C	2 C	5 C	10 C
Paper-based Capacity	376 mAh/g	368 mAh/g	335 mAh/g	283 mAh/g	262 mAh/g	227 mAh/g	206 mAh/g
Metallic Capacity	296 mAh/g	257 mAh/g	235 mAh/g	196 mAh/g	154 mAh/g	112 mAh/g	93 mAh/g

The comparison shows that there is a to a 27.0, 43.2, 42.6, 44.4, 70.1, 102.7 and 121.5% specific capacity increase for paper-based cells at the different rates (from 0.1 to 10 C), respectively. Such a huge improvement of rate performance of electrode on CNT-microfiber paper over metallic current collectors after bending tests suggests that the CNT-microfiber paper is a great choice to make long-lasting and high capacity flexible electrodes. The same trend can also be observed from the CV results, as it is shown in Figure 4-19 e and 4-19 f. With comparable CV results for CNT-microfiber electrodes before and after bending (solid and dashed arrows shown in Figure 4-19 e respectively) the curve of electrode on aluminum sheet shifted severely from a symmetric redox peak to a shuttle-shaped curve without any obvious redox peaks after the bending test (solid and dashed arrows shown in Figure 4-25 respectively). This shows that there was damage or change in the contact between the current collector layer and active material film resulted in an abnormality in the electrochemical reactions. After bending, the apparent diffusion coefficient of V_2O_5/G electrode calculated from EIS dropped 55.1% and 12.2% for both paper-based and metallic (aluminum) electrodes respectively, as is reported in Figure 4-19 g. The diffusion

coefficients have been calculated considering the whole surface of the electrode was participating in electrochemical reactions. Thus, it can be observed that after the bending test, the CNT-microfiber paper can hold more active material compared to the metallic cells while there is no big drop in the real diffusion coefficient.

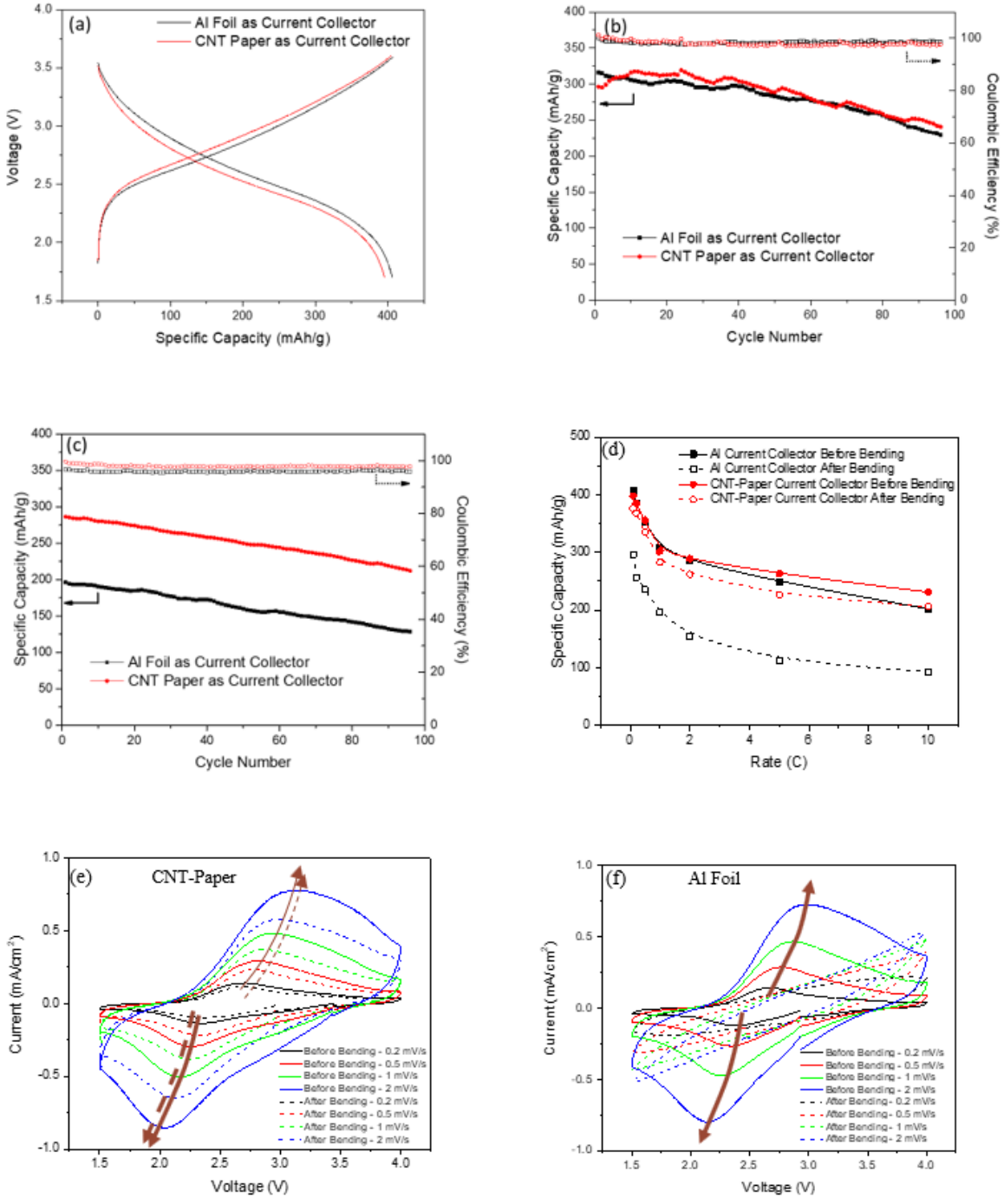

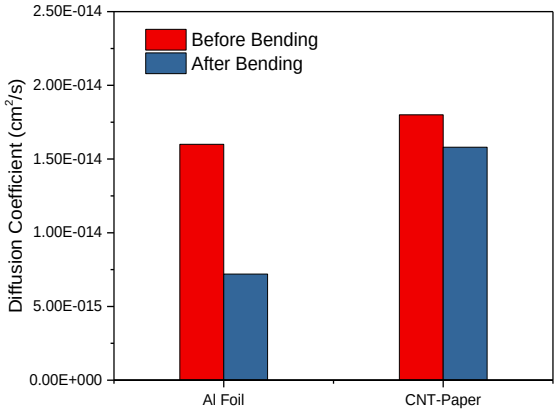

Figure 4-19 Electrochemical performance of the paper-based V_2O_5/G Half-cells. (a) Initial charge/discharge of the V_2O_5/G electrode on both CNT-microfiber paper and aluminum current collectors at 0.1 C. (b) Specific capacity and Coulombic efficiency at 1 C. (c) Specific capacity and Coulombic efficiency after 3 180º bending at 1 C. (d) C-rate performance of metallic and paper-based cells before and after bending. CV scan at different voltage levels of (e) paper-based V_2O_5/G electrodes before (solid) and after (dashed) bending and (f) metallic V_2O_5/G electrode before (solid) and after (dashed) bending. (g) Apparent lithium diffusion coefficient for paper-based and metallic V_2O_5/G electrode before and after bending

Here, by utilization of the CNT-microfiber paper with a good mechanical property and excellent electrochemical stability quality and flexibility of the electrodes have been improved and by taking advantage of the ultra-high capacity and stable of V_2O_5/G materials a complete ultra-high capacity flexible lithium ion battery has been developed using the CNT-microfiber paper. The electrochemical stability of CNT-microfiber paper proved that this paper can be used as a flexible and stable current collector for lithium ion battery electrodes. This paper-based electrode provides a simple fabrication, safety, lower weight, integration, recyclability and flexibility to lithium-ion batteries. The nanostructured V_2O_5/G hybrid composite active material was also applied to the CNT-microfiber paper current collectors and demonstrated excellent performance. The fabricated V_2O_5/G paper-based cell could achieve the capacities up to 396 mAh/g at 0.1 C and 300 mAh/g at 1 C with more than 80% capacity retention after 100 cycles. CNT-microfiber paper is a promising candidate as the current collector for high-performance and flexible electrodes to construct novel ultra-high capacity lithium ion batteries.

4.4 Reduced Graphene Microfiber Paper

4.4.1 Paper Characterization

Figure 4-20 a shows the alternating deposition of PEI and GO layers on wood microfibers. The thickness (obtained use a quartz crystal microbalance) and the zeta potential of each deposited layer is shown in Figure 4-20 b and 4-20 c respectively. As it is shown in Figure 4-20, the surface charge alternation after deposition of each layer confirms that layers of PEI and GO are coated over the negatively charged paper surface through LbL self-assembly. The anionic GO and the cationic PEI layers attach via electrostatic potential with PEI acting like a binding layer to keep GO on the surface of the microfibers. The zeta potential magnitude of each layer is always above 40 mV, providing high stability of each material in dispersion form and after they are deposited over the microfibers. Figure 4-20 b also reveals a uniform growth of the alternating layers. The QCM results are revealing that the thickness of each layer is between 5 to 20 um. This thin layer will not change the properties of the microfibers such as flexibility or porosity but acts as a high surface area highly conductive active material for lithium ion battery electrodes. In addition, the nanometer thickness of active layer reduces the lithium penetration dept and improves the reversibility and capacity of rGO microfiber cells.

The GO-coated microfibers were then reduced using the microwave thermal assisted reduction method described above. The final length resistance of the fabricated rGO fibers was measured to be 74.6 ±3.4 Ω/cm. Here the resistance and dimension of 20 randomly selected coated fibers were measured individually using a Keithley CV measurement microprobe station. The average of the resistance divided by the average length of the fiber then reported as the length resistance. This low length resistance makes the developed rGO microfibers suitable for thin, flexible electronic applications.

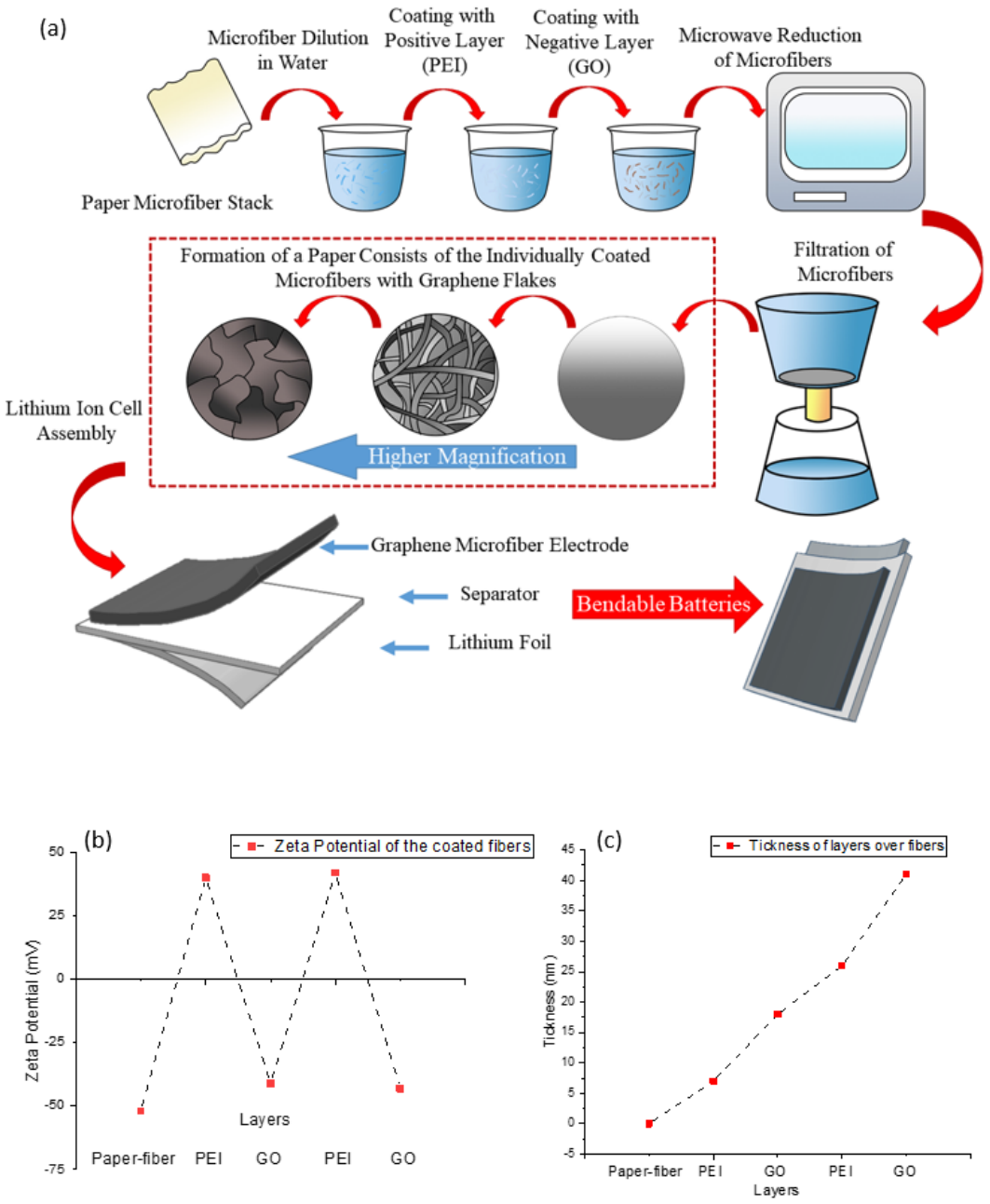

Figure 4-20 (a) Schematics of the rGO microfiber paper fabrication, (b) Surface potential, and (c) thickness of the deposited layers over the microfibers

Figure 4-21 a shows the associated color change of the fibers before and after microwave baking and Figure 4-21 b reveals the resulting Raman shift. The color change provides visual cue of the rGO formation via microwave thermal assist method [156]. The presence of rGO was validated using Raman spectroscopy of the fibers. Here, the G band and D bands were observed for GO and

rGO (graphene) samples. Here the D band from 1315 to 1326 is related to the defected in-plane sheet sp2 carbon bands so mainly corresponds to sp3 bonds made by disorders such as oxidations, and G band from 1597 to 1602 is related to in-plane sheet sp2 hybridized carbon corresponds to graphitic layers. Here the D/G intensity changed significantly from 1.28 to 0.92 after reduction which is related to the removal of oxygen from GO nanoflakes and formation of rGO. Here the D/G intensity changed significantly from 1.28 to 0.92 after reduction which is related to the removal of oxygen from GO nanoflakes and formation of rGO [157]. This reduction process is well known and backed by theory. In this case the particle size of GO is larger than rGO, therefore the intensity of the G band is also decreased after microwave assisted reduction.

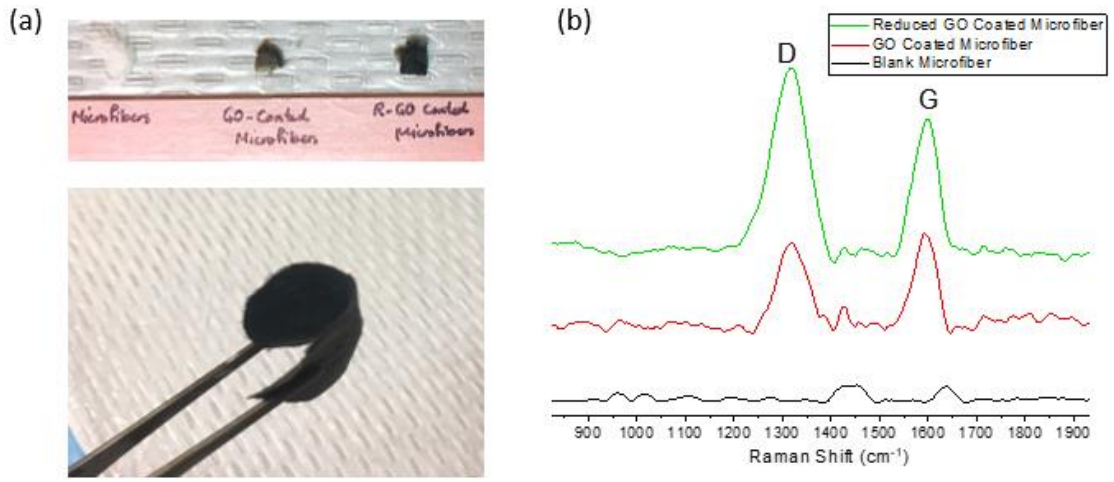

Figure 4-21 (a) Image of blank, graphene oxide coated, and microwave reduces graphene oxide microfibers and fabricated graphene microfiber paper and (b) Raman spectra of the paper fiber, GO and the microwave reduced graphene oxide rGO coated microfibers

The XRD results before and after the microwave reduction process of graphene oxide to rGO are shown in Figure 4-22. In this case the change in the XRD peaks is well visible. The main peak of GO is observed at 9.6°, which is related to the (001) plane of GO particles. The spacing of the crystal here is 9.2 Å which is associated to the GO crystals. The other peak at 24.1° is related to the (002) plane, which represents an indicator for rGO formation. In this case, having the 24.1° peak shows a spacing of 3.7 Å due to the removal of oxygen from GO [156, 158, 159]. Results, therefore indicate GO reduction to rGO using microwave thermal assisted reduction.

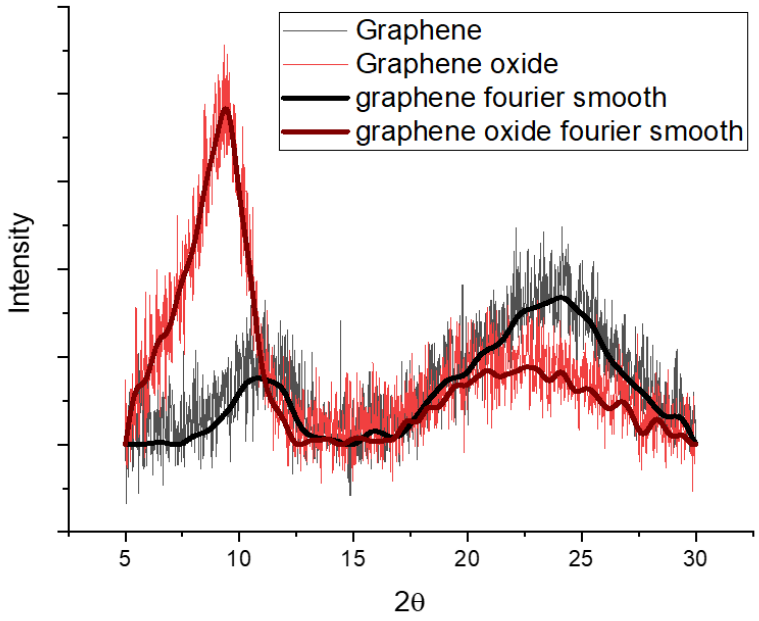

Figure 4-22 X-ray diffraction pattern of GO and microwaved reduced rGO fibers

The SEM images of wood microfibers, before and after GO reduction, as well as the final paper sheet product, are shown in Figure 4-23. A comparison between the uncoated (Figure 4-23 a) and coated (Figure 4-23 b and 4-23 c) microfibers shows the presence of a uniform GO (Figure 4-23 b) and subsequent rGO (Figure 4-23 c) coatings. The SEM images also reveal that the fibers are still porous after LbL and reduction processes. This porosity increases the total surface area of rGO, which should afford better capacity and lower internal resistance. In this case the liquid electrolyte can reach to more active material and provide higher chemical reactions. In this case,

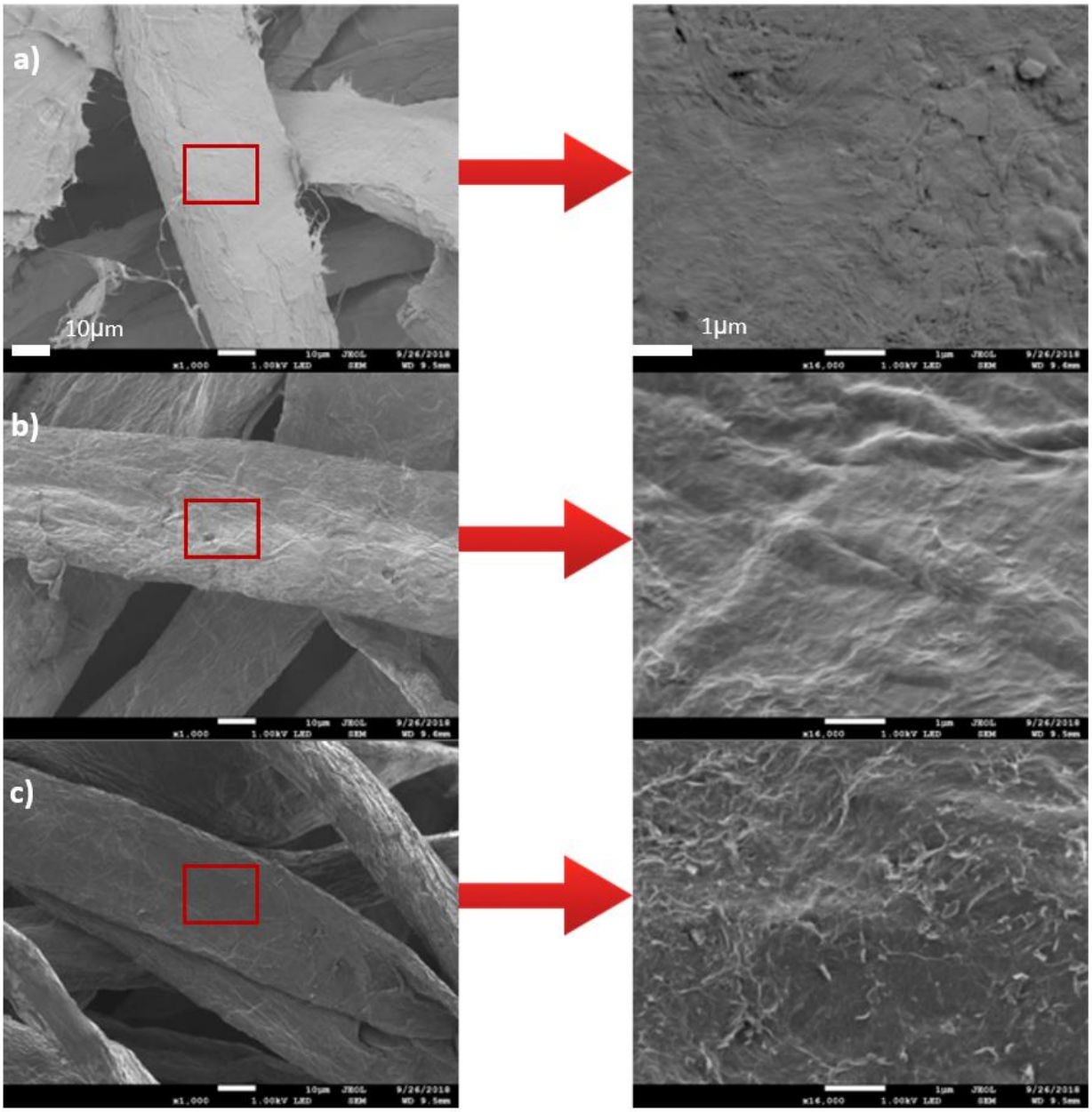

Figure 4-23 SEM images of the (a) paper fibers, (b) GO coated fiber, (c) microwave reduced rGO fibers

4.4.2 Lithium-ion Capacity

The fabricated rGO microfiber paper sheets were used in a half cell battery configuration. Figure 4-24 a shows the 1st and 10th cycles of the fabricated cells. The capacity of the cell was measured at 814 mAh/g for the 1st discharge, 546mAh/g for the 2nd cycle and 496 mAh/g for the 10th discharge. The high specific capacity of the first cycle is a well-known phenomenon related to the

lithium uptake on graphene flakes, and some decomposition of electrolyte in 1st cycle [160]. These values reveal that, by using this technique, a maximum number of rGO sheets are reacting with lithium due to the high surface area of the coated layers and very low effective thickness. The CV measurements presented below also support this. In this case, when lithium penetration depth is very small (around 50nm), maximum capacity will be achieved with C/5 rate. As is also shown in Figure 4-24 a the cell has stable performance after the 2nd cycle; the drop in the capacity after the 1st cycle is a well-known phenomenon due to a non-reversible lithiation of rGO, which has been previously reported [161]. The coulombic efficiency of the cell also has been reported in Figure 4-24 b. The first cycle efficiency is 69% due to the difference of charge and discharge capacity but after stabilization of the cell, this efficiency reached up to 96% and stayed almost the same through all 50 cycles.

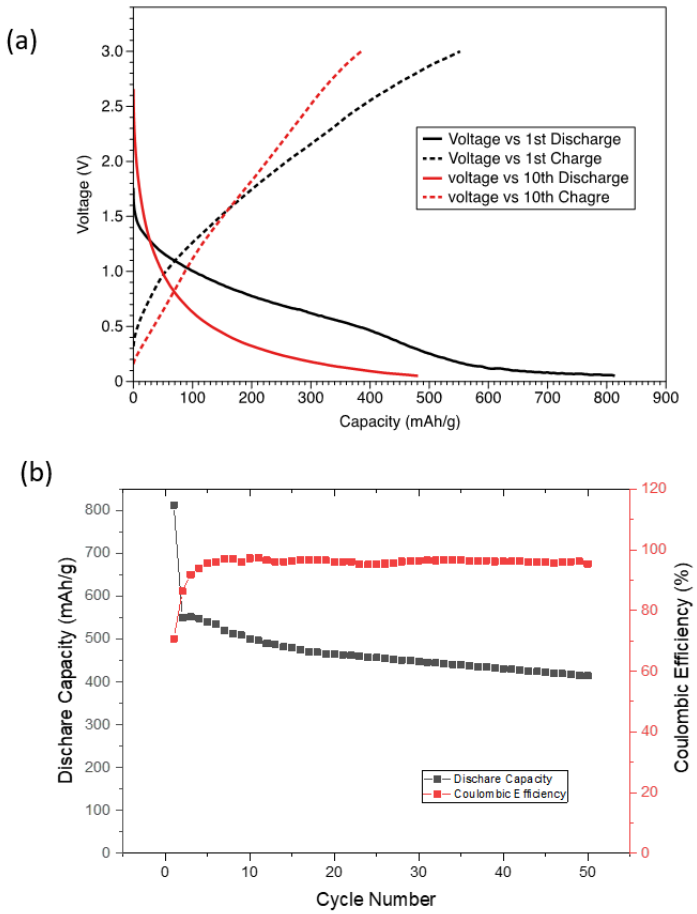

Figure 4-24 (a) Charge/Discharge capacity of the 1st and 10th cycle of the rGO microfiber paper sheet half cell, and (b) the cycle life of the rGO microfiber paper sheet half cell with C/5 discharge rate and coulombic efficiency

The internal resistance and galvanometry results of the half-cell also are shown in Figure 4-25 a. Internal resistance was calculated using the Warburg model with a lithium counter electrode. The DC potential and conductivity for the fabricated half cell (with 200 µm thick microfiber paper) was measured to be 0.5 mV and 1.2×10^{-3} S cm^{-1}, respectively. This is slightly higher than regular electrodes, making it particularly suitable for lower current applications where flexibility and durability are required. Figure 4-25 b reveals the cyclic voltammograms (CV) for the rGO microfiber paper as the anode. These half cells were made using a lithium cathode and demonstrated a voltage range was between 0.2 to 3 volts. The graph also shows the difference in the capacity of the fabricated cell after the 1st and 2nd cycles. This change in capacity and CV between the 1st and 2nd cycles is well known for graphene [27, 162].

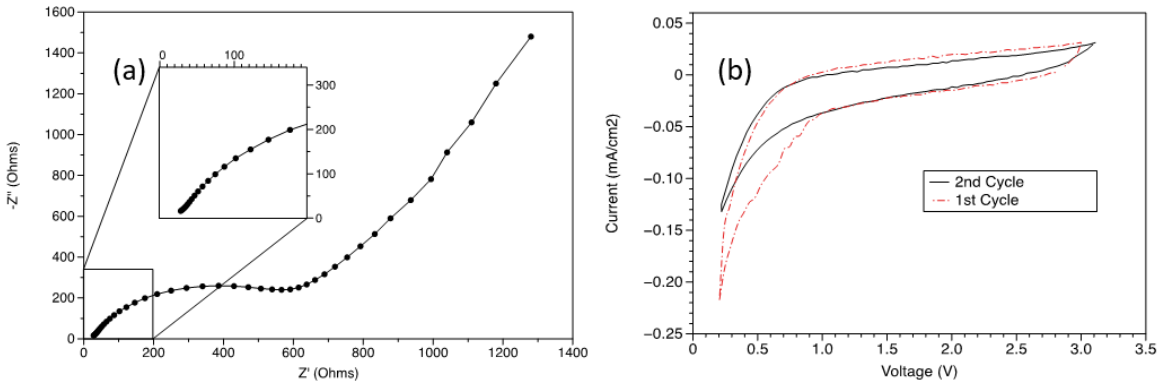

Figure 4-25 (a) Impedance measurements, and (b) Cyclic voltammogram of the rGO microfiber paper cell

In conclusion, rGO microfiber paper has been developed as a flexible electrode for lithium ion battery applications. Here, a fully flexible paper-based rGO electrode was created through the direct deposition of graphene oxide over paper microfibers, followed by mild microwave thermal reduction. This method forms a uniform coating of rGO over the fibers, which provides flexible lithium ion storage and eliminates the need for the addition of subsequent conductive materials such as carbon black, and super P lithium. The latter also reduces the total weight of the fabricated cells by up to 20%. Using the rGO microfiber paper as the anode for high capacity lithium ion batteries offers both cyclic performance and flexibility.

CHAPTER 5. SUMMARY, CONCLUSIONS, AND RECOMMENDATIONS

Paper-based flexible devices represent a new frontier in electronics technology. Recently there has been a surge in the development of flexible electronic devices, from smart watches to flexible displays. Thus, there is high demand for reliable and flexible energy storage strategies for use in these devices. The development of lightweight and flexible energy storage devices using a paper-based platform was the main goal of this research. Here, paper fibers coated with highly conductive materials, such as carbon nanotubes, in conjunction with ultra-high capacity lithium ion active materials were used to develop electrodes for flexible lithium ion batteries. The developed paper fibers can also be coated with other novel nanomaterials, such as reduced graphene oxide, to make standalone paper-based electrodes. In addition, development of a fully flexible and leakproof polymer gel electrolyte is needed to eliminate the limitations of liquid electrolytes for flexible lithium ion batteries.

Paper is a tangible material that can be used as a base for flexible electronics due to its properties such as porosity, high surface area, flexibility, biodegradability and low fabrication cost. One of the main challenges of using paper for flexible electronics is to make the paper conductive. While paper can provide porosity, surface area, flexibility and reduced weight, it needs to be coated with other conductive materials. Highly conductive materials, including carbon nanotubes and graphene, are used to fabricate the conductive microfiber papers through layer-by-layer nanoassembly. The resulting CNT-microfiber paper is a conductive and porous base for flexible electronic devices, and importantly requires only small amounts of CNT. This CNT-microfiber paper used as the current collector in conjunction with lithium electrodes offers flexible paper-based electrodes. In addition, rGO microfiber paper has also been developed to act as the anode of flexible lithium ion batteries. By deposition of GO over paper fibers, through LbL self-assembly, and using microwave-assisted thermal reduction, rGO coated microfibers are transformed into conductive sheets. These sheets have been formed into half-cells as a standalone current collector and electrode material for lithium ion batteries with capacities up to 814 mAh/g, and a 20% weight reduction in electrodes.

CNT-microfiber-based electrodes were also made via deposition of lithium active materials over the conductive paper. These paper-based electrodes and solid polymer gel electrolytes have been employed to make flexible lithium ion batteries. This paper-based electrode brings flexibility, durability, and lightweight properties to the lithium ion batteries. A new type of gel electrolyte was also fabricated to overcome the problems of liquid electrolytes for flexible batteries. This electrolyte was made by infusing both liquid and ceramic electrolytes, inside a polymer gel structure, and provided ionic conductivities up to 10^{-4} S/cm. The paper-based battery created in this work has a comparable capacity to commercial lithium batteries, while offering light weight and flexibility. Different electrodes such LTO, LCO, LMO and V_2O_5 were also fabricated and tested. Gel electrolytes such as poly(vinylidene fluoride-co-hexafluoropropylene) (PVDF-HFP) mixed with a highly ionic conductive solution lithium bis(Trifluoromethanesulfonyl)Imide (LiTFSI) showed improved cycle life and degradation of the paper-based cells. The voltage plateau of 2.3 V was achieved for LTO/LCO paper-based cells. Here, the electrolyte consisted of a highly porous PVDF-HFP membrane enhanced with LATP and LiTFSI ionic solution, achieved an ionic conductivity of 2.1×10^{-3} S/cm. Combining the high ionic conductivity properties of ceramic materials and the mechanical flexibility of the polymer gel structure, the resulting electrolyte demonstrated both high flexibility and high ionic conductivity. The electrolyte membrane was fabricated into regular and paper-based cells using LTO and LCO electrode materials, and performances were studied. Capacities up to 123 mAh/g for metallic and 99.5 mAh/g for CNT-microfiber current collector based devices we achieved, respectively. The difference in the charge/discharge plateau between the paper-based and metallic cells is due to the difference in the total impedance of the cells. The higher internal resistance of the paper-based battery is attributed to a lower capacity from the first to second cycle. Efforts to overcome these challenges and further improve cycle-life of the developed batteries are ongoing. While the capacity and performance of the paper-based battery needs improvement, the solid paper-based battery shows promise in many applications that require only limited power, such as RFID, wireless sensors, electrochromic displays, and paper-based functional electronics.

To improve the capacity of the paper-based cells, V_2O_5-based cells were also made and tested. The V_2O_5/G and its nano-compounds were designed to improve capacity, cycle life and conductivity. This can lead to the formation of V_2O_5/G xerogel to be deposited over the paper structure. The

capacity of the ultra-high capacity paper-based batteries was improved by using vanadium compounds to reach 396 mAh/g at 0.1 C and 300 mAh/g at 1 C with more than 80% capacity retention after 100 cycles. The electrochemical stability of this conductive paper was characterized and proved that it can be used as the current collector for a cathode and importantly offers simple fabrication processes, high safety, lower weight, and more flexibility than current lithium-ion batteries. Thus, CNT-microfiber paper is a promising candidate as a current collector for high-performance electrodes to construct flexible lithium ion cells.

The future recommendation for this project is to make a vanadium pentoxide cell using a V_2O_5/G cathode, rGO microfiber paper anode and a gel polymer electrolyte. This method solves the issues of previously developed flexible batteries and can be used to make large scale flexible batteries. In fact, commercialization plans are already in progress. Further, to improve the flexibility and stability of the cell a fully flexible, polyethylene or polydimethylsiloxane packaging also needs to be developed to maintain the integrity of the flexible components. This can lead to developing a fully flexible lithium ion battery for many flexible electronic applications.

LIST OF REFERENCES

[1] J.-M. Tarascon and M. Armand, "Issues and challenges facing rechargeable lithium batteries," in *Materials for Sustainable Energy: A Collection of Peer-Reviewed Research and Review Articles from Nature Publishing Group*: World Scientific, 2011, pp. 171-179.

[2] L. Li, Z. Wu, S. Yuan, and X.-B. Zhang, "Advances and challenges for flexible energy storage and conversion devices and systems," *Energy & Environmental Science,* vol. 7, no. 7, pp. 2101-2122, 2014.

[3] Y. Zhang *et al.*, "Flexible and Stretchable Lithium-Ion Batteries and Supercapacitors Based on Electrically Conducting Carbon Nanotube Fiber Springs," *Angewandte Chemie,* vol. 126, no. 52, pp. 14792-14796, 2014.

[4] Y. Qian, A. Vu, W. Smyrl, and A. Stein, "Facile preparation and electrochemical properties of V2O5-graphene composite films as free-standing cathodes for rechargeable lithium batteries," *Journal of the Electrochemical Society,* vol. 159, no. 8, pp. A1135-A1140, 2012.

[5] S. H. Ng *et al.*, "Synthesis and electrochemical properties of V2O5 nanostructures prepared via a precipitation process for lithium-ion battery cathodes," *Journal of Power Sources,* vol. 174, no. 2, pp. 1032-1035, 2007.

[6] N. Singh *et al.*, "Paintable battery," *Scientific reports,* vol. 2, p. 481, 2012.

[7] J. B. Goodenough and K.-S. Park, "The Li-ion rechargeable battery: a perspective," *Journal of the American Chemical Society,* vol. 135, no. 4, pp. 1167-1176, 2013.

[8] M. Wakihara, "Recent developments in lithium ion batteries," *Materials Science and Engineering: R: Reports,* vol. 33, no. 4, pp. 109-134, 2001.

[9] P. G. Bruce, B. Scrosati, and J. M. Tarascon, "Nanomaterials for rechargeable lithium batteries," *Angewandte Chemie International Edition,* vol. 47, no. 16, pp. 2930-2946, 2008.

[10] M. Armand and J.-M. Tarascon, "Building better batteries," *nature,* vol. 451, no. 7179, p. 652, 2008.

[11] C. Jiang, E. Hosono, and H. Zhou, "Nanomaterials for lithium ion batteries," *Nano today,* vol. 1, no. 4, pp. 28-33, 2006.

[12] G. N. Lewis and F. G. Keyes, "THE POTENTIAL OF THE LITHIUM ELECTRODE," *Journal of the American Chemical Society,* vol. 35, no. 4, pp. 340-344, 1913.

[13] J. W. Choi and D. Aurbach, "Promise and reality of post-lithium-ion batteries with high energy densities," *Nature Reviews Materials,* vol. 1, no. 4, p. 16013, 2016.

[14] D. Linden, "Handbook of batteries and fuel cells," *New York, McGraw-Hill Book Co., 1984, 1075 p. No individual items are abstracted in this volume.*, 1984.

[15] M. S. Whittingham, "Lithium batteries and cathode materials," *Chemical reviews,* vol. 104, no. 10, pp. 4271-4302, 2004.

[16] W. Van Schalkwijk and B. Scrosati, "Advances in lithium ion batteries introduction," in *Advances in Lithium-Ion Batteries*: Springer, 2002, pp. 1-5.

[17] B. K. Miremadi and S. R. Morrison, "The intercalation and exfoliation of tungsten disulfide," *Journal of applied physics*, vol. 63, no. 10, pp. 4970-4974, 1988.

[18] M. Yoshio, R. J. Brodd, and A. Kozawa, *Lithium-ion batteries: science and technologies*. Springer Science & Business Media, 2010.

[19] G. Pistoia, *Lithium-ion batteries: advances and applications*. Newnes, 2013.

[20] H. Huang, S.-C. Yin, and L. s. Nazar, "Approaching theoretical capacity of LiFePO4 at room temperature at high rates," *Electrochemical and Solid-State Letters*, vol. 4, no. 10, pp. A170-A172, 2001.

[21] R. Gummow, M. Thackeray, W. David, and S. Hull, "Structure and electrochemistry of lithium cobalt oxide synthesised at 400 C," *Materials research bulletin*, vol. 27, no. 3, pp. 327-337, 1992.

[22] K. Amine *et al.*, "Nanostructured anode material for high-power battery system in electric vehicles," *Advanced materials*, vol. 22, no. 28, pp. 3052-3057, 2010.

[23] X. B. Cheng, R. Zhang, C. Z. Zhao, F. Wei, J. G. Zhang, and Q. Zhang, "A review of solid electrolyte interphases on lithium metal anode," *Advanced Science*, vol. 3, no. 3, p. 1500213, 2016.

[24] S. Lux, F. Schappacher, A. Balducci, S. Passerini, and M. Winter, "Low cost, environmentally benign binders for lithium-ion batteries," *Journal of the Electrochemical Society*, vol. 157, no. 3, pp. A320-A325, 2010.

[25] M.-H. Park *et al.*, "Flexible high-energy Li-ion batteries with fast-charging capability," *Nano letters*, vol. 14, no. 7, pp. 4083-4089, 2014.

[26] G. Eda, G. Fanchini, and M. Chhowalla, "Large-area ultrathin films of reduced graphene oxide as a transparent and flexible electronic material," *Nature nanotechnology*, vol. 3, no. 5, p. 270, 2008.

[27] G. Wang, X. Shen, J. Yao, and J. Park, "Graphene nanosheets for enhanced lithium storage in lithium ion batteries," *Carbon*, vol. 47, no. 8, pp. 2049-2053, 2009.

[28] Q. Liu *et al.*, "Graphene-modified nanostructured vanadium pentoxide hybrids with extraordinary electrochemical performance for Li-ion batteries," *Nature communications*, vol. 6, p. 6127, 2015.

[29] E. Yoo, J. Kim, E. Hosono, H.-s. Zhou, T. Kudo, and I. Honma, "Large reversible Li storage of graphene nanosheet families for use in rechargeable lithium ion batteries," *Nano letters*, vol. 8, no. 8, pp. 2277-2282, 2008.

[30] L. Ji, Z. Lin, M. Alcoutlabi, and X. Zhang, "Recent developments in nanostructured anode materials for rechargeable lithium-ion batteries," *Energy & Environmental Science*, vol. 4, no. 8, pp. 2682-2699, 2011.

[31] N. Nitta, F. Wu, J. T. Lee, and G. Yushin, "Li-ion battery materials: present and future," *Materials today*, vol. 18, no. 5, pp. 252-264, 2015.

[32] S. v. Laszczynski and S. v. Gorski, "Leitfähigkeit von Lösungen Eniger Saltze in Pyridin," *Z. Elektrochem*, vol. 4, pp. 290-293, 1897.

[33] B. Scrosati, "Recent advances in lithium ion battery materials," *Electrochimica Acta,* vol. 45, no. 15-16, pp. 2461-2466, 2000.

[34] S.-H. Kim, K.-H. Choi, S.-J. Cho, S. Choi, S. Park, and S.-Y. Lee, "Printable solid-state lithium-ion batteries: a new route toward shape-conformable power sources with aesthetic versatility for flexible electronics," *Nano letters,* vol. 15, no. 8, pp. 5168-5177, 2015.

[35] G. Chen, F. Zhang, Z. Zhou, J. Li, and Y. Tang, "A Flexible Dual-Ion Battery Based on PVDF-HFP-Modified Gel Polymer Electrolyte with Excellent Cycling Performance and Superior Rate Capability," *Advanced Energy Materials,* vol. 8, no. 25, p. 1801219, 2018.

[36] M. Agarwal, Y. Lvov, and K. Varahramyan, "Conductive wood microfibres for smart paper through layer-by-layer nanocoating," *Nanotechnology,* vol. 17, no. 21, p. 5319, 2006.

[37] Y.-H. Kim, D.-G. Moon, and J.-I. Han, "Organic TFT array on a paper substrate," *IEEE electron device letters,* vol. 25, no. 10, pp. 702-704, 2004.

[38] J. Kim, C.-S. Song, and S.-R. Yun, "Cellulose based electro-active papers: performance and environmental effects," *Smart Materials and Structures,* vol. 15, no. 3, p. 719, 2006.

[39] J. Qi and L. Buechley, "Electronic popables: exploring paper-based computing through an interactive pop-up book," in *Proceedings of the fourth international conference on Tangible, embedded, and embodied interaction*, 2010, pp. 121-128: ACM.

[40] A. C. Siegel, S. T. Phillips, M. D. Dickey, N. Lu, Z. Suo, and G. M. Whitesides, "Foldable printed circuit boards on paper substrates," *Advanced Functional Materials,* vol. 20, no. 1, pp. 28-35, 2010.

[41] T. H. Nguyen, A. Fraiwan, and S. Choi, "Paper-based batteries: A review," *Biosensors and Bioelectronics,* vol. 54, pp. 640-649, 2014.

[42] J. Lessing, A. C. Glavan, S. B. Walker, C. Keplinger, J. A. Lewis, and G. M. Whitesides, "Inkjet Printing of Conductive Inks with High Lateral Resolution on Omniphobic “RF Paper” for Paper-Based Electronics and MEMS," *Advanced Materials,* vol. 26, no. 27, pp. 4677-4682, 2014.

[43] M. Agarwal, K. Varahramyan, S. Shrestha, and N. Aliahmad, "Paper-Based Lithium- Ion Batteries," ed: Google Patents, 2014.

[44] M. Agarwal, Q. Xing, B. S. Shim, N. Kotov, K. Varahramyan, and Y. Lvov, "Conductive paper from lignocellulose wood microfibers coated with a nanocomposite of carbon nanotubes and conductive polymers," *Nanotechnology,* vol. 20, no. 21, p. 215602, 2009.

[45] N. Aliahmad, M. Agarwal, S. Shrestha, and K. Varahramyan, "Paper-based lithium-ion batteries using carbon nanotube-coated wood microfibers," 2013.

[46] H. S. Nalwa, *Handbook of nanostructured materials and nanotechnology, five-volume set*. Academic Press, 1999.

[47] M. J. Allen, V. C. Tung, and R. B. Kaner, "Honeycomb carbon: a review of graphene," *Chemical reviews,* vol. 110, no. 1, pp. 132-145, 2009.

[48] M. Yoshio, H. Wang, K. Fukuda, T. Umeno, T. Abe, and Z. Ogumi, "Improvement of natural graphite as a lithium-ion battery anode material, from raw flake to carbon-coated sphere," *Journal of Materials Chemistry,* vol. 14, no. 11, pp. 1754-1758, 2004.

[49] S. Pei and H.-M. Cheng, "The reduction of graphene oxide," *Carbon,* vol. 50, no. 9, pp. 3210-3228, 2012.

[50] L. Hu *et al.*, "Highly conductive paper for energy-storage devices," *Proceedings of the National Academy of Sciences,* vol. 106, no. 51, pp. 21490-21494, 2009.

[51] J. Wang, L. Li, C. L. Wong, and S. Madhavi, "Flexible single-walled carbon nanotube/polycellulose papers for lithium-ion batteries," *Nanotechnology,* vol. 23, no. 49, p. 495401, 2012.

[52] B. J. Landi, M. J. Ganter, C. D. Cress, R. A. DiLeo, and R. P. Raffaelle, "Carbon nanotubes for lithium ion batteries," *Energy & Environmental Science,* vol. 2, no. 6, pp. 638-654, 2009.

[53] L. Hu, H. Wu, F. La Mantia, Y. Yang, and Y. Cui, "Thin, flexible secondary Li-ion paper batteries," *ACS nano,* vol. 4, no. 10, pp. 5843-5848, 2010.

[54] H. Zhang, Z. Wang, Z. Zhang, J. Wu, J. Zhang, and J. He, "Regenerated-cellulose/multiwalled-carbon-nanotube composite fibers with enhanced mechanical properties prepared with the ionic liquid 1-allyl-3-methylimidazolium chloride," *Advanced Materials,* vol. 19, no. 5, pp. 698-704, 2007.

[55] L. Jabbour, R. Bongiovanni, D. Chaussy, C. Gerbaldi, and D. Beneventi, "Cellulose-based Li-ion batteries: a review," *Cellulose,* vol. 20, no. 4, pp. 1523-1545, 2013.

[56] G. Zhou, F. Li, and H.-M. Cheng, "Progress in flexible lithium batteries and future prospects," *Energy & Environmental Science,* vol. 7, no. 4, pp. 1307-1338, 2014.

[57] G. Broza, M. Kwiatkowska, Z. Rosłaniec, and K. Schulte, "Processing and assessment of poly (butylene terephthalate) nanocomposites reinforced with oxidized single wall carbon nanotubes," *Polymer,* vol. 46, no. 16, pp. 5860-5867, 2005.

[58] J.-M. Tarascon and M. Armand, "Issues and challenges facing rechargeable lithium batteries," *Nature,* vol. 414, no. 6861, pp. 359-367, 2001.

[59] C. Wang, W. Zheng, Z. Yue, C. O. Too, and G. G. Wallace, "Buckled, stretchable polypyrrole electrodes for battery applications," *Advanced materials,* vol. 23, no. 31, pp. 3580-3584, 2011.

[60] N. Aliahmad, S. Shrestha, K. Varahramyan, and M. Agarwal, "Poly (vinylidene fluoride-hexafluoropropylene) polymer electrolyte for paper-based and flexible battery applications," *AIP Advances,* vol. 6, no. 6, p. 065206, 2016.

[61] B. Mi, "Graphene oxide membranes for ionic and molecular sieving," *Science,* vol. 343, no. 6172, pp. 740-742, 2014.

[62] T. Müller and B. Friedrich, "Development of a recycling process for nickel-metal hydride batteries," *Journal of power sources,* vol. 158, no. 2, pp. 1498-1509, 2006.

[63] J. X. Weinert, A. F. Burke, and X. Wei, "Lead-acid and lithium-ion batteries for the Chinese electric bike market and implications on future technology advancement," *Journal of Power Sources,* vol. 172, no. 2, pp. 938-945, 2007.

[64] C. Yan *et al.*, "Stretchable Silver-Zinc Batteries Based on Embedded Nanowire Elastic Conductors," *Advanced Energy Materials,* vol. 4, no. 5, p. 1301396, 2014.

[65] B. Diouf and R. Pode, "Potential of lithium-ion batteries in renewable energy," *Renewable Energy,* vol. 76, pp. 375-380, 2015.

[66] D. Aurbach *et al.*, "A short review on the comparison between Li battery systems and rechargeable magnesium battery technology," *Journal of Power Sources,* vol. 97, pp. 28-32, 2001.

[67] A. Manthiram, "Materials challenges and opportunities of lithium ion batteries," *The Journal of Physical Chemistry Letters,* vol. 2, no. 3, pp. 176-184, 2011.

[68] N. Aliahmad, Y. Liu, J. Xie, and M. Agarwal, "V2O5/Graphene Hybrid Supported on Paper Current Collectors for Flexible Ultrahigh-Capacity Electrodes for Lithium-Ion Batteries," *ACS applied materials & interfaces,* vol. 10, no. 19, pp. 16490-16499, 2018.

[69] N. Aliahmad, M. Agarwal, S. Shrestha, and K. Varahramyan, "based lithium-ion batteries using carbon nanotube-coated wood microfibers," *IEEE Transactions on Nanotechnology,* vol. 12, no. 3, pp. 408-412, 2013.

[70] G. Taillades and J. Sarradin, "Silver: high performance anode for thin film lithium ion batteries," *Journal of power sources,* vol. 125, no. 2, pp. 199-205, 2004.

[71] C.-T. Hsieh, C.-Y. Lin, Y.-F. Chen, J.-S. Lin, and H. Teng, "Silver nanorods attached to graphene sheets as anode materials for lithium-ion batteries," *Carbon,* vol. 62, pp. 109-116, 2013.

[72] C. K. Chan *et al.*, "High-performance lithium battery anodes using silicon nanowires," *Nature nanotechnology,* vol. 3, no. 1, p. 31, 2008.

[73] J. Zhu, D. Yang, Z. Yin, Q. Yan, and H. Zhang, "Graphene and graphene-based materials for energy storage applications," *Small,* vol. 10, no. 17, pp. 3480-3498, 2014.

[74] C. Fu, G. Zhao, H. Zhang, and S. Li, "Evaluation and characterization of reduced graphene oxide nanosheets as anode materials for lithium-ion batteries," *Int. J. Electrochem. Sci,* vol. 8, no. 5, pp. 6269-6280, 2013.

[75] C. Liu and H.-M. Cheng, "Carbon nanotubes for clean energy applications," *Journal of Physics D: Applied Physics,* vol. 38, no. 14, p. R231, 2005.

[76] A. Mansourizadeh and A. Ismail, "Preparation and characterization of porous PVDF hollow fiber membranes for CO< sub> 2</sub> absorption: Effect of different non-solvent additives in the polymer dope," *International Journal of Greenhouse Gas Control,* vol. 5, no. 4, pp. 640-648, 2011.

[77] F. Lin *et al.*, "Surface reconstruction and chemical evolution of stoichiometric layered cathode materials for lithium-ion batteries," Article vol. 5, p. 3529, 03/27/online 2014.

[78] M.-J. Lee, S. Lee, P. Oh, Y. Kim, and J. Cho, "High Performance LiMn2O4 Cathode Materials Grown with Epitaxial Layered Nanostructure for Li-Ion Batteries," *Nano Letters,* vol. 14, no. 2, pp. 993-999, 2014/02/12 2014.

[79] J. W. Park, "Effects of Non-Uniform Temperature on in-Situ Current Distribution and Non-Uniform State of Charge Measurements for LiFePO 4 and LiNiMnCoO 2 Cells," in *231st ECS Meeting (May 28-June 1, 2017),* 2017: Ecs.

[80] D. Guan, J. A. Jeevarajan, and Y. Wang, "Enhanced cycleability of LiMn2O4 cathodes by atomic layer deposition of nanosized-thin Al2O3 coatings," *Nanoscale,* vol. 3, no. 4, pp. 1465-1469, 2011.

[81] D. Murphy, P. Christian, F. DiSalvo, and J. Waszczak, "Lithium incorporation by vanadium pentoxide," *Inorganic Chemistry,* vol. 18, no. 10, pp. 2800-2803, 1979.

[82] A. M. Cao, J. S. Hu, H. P. Liang, and L. J. Wan, "Self-assembled vanadium pentoxide (V2O5) hollow microspheres from nanorods and their application in lithium-Ion batteries," *Angewandte Chemie International Edition,* vol. 44, no. 28, pp. 4391-4395, 2005.

[83] L. Mai *et al.*, "Electrospun ultralong hierarchical vanadium oxide nanowires with high performance for lithium ion batteries," *Nano letters,* vol. 10, no. 11, pp. 4750-4755, 2010.

[84] A. Pan *et al.*, "Facile synthesized nanorod structured vanadium pentoxide for high-rate lithium batteries," *J. Mater. Chem.,* vol. 20, no. 41, pp. 9193-9199, 2010.

[85] Y. J. Mai *et al.*, "CuO/graphene composite as anode materials for lithium-ion batteries," *Electrochimica Acta,* vol. 56, no. 5, pp. 2306-2311, 2/1/ 2011.

[86] Y. Wang, K. Takahashi, K. H. Lee, and G. Cao, "Nanostructured Vanadium Oxide Electrodes for Enhanced Lithium-Ion Intercalation," *Advanced Functional Materials,* vol. 16, no. 9, pp. 1133-1144, 2006.

[87] L. Gu *et al.*, "Direct Observation of Lithium Staging in Partially Delithiated LiFePO4 at Atomic Resolution," *Journal of the American Chemical Society,* vol. 133, no. 13, pp. 4661-4663, 2011/04/06 2011.

[88] Z.-F. Li, H. Zhang, Q. Liu, Y. Liu, L. Stanciu, and J. Xie, "Hierarchical Nanocomposites of Vanadium Oxide Thin Film Anchored on Graphene as High-Performance Cathodes in Li-Ion Batteries," *ACS Applied Materials & Interfaces,* vol. 6, no. 21, pp. 18894-18900, 2014/11/12 2014.

[89] Q. Liu *et al.*, "Graphene-modified nanostructured vanadium pentoxide hybrids with extraordinary electrochemical performance for Li-ion batteries," *Nature communications,* vol. 6, 2015.

[90] F. M. Gray, *Solid polymer electrolytes*. VCH New Tork etc., 1991.

[91] J. B. Goodenough and Y. Kim, "Challenges for rechargeable Li batteries†," *Chemistry of Materials,* vol. 22, no. 3, pp. 587-603, 2009.

[92] A. M. Stephan, "Review on gel polymer electrolytes for lithium batteries," *European polymer journal,* vol. 42, no. 1, pp. 21-42, 2006.

[93] C. Tao *et al.*, "A promising TPU/PEO blend polymer electrolyte for all-solid-state lithium ion batteries," *Electrochimica Acta,* vol. 257, pp. 31-39, 2017.

[94] J. Płcharski and W. Weiczorek, "PEO based composite solid electrolyte containing nasicon," *Solid State Ionics,* vol. 28, pp. 979-982, 1988.

[95] M. Michael, M. Jacob, S. Prabaharan, and S. Radhakrishna, "Enhanced lithium ion transport in PEO-based solid polymer electrolytes employing a novel class of plasticizers," *Solid State Ionics,* vol. 98, no. 3-4, pp. 167-174, 1997.

[96] H.-H. Kuo, W.-C. Chen, T.-C. Wen, and A. Gopalan, "A novel composite gel polymer electrolyte for rechargeable lithium batteries," *Journal of power sources,* vol. 110, no. 1, pp. 27-33, 2002.

[97] A. Arya and A. Sharma, "Insights into the use of polyethylene oxide in energy storage/conversion devices: a critical review," *Journal of Physics D: Applied Physics,* vol. 50, no. 44, p. 443002, 2017.

[98] T.-C. Wen and W.-C. Chen, "Gelled composite electrolyte comprising thermoplastic polyurethane and poly (ethylene oxide) for lithium batteries," *Journal of power sources,* vol. 92, no. 1, pp. 139-148, 2001.

[99] S. Abbrent, J. Plestil, D. Hlavata, J. Lindgren, J. Tegenfeldt, and Å. Wendsjö, "Crystallinity and morphology of PVdF–HFP-based gel electrolytes," *Polymer,* vol. 42, no. 4, pp. 1407-1416, 2001.

[100] H.-L. Wang, H.-M. Kao, and T.-C. Wen, "Direct 7Li NMR Spectral Evidence for Different Li+ Local Environments in a Polyether Poly (urethane urea) Electrolyte," *Macromolecules,* vol. 33, no. 19, pp. 6910-6912, 2000.

[101] M. Kammoun, S. Berg, and H. Ardebili, "Flexible thin-film battery based on graphene-oxide embedded in solid polymer electrolyte," *Nanoscale,* vol. 7, no. 41, pp. 17516-17522, 2015.

[102] Q. Li and H. Ardebili, "Flexible thin-film battery based on solid-like ionic liquid-polymer electrolyte," *Journal of Power Sources,* vol. 303, pp. 17-21, 2016.

[103] Q. Cheng *et al.*, "Folding paper-based lithium-ion batteries for higher areal energy densities," *Nano letters,* vol. 13, no. 10, pp. 4969-4974, 2013.

[104] H. Ye, J. Huang, J. J. Xu, A. Khalfan, and S. G. Greenbaum, "Li ion conducting polymer gel electrolytes based on ionic liquid/PVDF-HFP blends," *Journal of the Electrochemical Society,* vol. 154, no. 11, pp. A1048-A1057, 2007.

[105] J. Song, Y. Wang, and C. Wan, "Review of gel-type polymer electrolytes for lithium-ion batteries," *Journal of Power Sources,* vol. 77, no. 2, pp. 183-197, 1999.

[106] D. Saikia and A. Kumar, "Ionic conduction in P (VDF-HFP)/PVDF–(PC+ DEC)–LiClO< sub> 4</sub> polymer gel electrolytes," *Electrochimica acta,* vol. 49, no. 16, pp. 2581-2589, 2004.

[107] Y. Cao, G. Yu, A. J. Heeger, and C. Yang, "Efficient, fast response light-emitting electrochemical cells: Electroluminescent and solid electrolyte polymers with interpenetrating network morphology," *Applied physics letters,* vol. 68, no. 23, pp. 3218-3220, 1996.

[108] M. Moshkovich, M. Cojocaru, H. Gottlieb, and D. Aurbach, "The study of the anodic stability of alkyl carbonate solutions by in situ FTIR spectroscopy, EQCM, NMR and MS," *Journal of Electroanalytical Chemistry,* vol. 497, no. 1, pp. 84-96, 2001.

[109] Y. Liang, Z. Lin, Y. Qiu, and X. Zhang, "Fabrication and characterization of LATP/PAN composite fiber-based lithium-ion battery separators," *Electrochimica Acta,* vol. 56, no. 18, pp. 6474-6480, 7/15/ 2011.

[110] M. Yang and J. Hou, "Membranes in lithium ion batteries," *Membranes,* vol. 2, no. 3, pp. 367-383, 2012.

[111] S. Kim, "CNT sensors for detecting gases with low adsorption energy by ionization," *Sensors,* vol. 6, no. 5, pp. 503-513, 2006.

[112] L. Yang, R. Zhang, D. Staiculescu, C. Wong, and M. M. Tentzeris, "A novel conformal RFID-enabled module utilizing inkjet-printed antennas and carbon nanotubes for gas-detection applications," *IEEE Antennas and Wireless Propagation Letters,* vol. 8, pp. 653-656, 2009.

[113] C. K. Fung, M. Q. Zhang, Z. Dong, and W. J. Li, "Fabrication of CNT-based MEMS piezoresistive pressure sensors using DEP nanoassembly," in *5th IEEE Conference on Nanotechnology, 2005.*, 2005, pp. 199-202: IEEE.

[114] J.-W. Han, B. Kim, J. Li, and M. Meyyappan, "Carbon nanotube based humidity sensor on cellulose paper," *The Journal of Physical Chemistry C,* vol. 116, no. 41, pp. 22094-22097, 2012.

[115] J. Kong, M. G. Chapline, and H. Dai, "Functionalized carbon nanotubes for molecular hydrogen sensors," *Advanced Materials,* vol. 13, no. 18, pp. 1384-1386, 2001.

[116] B. Serban *et al.*, "Polymer-amino carbon nanotube nanocomposites for surface acoustic wave CO2 detection," *Rom J Inf Sci Technol,* vol. 12, no. 3, pp. 376-384, 2009.

[117] N. Sinha, J. Ma, and J. T. Yeow, "Carbon nanotube-based sensors," *Journal of nanoscience and nanotechnology,* vol. 6, no. 3, pp. 573-590, 2006.

[118] D. R. Kauffman and A. Star, "Carbon nanotube gas and vapor sensors," *Angewandte Chemie International Edition,* vol. 47, no. 35, pp. 6550-6570, 2008.

[119] Y. Wang and J. T. Yeow, "A review of carbon nanotubes-based gas sensors," *Journal of sensors,* vol. 2009, 2009.

[120] T. Zhang, S. Mubeen, N. V. Myung, and M. A. Deshusses, "Recent progress in carbon nanotube-based gas sensors," *Nanotechnology,* vol. 19, no. 33, p. 332001, 2008.

[121] J. Newman, K. E. Thomas, H. Hafezi, and D. R. Wheeler, "Modeling of lithium-ion batteries," *Journal of power sources,* vol. 119, pp. 838-843, 2003.

[122] L. Cai and R. E. White, "Mathematical modeling of a lithium ion battery with thermal effects in COMSOL Inc. Multiphysics (MP) software," *Journal of Power Sources,* vol. 196, no. 14, pp. 5985-5989, 2011.

[123] Y. Ren, *Heat and Mass Transfer: Advances in Modelling and Experimental Study for Industrial Applications*. BoD–Books on Demand, 2018.

[124] M. Doyle and Y. Fuentes, "Computer simulations of a lithium-ion polymer battery and implications for higher capacity next-generation battery designs," *Journal of The Electrochemical Society,* vol. 150, no. 6, pp. A706-A713, 2003.

[125] E. Martínez-Rosas, R. Vasquez-Medrano, and A. Flores-Tlacuahuac, "Modeling and simulation of lithium-ion batteries," *Computers & Chemical Engineering,* vol. 35, no. 9, pp. 1937-1948, 2011.

[126] L. O. Valøen and J. N. Reimers, "Transport properties of LiPF6-based Li-ion battery electrolytes," *Journal of The Electrochemical Society,* vol. 152, no. 5, pp. A882-A891, 2005.

[127] S. Buller, M. Thele, R. W. De Doncker, and E. Karden, "Impedance-based simulation models of supercapacitors and Li-ion batteries for power electronic applications," *IEEE Transactions on Industry Applications,* vol. 41, no. 3, pp. 742-747, 2005.

[128] H. He, X. Zhang, R. Xiong, Y. Xu, and H. Guo, "Online model-based estimation of state-of-charge and open-circuit voltage of lithium-ion batteries in electric vehicles," *Energy,* vol. 39, no. 1, pp. 310-318, 2012.

[129] T. B. Reddy, *Linden's handbook of batteries*. McGraw-hill New York, 2011.

[130] L. Chen, M. Zhang, and W. Wei, "Graphene-based composites as cathode materials for lithium ion batteries," *Journal of Nanomaterials,* vol. 2013, p. 2, 2013.

[131] G. Appetecchi, J. Hassoun, B. Scrosati, F. Croce, F. Cassel, and M. Salomon, "Hot-pressed, solvent-free, nanocomposite, PEO-based electrolyte membranes: II. All solid-state Li/LiFePO4 polymer batteries," *Journal of power sources,* vol. 124, no. 1, pp. 246-253, 2003.

[132] M. J. Reddy, J. S. Kumar, U. S. Rao, and P. P. Chu, "Structural and ionic conductivity of PEO blend PEG solid polymer electrolyte," *Solid state ionics,* vol. 177, no. 3, pp. 253-256, 2006.

[133] X. Liang, Z. Wen, Y. Liu, H. Zhang, L. Huang, and J. Jin, "Highly dispersed sulfur in ordered mesoporous carbon sphere as a composite cathode for rechargeable polymer Li/S battery," *Journal of Power Sources,* vol. 196, no. 7, pp. 3655-3658, 2011.

[134] S. S. Zhang, "A review on the separators of liquid electrolyte Li-ion batteries," *Journal of Power Sources,* vol. 164, no. 1, pp. 351-364, 2007.

[135] A. Du Pasquier, P. Warren, D. Culver, A. Gozdz, G. Amatucci, and J.-M. Tarascon, "Plastic PVDF-HFP electrolyte laminates prepared by a phase-inversion process," *Solid State Ionics,* vol. 135, no. 1, pp. 249-257, 2000.

[136] J. Zhao, L. Wang, X. He, C. Wan, and C. Jiang, "Determination of lithium-ion transference numbers in LiPF6–PC solutions based on electrochemical polarization and NMR measurements," *Journal of The Electrochemical Society,* vol. 155, no. 4, pp. A292-A296, 2008.

[137] S. Rajabzadeh, T. Maruyama, T. Sotani, and H. Matsuyama, "Preparation of PVDF hollow fiber membrane from a ternary polymer/solvent/nonsolvent system via thermally induced phase separation (TIPS) method," *Separation and Purification Technology,* vol. 63, no. 2, pp. 415-423, 2008.

[138] J. W. Fergus, "Ceramic and polymeric solid electrolytes for lithium-ion batteries," *Journal of Power Sources,* vol. 195, no. 15, pp. 4554-4569, 2010.

[139] P. G. Bruce, *Solid state electrochemistry*. Cambridge University Press, 1997.

[140] J. Song, Y. Wang, and C. C. Wan, "Review of gel-type polymer electrolytes for lithium-ion batteries," *Journal of power sources,* vol. 77, no. 2, pp. 183-197, 1999.

[141] A. Daneshkhah, S. Shrestha, M. Agarwal, and K. Varahramyan, "Poly (vinylidene fluoride-hexafluoropropylene) composite sensors for volatile organic compounds detection in breath," *Sensors and Actuators B: Chemical,* vol. 221, pp. 635-643, 2015.

[142] S.-H. Yeon, K.-S. Kim, S. Choi, J.-H. Cha, and H. Lee, "Characterization of PVdF(HFP) Gel Electrolytes Based on 1-(2-Hydroxyethyl)-3-methyl Imidazolium Ionic Liquids," *The Journal of Physical Chemistry B,* vol. 109, no. 38, pp. 17928-17935, 2005/09/01 2005.

[143] P. Arora, R. E. White, and M. Doyle, "Capacity fade mechanisms and side reactions in lithium-ion batteries," *Journal of the Electrochemical Society,* vol. 145, no. 10, pp. 3647-3667, 1998.

[144] S.-H. Yeon, K.-S. Kim, S. Choi, J.-H. Cha, and H. Lee, "Characterization of PVdF (HFP) gel electrolytes based on 1-(2-hydroxyethyl)-3-methyl imidazolium ionic liquids," *The Journal of Physical Chemistry B,* vol. 109, no. 38, pp. 17928-17935, 2005.

[145] A. Du Pasquier, I. Plitz, J. Gural, F. Badway, and G. Amatucci, "Power-ion battery: bridging the gap between Li-ion and supercapacitor chemistries," *Journal of Power Sources,* vol. 136, no. 1, pp. 160-170, 2004.

[146] H. He *et al.,* "Failure Investigation of LiFePO4 Cells in Over-Discharge Conditions," *Journal of The Electrochemical Society,* vol. 160, no. 6, pp. A793-A804, January 1, 2013 2013.

[147] F. Xu *et al.,* "Failure Investigation of LiFePO4 Cells under Overcharge Conditions," *Journal of The Electrochemical Society,* vol. 159, no. 5, pp. A678-A687, January 1, 2012 2012.

[148] S. Zhang and T. Jow, "Aluminum corrosion in electrolyte of Li-ion battery," *Journal of Power Sources,* vol. 109, no. 2, pp. 458-464, 2002.

[149] S.-T. Myung, Y. Hitoshi, and Y.-K. Sun, "Electrochemical behavior and passivation of current collectors in lithium-ion batteries," *Journal of Materials Chemistry,* vol. 21, no. 27, pp. 9891-9911, 2011.

[150] Q. Liu *et al.,* "Capacity fading mechanism of the commercial 18650 LiFePO4-based lithium-ion batteries: an in situ time-resolved high-energy synchrotron XRD study," *ACS applied materials & interfaces,* vol. 10, no. 5, pp. 4622-4629, 2018.

[151] Y. Liu *et al.,* "Failure study of commercial LiFePO4 cells in over-discharge conditions using electrochemical impedance spectroscopy," *Journal of The Electrochemical Society,* vol. 161, no. 4, pp. A620-A632, 2014.

[152] Y. Liu and J. Xie, "Failure Study of Commercial LiFePO4 Cells in Overcharge Conditions Using Electrochemical Impedance Spectroscopy," *Journal of The Electrochemical Society,* vol. 162, no. 10, pp. A2208-A2217, 2015.

[153] A. Yamada, S. C. Chung, and K. Hinokuma "Optimized LiFePO4 for Lithium Battery Cathodes," *Journal of The Electrochemical Society,* vol. 148, no. 3, pp. A224-A229, March 1, 2001 2001.

[154] J. Cho, Y.-W. Kim, B. Kim, J.-G. Lee, and B. Park, "A Breakthrough in the Safety of Lithium Secondary Batteries by Coating the Cathode Material with AlPO4 Nanoparticles," *Angewandte Chemie International Edition,* vol. 42, no. 14, pp. 1618-1621, 2003.

[155] F. Lin *et al.*, "Surface reconstruction and chemical evolution of stoichiometric layered cathode materials for lithium-ion batteries," *Nature Communications,* Article vol. 5, p. 3529, 03/27/online 2014.

[156] H. M. Hassan *et al.*, "Microwave synthesis of graphene sheets supporting metal nanocrystals in aqueous and organic media," *Journal of Materials Chemistry,* vol. 19, no. 23, pp. 3832-3837, 2009.

[157] G. Lalwani, W. Xing, and B. Sitharaman, "Enzymatic degradation of oxidized and reduced graphene nanoribbons by lignin peroxidase," *Journal of Materials Chemistry B,* vol. 2, no. 37, pp. 6354-6362, 2014.

[158] W. Chen, L. Yan, and P. R. Bangal, "Preparation of graphene by the rapid and mild thermal reduction of graphene oxide induced by microwaves," *Carbon,* vol. 48, no. 4, pp. 1146-1152, 2010.

[159] S. R. Sahu, M. M. Devi, P. Mukherjee, P. Sen, and K. Biswas, "Optical property characterization of novel graphene-X (X= Ag, Au and Cu) nanoparticle hybrids," *Journal of Nanomaterials,* vol. 2013, p. 6, 2013.

[160] J. Hassoun *et al.*, "An advanced lithium-ion battery based on a graphene anode and a lithium iron phosphate cathode," *Nano letters,* vol. 14, no. 8, pp. 4901-4906, 2014.

[161] K.-H. Lin and C.-L. Kuo, "Lithiation mechanisms and lithium storage capacity of reduced graphene oxide nanoribbons: a first-principles study," *Journal of Materials Chemistry A,* vol. 5, no. 10, pp. 4912-4922, 2017.

[162] C. Gómez-Navarro *et al.*, "Electronic transport properties of individual chemically reduced graphene oxide sheets," *Nano letters,* vol. 7, no. 11, pp. 3499-3503, 2007.